Elucidating Regulatory Mechanisms of Cardiac $Ca_V1.2$ and $Na_V1.5$ Channels

Daniel Dennis Roybal

Submitted in partial fulfillment of the
requirements for the degree of
Doctor of Philosophy
under the Executive Committee
of the Graduate School of Arts and Sciences

COLUMBIA UNIVERSITY

2021

Abstract

Elucidating Regulatory Mechanisms of Cardiac $Ca_V1.2$ and $Na_V1.5$ Channels

Daniel Dennis Roybal

In the heart, sodium (Na^+) influx via $Na_V1.5$ channels initiates the action potential, and calcium (Ca^{2+}) influx via $Ca_V1.2$ channels has a key role in excitation-contraction coupling and determining the plateau phase of the action potential. Mutations in the genes that encode these ion channels or in proteins that modulate them are linked to arrhythmias and cardiomyopathy, underscoring the need for characterizing mechanisms of regulation. The work presented in this thesis is subdivided into three different chapters, each with a distinct focus on ion channel modulation.

The first chapter details our investigation of the functional PKA phosphorylation target for β-adrenergic regulation of $Ca_V1.2$. Physiologic β-adrenergic activation of PKA during the sympathetic "fight or flight" response increases Ca^{2+} influx through $Ca_V1.2$ in cardiomyocytes, leading to increased cardiac contractility. The molecular mechanisms of β-adrenergic regulation of $Ca_V1.2$ in cardiomyocytes are incompletely known, but activation of PKA is required for this process. Recent data suggest that β-adrenergic regulation of $Ca_V1.2$ does not require any combination of PKA phosphorylation sites conserved in human, guinea pig, rabbit, rat, and mouse α_{1C} subunits. To test if any non-conserved sites are required for regulation, we generated mice with inducible cardiac-specific expression of α_{1C} with mutations at both conserved and non-conserved predicted PKA phosphorylation sites (35-mutant α_{1C}). Additionally, we created

another mouse with inducible cardiac-specific expression of β_2 with mutations at predicted PKA phosphorylation sites (28-mutant β_{2B}). In each of these mice, β-adrenergic stimulation of Ca^{2+} current was unperturbed. Finally, to test the hypothesis that redundant functional PKA phosphorylation sites exist on the α_{1C} subunit and β_2 subunit or that several sites confer incremental regulation, we crossed the 35-mutant α_{1C} mice with the 28-mutant β_{2B} mice to generate offspring expressing both mutant subunits. In these offspring, intact regulation was observed. These results provide the definitive answer that phosphorylation of the α_{1C} subunit or β_2 subunit is not required for β-adrenergic regulation of $Ca_V1.2$ in the heart.

In the second chapter, we study the influence of calmodulin and fibroblast growth homologous factor (FHF) FGF13 on late Na^+ current. Studies in heterologous expression systems show that the Ca^{2+}-binding protein calmodulin plays a key role in decreasing late Na^+ current. The effect of loss of calmodulin binding to $Na_V1.5$ on late Na^+ current has yet to be resolved in native cardiomyocytes. We created transgenic mice with cardiac-specific expression of human $Na_V1.5$ channels with alanine substitutions for the IQ motif (IQ/AA), disrupting calmodulin binding to the C-terminus. Surprisingly, we found that the IQ/AA mutation did not cause an increase late Na^+ current in cardiomyocytes. These findings suggest the existence of endogenous protective mechanisms that counteract the increase in late Na^+ current that occurs with loss of calmodulin binding. We reasoned that FGF13, a known modulator of late Na^+ current that is endogenously expressed in cardiomyocytes but not HEK cells, might play a protective role in limiting late Na^+ current. Finally, we coexpressed the IQ/AA mutant $Na_V1.5$ channel in HEK293 cells with FGF13 and found that FGF13 diminished the late Na^+ current

compared to cells without FGF13, suggesting that endogenous FHFs may serve to prevent late Na^+ current in mouse cardiomyocytes.

The third chapter of this thesis focuses on the use of proximity labeling and multiplexed quantitative proteomics to define changes in the $Na_V1.5$ macromolecular complex in Duchenne muscular dystrophy (DMD), in which the absence of dystrophin predisposes affected individuals to arrhythmias and cardiac dysfunction.. Standard methods to characterize macromolecular complexes have relied on candidate immunoprecipitation or immunocytochemistry techniques that fall short of providing a comprehensive view of the numbers and types of interactors, as well as the potential dynamic nature of the interactions that may be perturbed by disease states. To provide an inclusive understanding of $Na_V1.5$ macromolecular complexes, we utilize live-cell APEX2 proximity labeling in cardiomyocytes. We identify several proximal changes that align with the electrophysiological $Na_V1.5$ phenotype of young dystrophin-deficient mice, including a decrease in Ptpn3 and Gdp1l and an increase in proteasomal machinery. Whole-cell protein expression fold-change results were used to reveal the altered global expression profile and to place context behind $Na_V1.5$-proximal changes. Finally, we leveraged the neighborhood-specificity of proteins at the lateral membrane, intercalated disc, and transverse tubules of cardiomyocytes to demonstrate that $Na_V1.5$ channels can traffic to all three membrane compartments even in the absence of dystrophin. Thus, the approach of proximity labeling in cardiomyocytes from an animal model of human disease offers new insights into molecular mechanisms of $Na_V1.5$ dysfunction in DMD and provides a template for similar investigations in other cardiac diseases.

Table of Contents

List of Charts, Graphs, Illustrations

Introduction

Chapter 1

Chapter 2

Chapter 3

List of Abbreviations

α-MHC	α-Myosin Heavy Chain
AID	α-Interacting Domain
APEX2	Ascorbate-Peroxidase
apoCaM	Ca^{2+}-free Calmodulin
ATP	Adenosine Triphosphate
Ca^{2+}	Calcium
CaM	Calmodulin
cAMP	Cyclic Adenosine Monophosphate
CDI	Ca^{2+}-Dependent Inactivation
CICR	Ca^{2+}-Induced Ca^{2+} Release
DGC	Dystrophin-Glycoprotein Complex
DHP	Dihydropyridine
DMD	Duchenne muscular Dystrophy
E-C	Excitation-Contraction
GFP	Green Fluorescent Protein
$I_{Na,L}$	Late Na^+ Current
LQTS3	Long QT Syndrome 3
LTCC	L-type Ca^{2+} channel
Na^+	Sodium
NCX	Na^+/Ca^{2+} exchanger
PKA	Protein Kinase A

Plb	Phospholamban
rtTA	Reverse Tetracycline-Controlled Transactivator
RyR2	Ryanodine Receptor
SERCA	SR Ca^{2+}–ATPase
SR	Sarcoplasmic Reticulum
T-tubule	Transverse Tubule
TMT	Tandem Mass Tag
TTX	Tetrodotoxin
VDI	Voltage-Dependent Inactivation

Acknowledgments

Writing up scientific findings in clear, pithy story often doesn't fully illustrate the love and labor that goes into making significant discoveries, and I fear that any statement here on my graduate school experiences will be the same. The last 6 years stand as the most eventful time in my life. I experienced remarkable highs and weighty lows, many of which were shared with friends and colleagues. Importantly, the work presented here would not have been possible without the invaluable contributions, guidance, and kindness of others.

First, I'd like to thank my thesis committee: Dr. Henry Colecraft, Dr. Rocky Kass, and Dr. Masa Yazawa. With them, I gained valuable experience exploring the nuances of ion channel regulation. Their comments and questions challenged me to critically think of approaches that tested the validity of my findings and, without them, I wouldn't be the scientist that I am today. My rotations in the labs of Dr. Kass and Dr. Colecraft is where my fascination with ion channel electrophysiology was fostered and were valuable learning affairs. Each of them showed me great kindness in encouraging me to pursue my interests. Dr. Yazawa has been a fantastic leader both in his position as my thesis committee chair and in his tenure as program director. I have very high hopes for the future of the pharmacology graduate program with him at the helm. I would also like to thank Dr. Mario Delmar and Dr. Barry Fine for participating in my thesis defense committee.

I would like to thank the wonderful people in the Pharmacology department at Columbia. This department has fostered an open-door policy from day one and their vast experience in

working with students shows deeply. Thank you to Karen Allis, Janice Savage, and past administrators for your warmth and direction. Thank you to past program directors Dr. Neil Harrison and Dr. Susan Steinburg. Our individual meetings were distinguished by deep assistance and quip, and you both played an important role in my thesis committee meeting and qualifying exam. Thank you to Dr. Corey Abate-Shen for connecting with pharmacology graduate students and your efforts in transforming the department. Thank you, Dr. Jamie Rubin, for your unparalleled advice and assistance during my efforts in grant writing. Additionally, I'm proud to have known almost every student in the pharmacology department over nearly 10 cohorts. I have always felt a strong comradery with my fellow pharm students due to our shared experiences. This is especially true for the 5 others in my own cohort. I'll never forget the closeness that I built with them during my first experiences exploring New York.

A very large gratitude is owed to everyone that I worked with in the lab. Thank you to Dr. Guoxia Liu and Dr. Lin Yang for my first real education in laboratory molecular biology. Although I had some previous experience with techniques, your deep knowledge and guidance on experimental design was fundamental to my growth as a scientist. Thank you Bi-Xing Chen, your strong organization skills and dedication to project timelines was essential to my success and very much appreciated. Thank you to Dr. Alex Katchman and Dr. Sergey Zakharov for sharing pieces of your extensive insight on electrophysiology techniques and theory. Additionally, a very big thanks to Dr. Jared Kushner, Arianne Papa (soon-to-be Dr.), and Dr. Jessica Hennessey. Not only for their knowledge, resources, and enthusiasm, but for being great friends. The work in this thesis would not be possible without the profound expertise and assistance of Dr. Marian Kalocsay, Dr. Robyn Eisert, Dr. Gary Bradshaw, Dr. Nourdine

Chakouri, and Dr. Manu Ben-Johny. I appreciate all your hard work. Additionally, thank you to Dr. John Morrow, Dr. Elaine Wan, Dr. Uma Avula, Dr. Leroy Joseph, Dr. Chris Ward, and others for your helpful advice along the way.

The friendships that I made after moving to New York have been an amazing source of happiness and I wouldn't be person I am today without these radiant people in my life. Thank you especially to Meghan, Aaron, Greg, Emma, Daniel, Tarun, Nick, Manny, Eric and Kei. I also appreciate the dozens of other friends not mentioned here that have made life in New York magical. Finally, a very huge thank you to my partner Elise. You never fail to prop me up in all my personal and professional endeavors and continue to inspire me to do great things. I can't wait to see you excel in your future ventures.

Thank you to my friends from high school and college and my cousins, aunts, uncles, and grandparents back in New Mexico, who have always showered me with unconditional support. Thank you especially to Mom, Dad, and Aaron, who have been at my side for everything, for the reliable and enormous love you share.

Finally, thank you to my mentor Dr. Steven Marx. Your guidance and encouragement from day 1 left me knowing that I had truly and finally found the perfect lab for my thesis research. I have very much appreciated our conversations and your advice on all my experiments and research proposals. Most importantly, you instilled in me a high level of scientific confidence that I didn't think possible for myself. I look forward to hearing about the future high-impact findings that emerge from the lab under your stellar leadership.

Dedication

To Mom, Dad, and Aaron, with love.

Introduction

Ion Channels Facilitate Electrical Signals

Electrical signals occur in various tissues of the body, mediating cell-cell communication for physiologic organ function [1]. The phospholipid bilayer membrane acts as a barrier separating ionic species on the inside of the cell from the outside, and this compartmentalization allows the establishment of a voltage gradient across the cell membrane. Changes in cellular potential are mediated in part by protein complexes called ion channels, which form a transmembrane pore and modulate electrical signals by gating ionic flow across the cell membrane down their electrochemical concentration gradient. [2]. The ion channels detailed in this thesis belong to the voltage-gated ion channel family that open in response to a change in voltage across the cell membrane.

Ventricular Action Potential

Ion channels are essential to the proper function of the heart, where a brief spike in membrane potential called the action potential allows the augmentation and propagation of an electrical signal, culminating in myocyte and heart tissue contraction. The ventricular action potential is defined by four phases, each shaped by depolarizing inward currents and/or repolarizing outward currents [3]. The resting potential of a healthy heart is about -85mV. Influx of cations from gap junctions at the intercalated disc depolarize the membrane potential to about -55mV, resulting in the opening of voltage-gated Na^+ channels, including $Na_V1.5$, and initiating the phase 0 rapid upstroke of the action potential [4]. After the membrane depolarizes to about

+50 mV, Na^+ channels rapidly inactivate and voltage gated K^+ channels open, initiating the phase 1 initial repolarization of the action potential and facilitating outward K^+ movement. Membrane depolarization also activates L-type voltage-gated Ca^{2+} channels, including $Ca_V1.2$, prompting excitation-contraction coupling in the heathy heart. During phase 2, Ca^{2+} entry through voltage activated Ca^{2+} channels balances K^+ efflux, resulting in a plateau in the action potential [5]. During phase 3 of the cardiac action potential, voltage- and Ca^{2+}-dependent inactivation of L-type voltage-gated Ca^{2+} channels occurs while K^+ channels remain open, ensuring a net flow of positive ions out of the cell and a repolarization of the cell. Several K^+ channels with distinguishing voltage-gating relationships as well as ionic pumps contribute to the repolarization and eventual resting potential of the cardiomyocyte during phase 4, resetting the process for the next depolarization [3].

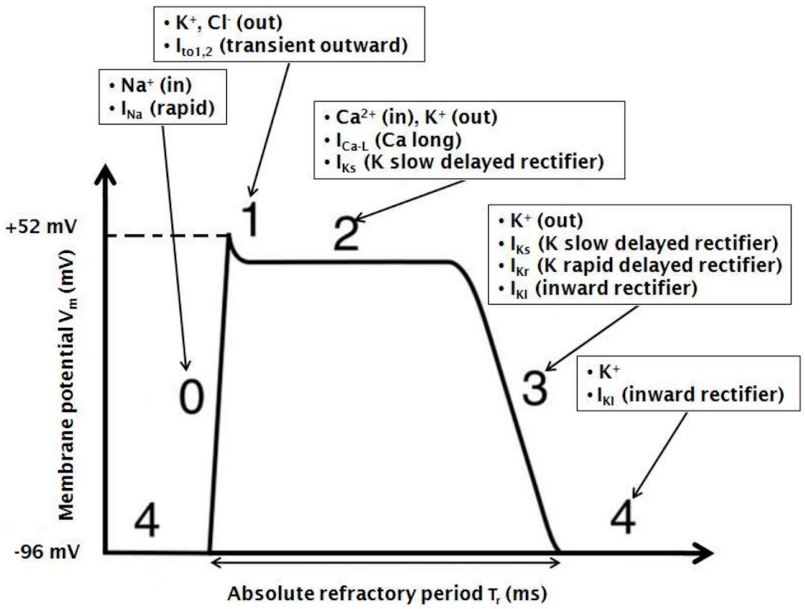

Figure 1. Ventricular action potential. Sequential openings of ion channels and subsequent movement of ions down their electrochemical gradients results in the characteristic ventricular action potential waveform. The ventricular action potential is divided into four phases based on the specific channels that are predominantly active. Figure taken from [6].

$Ca_V1.2$ Structure and Function

$Ca_V1.2$, encoded by *CACNA1C*, is an L-type Ca^{2+} channel (LTCC) that is comprised of a pore-forming α_{1C} subunit in complex with several auxiliary subunits including β, $\alpha_{2\delta}$, and γ [7, 8]. In the heart, α_{1C} consists of a 240kDa protein that is organized into four homologous domains (I–IV), each containing six transmembrane segments (S1–S6) and a pore-forming region between S5 and S6 [9]. The alternating positively charged arginine or lysine residues at every third or fourth position in the S4 segment of each domain regulate voltage sensitivity. The pore region contains the binding sites of L-type Ca^{2+} channel blocking agents including dihydropyridines, phenylalkylamines, and benzothiazepines [10]. There are four subfamilies of Ca_Vβs (β_1-β_4), each with splice variants, encoded by four distinct genes. The guanylate kinase (GK) domain and Src-homology 3 (SH3) domain are similar among the Ca_Vβs, whereas the N-termini, the linker between the SH3 and GK domains, and the C-termini are different [7]. All Ca_Vβs increase trafficking of α_{1C} to the plasma membrane and regulate voltage dependence of activation. β_2 is the predominantly expressed isoform in the adult murine heart [11]. A hydrophobic groove on the GK domain interacts with the α-interacting domain (AID) on the α_{1C} I-II linker [12, 13].

$Ca_V1.2$ is activated at voltages positive to -40 mV and Ca^{2+} current peaks at 0 to +10 mV. On a single-channel level, multiple modes of gating were described for $Ca_V1.2$. A null "mode 0" is used to describe a state of very rare opening upon depolarization. The term "mode 1" describes a mode of low probability and brief activation, while "mode 2" describes a high probability and longer-lasting activation [14]. β-adrenergic stimulation of $Ca_V1.2$ is postulated to shift the gating

mode from mode 0 to mode 1 and mode 2 by shifting a number of channels incapable of activation to activable and by increasing the probability of activation for activable channels [15]. After activation, $Ca_V1.2$ undergoes both voltage-dependent inactivation (VDI) as well as Ca^{2+}-dependent inactivation (CDI). VDI depends on the cytosolic ends of the S6 segments, the I-II linker, and the N- and C-termini of the α_{1C} subunit [16]. CDI occurs via calmodulin (CaM), which is constitutively bound to the IQ domain on the α_{1C} C-terminus [17]. Following LTCC activation, influx of Ca^{2+} and the subsequent increase in local Ca^{2+} concentration triggers C-terminal rearrangements that inhibit channel opening. Upon β-adrenergic stimulation, CDI has been suggested to dominate $Ca_V1.2$ kinetics over VDI as a result of increased Ca^{2+} influx leading to more CaM binding to Ca^{2+} [18, 19]. The same domain is required for Ca^{2+}-dependent facilitation in which Ca^{2+} current via $Ca_V1.2$ increases as a function of pacing frequency [17].

Mutations that confer gain/loss-of-function properties on $Ca_V1.2$ can result in a number of human diseases that have cardiac manifestations. Gain-of-function mutations in *CACNA1C* that increase Ca^{2+} influx that can counteract repolarization, resulting in prolongation of the action potential duration and QT interval prolongation. Classically, gain-of-function mutations in *CACNA1C* have been associated with Timothy syndrome where syndactyly, cardiac arrhythmia, congenital heart disease, and neurological dysfunction are observed [20, 21]. Slowed voltage-dependent inactivation and calcium-dependent inactivation of $Ca_V1.2$ is the predicted basis of Timothy syndrome phenotypes [22]. Loss-of-function mutations in the $Ca_V\alpha_1$, $Ca_V\beta$, and $Ca_V\alpha_2\delta$ subunits can also cause Brugada syndrome [23].

Excitation-Contraction (E-C) Coupling

The initiation of the systolic Ca^{2+} transient and subsequent contraction of cardiomyocytes is dependent on subcellular structures called dyads [24]. Here the sarcoplasmic reticulum (SR) is in very close contact with the T-tubule membrane so that the ryanodine receptor (RyR2) on the SR is directly adjacent to $Ca_V1.2$ on the T-tubule [25, 26]. After $Ca_V1.2$ is activated by depolarization, Ca^{2+} current passes through the channel and binds and activates RyR2s [27]. RyR2 acts both as a Ca^{2+} sensor and a Ca^{2+} channel, releasing stored Ca^{2+} from the SR and amplifying the relatively small Ca^{2+} signal from $Ca_V1.2$ in a process termed Ca^{2+}-induced Ca^{2+} release (CICR). [28]. Increased intracellular Ca^{2+} binds to troponin on the actin thin filaments and induces a conformational change that allows the heads of the myosin thick filament to bind to the actin forming crossbridges [29]. Myosin uses the energy stored as adenosine triphosphate (ATP) to tilt the myosin head, pulling on the actin filament to create sarcomere shortening and cellular contraction. For relaxation to occur, intracellular Ca^{2+} is removed from the cytosol mainly by the SR Ca^{2+}–ATPase (SERCA), which pumps Ca^{2+} back into the SR, and the sarcolemmal Na^+/Ca^{2+} exchanger (NCX), which extrudes Ca^{2+} from the cell [30]. When cytosolic Ca^{2+} concentration decreases, troponin changes back to its original shape, blocking the binding sites on actin and preventing crossbridge formation.

Adrenergic Regulation of the Heart

The body's sympathetic nervous system regulates the fight-or-flight response that occurs in response to an acute stress event. The sympathetic nervous system is responsible for readying the body for action during a perceived harmful event and regulates cardiac function to meet the amplified needs of the body [31]. Sympathetic neurohormonal control of cardiac function is

exerted by adrenaline and norepinephrine, which is synthesized and released into the bloodstream from the adrenal medulla and sympathetic nerve endings [27, 32]. Adrenaline and norepinephrine bind to β-adrenergic G protein-coupled receptors on the membrane of cardiomyocytes and other cell types. The ensuing activation of adenylyl cyclase by the G-protein $G_S\alpha$ catalyzes the conversion of cytosolic ATP to cyclic adenosine monophosphate (cAMP). cAMP binds to heterotetramer protein kinase A (PKA), resulting in the dissociation of the regulatory subunits from the catalytic subunits of PKA, readying the enzyme for phosphorylation of target proteins [33].

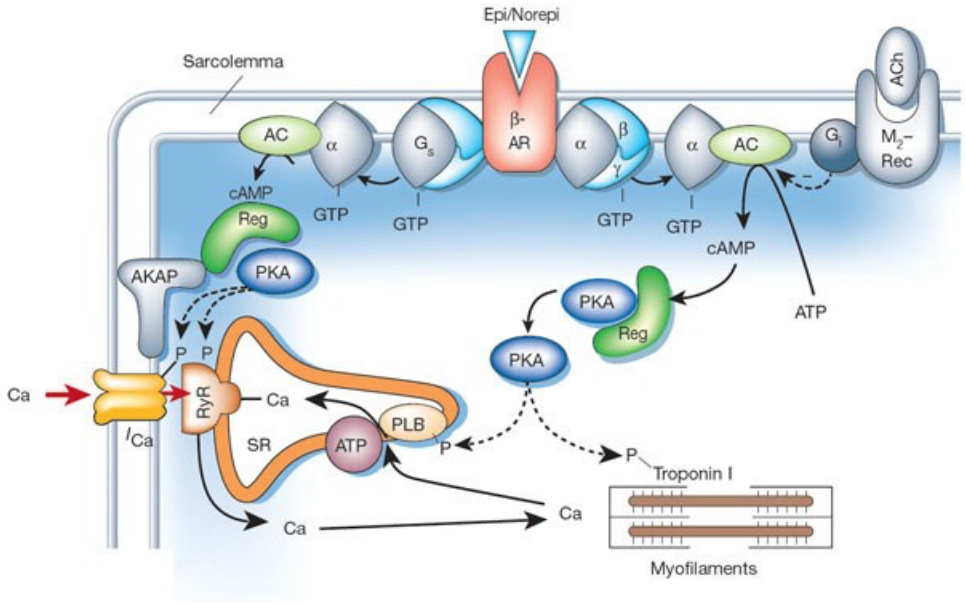

Figure 2: β-Adrenergic receptor activation and phosphorylation targets relevant to excitation–contraction coupling. AC, adenylyl cyclase; ACh, acetylcholine; AKAP, A kinase anchoring protein; β-AR, β-adrenergic receptor; M_2-Rec, M_2-muscarinic receptor; PLB, phospholamban; Reg, PKA regulatory subunit; SR, sarcoplasmic reticulum. Figure taken from [27].

In ventricular myocytes, PKA activation leads to the phosphorylation of a number of proteins involved in E-C coupling to increase chronotropy (heart rate), inotropy (strength of contraction) and lusitropy (extent of relaxation) [27]. The increase in inotropy is critically dependent on the amplitude and kinetics of the Ca^{2+} signal generated by $Ca_V1.2$ channels. A

PKA-dependent increase in $Ca_V1.2$ activity and availability is observed after activation of the β-adrenergic signaling pathway, although it is unclear which members of the $Ca_V1.2$ macromolecular complex are the phosphorylated targets [34]. Prominent candidates for the PKA phosphorylation targets that mediate upregulation of $Ca_V1.2$ include the α_{1C} and β_2 subunits, forming the basis for the investigations conducted in Chapter 1 of this thesis. Another target of PKA phosphorylation is phospholamban (Plb), which is a partial inhibitor of SERCA [35]. Plb dissociates from SERCA after phosphorylation, relieving its inhibition of SERCA and accelerating SR Ca^{2+} refilling during diastole. Troponin is also phosphorylated, decreasing the Ca^{2+} affinity of myofilaments and accelerating cross-bridge detachment [36]. These events result in larger and faster Ca^{2+} off rate transients, which increases contractile force and accelerates relaxation. PKA also phosphorylates RyR2, but the physiological role of this is controversial and beyond the scope of this thesis [37-39].

$Na_V1.5$ Structure and Function

$Na_V1.5$, encoded by *SCN5A*, is the primary cardiac isoform of the voltage-gated Na^+ channel responsible for phase 0 of the ventricular action potential [40]. $Na_V1.5$ consists of a pore-forming ~220kDa α subunit in complex with one or two auxiliary ~33kDa β-subunits and modulatory proteins that are part of the larger $Na_V1.5$ macromolecular complex [41]. The α-subunit is comprised of four homologous domains (I–IV), each containing six transmembrane segments (S1–S6) and a pore-forming region between S5 and S6 [42, 43]. Voltage-gated activation of $Na_V1.5$ is dependent on movement of the S4 segment, which contains positively-charged amino acids at every third position and serves a voltage-sensing function [4]. In the closed state, the negative membrane potential of -70 mV to -90 mV pulls the charges inward by

electrostatic force [44, 45]. Activation of the Na^+ channels in response to membrane depolarization derives from outward movement and rotation of S4, initiating a confirmational change that opens the channel pore [46]. Movement of the four S4 segments results in conformational changes within the channel that culminate in S6 segments moving to open the pore, allowing $Na_V1.5$ to transition to an open state in which Na^+ ions can diffuse down their electrochemical gradient. [47].

After 1-2 milliseconds, Na^+ channels conform into a non-conducting inactivated state through a process termed "fast inactivation". This occurs via an inactivation gate formed by the intracellular loop between domains III and IV that binds to and blocks the intracellular side of the pore, terminating Na^+ influx through $Na_V1.5$ [41]. Mutagenesis studies have revealed a three-residue hydrophobic IFM (isoleucine, phenylalanine, methionine) motif in III–IV linker that interacts with a hydrophobic pocket between domains III and IV [48, 49]. Disruption of this mechanism through intracellular perfusion of proteases prevents fast inactivation [50]. Additionally, mutations in the Na^+ channel C-terminus have been shown to impair inactivation, leading to the hypothesis that this region participates in the fast inactivation process [51, 52]. The relationship between the III-IV linker and the C-terminus is not clear, but both of these domains are required for complete inactivation [53]. The C-terminal domain interacts with CaM as well as FGF13, suggesting that these proteins may play a role in the interaction between the channel's C-terminus and III-IV linker region [54, 55]. In addition to fast inactivation, a separate "slow inactivation" process occurs on the time scale of hundreds of milliseconds [56]. The molecular mechanism of slow inactivation is not as defined as fast inactivation, but structure–function studies implicate conformational changes in the selectivity filter [57, 58]

Late Na^+ Current

Na^+ channel "peak current" represents the maximum inward Na^+ current in response to a depolarizing stimulus during phase 0 of the cardiac action potential, after which the majority transition to an inactivated, nonconducting state. However, some Na^+ channels either do not inactivate or inactivate and reopen, generating a sustained late Na^+ current ($I_{Na,L}$) [59]. $I_{Na,L}$ persists after phase 0 into phases 1 and 2 where it can lead to prolongation of the plateau phase, delayed repolarization, and prolongation of the QT-interval on the ECG [60]. Prolongation of the QT interval due to increased $I_{Na,L}$ is called long QT syndrome 3 (LQTS3) [3]. Although $I_{Na,L}$ represents less than 1% of the peak current [61], it has been shown to account for the LQT3 phenotype in computational and genetically altered mouse models [62, 63]. Failure of Na^+ channel inactivation during phase 2 or 3 of the cardiac action potential predisposes patients to asynchronous early afterdepolarizations (EADs), which result from reactivation of L-type Ca^{2+} channels and lead to premature action potentials [64, 65]. $I_{Na,L}$ is also linked to delayed afterdepolarizations (DADs) resulting from spontaneous Ca^{2+} release from the SR and subsequent increase in depolarizing currents via the NCX [66].

Even amongst LQT3 patients, heterogeneity in rate-dependence has been observed, and investigations have revealed divergent mechanisms of $I_{Na,L}$ generation. Multi-modal composition of Na^+ current is separated into three distinct gating modalities: transient (peak current), bursts, and late scattered openings [67]. Channel bursting describes a mode of gating characterized by persistent long-lasting channel openings [61]. This mode has been studied using the ΔKPQ (1505-1507del) deletion in the intracellular III-IV loop and, in heterologous expression systems,

modal transitions of $I_{Na,L}$ from ΔKPQ channels is an inversely dependent on slower pacing frequencies [68]. Indeed, LQT3 patients with the ΔKPQ are at higher risk for arrhythmias at rest [69, 70]. Late scattered openings are individual openings that are shorter-lasting than burst openings. Computational modeling of the S1904L mutation on the C-terminal region provided evidence that channel reopening arises due to a deficiency in slow inactivation, keeping channels in fast inactivated states from which they can reopen [52]. The multi-modal composition of the $I_{Na,L}$ may allow for pharmacological targeting of specific gating mode specific modulation.

Disruption of several $Na_V1.5$-interacting proteins have been reported to have a functional effect on $I_{Na,L}$. CaM binds to the IQ region on the $Na_V1.5$ C-terminal domain and, although effects of CaM on steady-state inactivation have been debated [54, 71], investigation on mutations in the IQ region on the C-terminus have shown an increase in $I_{Na,L}$ in heterologous expression systems [72, 73]. Likewise, mutations that affect the binding of FGF13 to the $Na_V1.5$ C-terminus increase $I_{Na,L}$, leading to arrhythmias [74]. Recently, evidence was reported supporting the hypothesis that CaM and FGF13 limit $I_{Na,L}$ by stabilizing an interaction between the channel's CTD and III-IV linker region [75]. In HEK293 cells, mutations in α-syntrophin caused ~1.5-fold increase in peak Na^+ current and ~2.5-fold increase in $I_{Na,L}$ [76]. Mutants of caveolin-3, which is a member of the dystrophin-glycoprotein complex along with α-syntrophin, were found in long-QT syndrome patients and showed an increase $I_{Na,L}$ [77, 78]. Finally, enzymatic regulation of $I_{Na,L}$ was described in results showing increased $I_{Na,L}$ after PKA phosphorylation of $Na_V1.5$ channels with a long QT-associated mutation in the C-terminus [79]. These results exemplify the complex network of $I_{Na,L}$ modulatory factors and underscore the

importance of elucidating their mechanisms in native cardiomyocytes where all regulatory components are expressed.

Considerable efforts are currently being made in the generation of drugs that selectively target $I_{Na,L}$ over peak Na^+ current. In the late 1980's, results of the CAST trial, whose goal was to assess the antiarrhythmic efficacy of Na^+ channel blockers, showed that Na^+ channel blockers increased mortality compared to placebo [80, 81]. This led to wide therapeutic discontinuation of use due, in part, to the inability of many Na^+ channel blockers to discriminate between peak Na^+ current and $I_{Na,L}$. Several drugs such as flecainide and lidocaine have demonstrated clinical usefulness, but only display a 2.9 to 5-fold and 2.7-fold selectivity for $I_{Na,L}$ compared to peak Na^+ current, respectively [82]. Ranolazine, on the other hand, displays a 9 to 38-fold selectivity for $I_{Na,L}$ and may prove beneficial for LQT3 patients in reducing action potential duration prolongation and suppressing the development of EADs [83].

$Na_V1.5$ Macromolecular Complexes

$Na_V1.5$ interacts with several proteins that have been shown to modulate Na^+ current density, activation and inactivation kinetics, and $I_{Na,L}$ [84]. Association of these proteins with $Na_V1.5$ is required for normal physiological function of $Na_V1.5$. Interestingly, many of the interacting proteins are specifically localized to subcellular regions of the cardiomyocytes, namely the intercalated disc and the lateral membrane. This has led to the hypothesis that two or more separate "pools" of $Na_V1.5$ macromolecular complexes exist in the cardiomyocyte with distinct functions [85].

The intercalated disc is a highly orchestrated cellular domain where several multicomponent complexes facilitate intercellular communication and cell excitability [86]. It is traditionally divided into three major complexes: gap junctions, desmosomes, and adherens junctions. Gap junctions, composed principally of connexin-43, connects the cytoplasm of adjacent cardiomyocytes to provide a pathway for passage of ions and small molecules between cardiomyocytes [87, 88]. Desmosomes and adherens junctions provide mechanical coupling between two cells by anchoring the actin cytoskeleton and intermediate filaments, respectively, to enhance the strength and stability of the myocardium [89, 90]. Although initial classification divided the different intercalated disc structures, recent studies have demonstrated interplay between complexes [91-93]. The additional integration of $Na_V1.5$ into complexes at the intercalated disc has been suggested through studies that show modulation of $Na_V1.5$ expression or function by ankyrin-G [94, 95], plakophilin-2 [96, 97], desmoglein-2 [98], desmoplakin [99], and connexin-43 [100, 101], although many of these studies do not demonstrate direct interaction. Taken together, these results support the idea of the molecular interaction network at the intercalated disc as a single functional unit to control the cardiac excitability, electric coupling, and intercellular adhesion.

The second pool of $Na_V1.5$ channels has been described outside the intercalated disc domain at the lateral membrane and the T-tubules [102]. $Na_V1.5$ expression at the lateral membrane is influenced by the dystrophin-glycoprotein complex (DGC) and the PDZ-binding motif of $Na_V1.5$ comprising its last three C-terminal amino acids Ser, Ile, and Val (SIV motif). Syntrophin, containing a PDZ domain, acts as an adaptor protein between the SIV motif of $Na_V1.5$ and dystrophin, and the stability of $Na_V1.5$ at the lateral membrane has been shown to

depend on this interaction [103, 104]. Recently, investigations using mice expressing $Na_V1.5$ lacking the SIV motif (ΔSIV) and syntrophin knockdown mice showed a reduction, but not abolition, of $Na_V1.5$ at the lateral membrane [105]. This indicates the presence of a subpopulation of $Na_V1.5$ at the lateral membrane whose expression is independent of DGC expression, a hypothesis that has been supported by single-molecule localization microscopy in dystrophin-deficient *Dmd*^{mdx} mice [106].

The reason for the different pools of $Na_V1.5$ at the lateral membrane and intercalated disc continues to be a subject of investigation. Macropatch cell-attached patch clamp methodology has been employed to show that the Na^+ current recorded in the lateral membrane of cardiac myocytes is of smaller amplitude than the current recorded at the intercalated disc [107, 108]. Steady-state inactivation was left-shifted in Na^+ recordings at the intercalated disc, suggesting that Na^+ channels in this region may be primarily responsible for action potential upstroke of a ventricular myocyte. Optical measurements in in isolated Langendorff-perfused hearts from ΔSIV mice, where $Na_V1.5$ expression is specifically decreased from the lateral membrane, have shown that ventricular conduction velocity was preferentially decreased in the transversal direction, indicating a role for this subpopulation in anisotropy of ventricular conduction [104]. These results support the conclusion that region-specific interactions in $Na_V1.5$ macromolecular complexes confer different biophysical properties to $Na_V1.5$.

Proximity Proteomics and TMT Mass Spectrometry Analysis

Specialized biological processes and reactions are compartmentalized into subcellular regions and are exerted through protein-protein interactions. Protein functions often correlate

with their subcellular interactions with a multi-protein macromolecular complex. Identification of protein interactions in these complexes and their alterations after a perturbation— such as activation of a pathway or in a disease state— is essential for understanding mechanisms that underlie intricate cellular processes. Affinity purification of a protein of interest followed by identification of direct and indirect interactors by mass spectrometry has been a widely-used approach, but this can be challenging when recovering structures or molecules that are difficult to solubilize or easily dissociate after purification [109, 110]. Moreover, even when purification techniques are modified to preserve interactions, such as with the use of chemical cross-linkers, the number of false positive interactions can increase. Overall, an approach that can identify all proteins within spatially resolved and potentially weakly interacting multicomponent complexes is needed to characterize protein interaction networks.

Most recently, proximity labeling has emerged as a biochemical approach to bypass the requirement of maintaining protein-protein interactions after solubilization [111, 112]. This method involves expression of an enzyme that catalyzes the covalent transfer of biotin onto endogenous proteins that are within a restricted spatial distance from the enzyme. Fusing the enzyme to a protein of interest allows specific localization to a subcellular compartment and proximity labeling is initiated in intact cells and tissues where protein complexes are maintained. Once labeled, the integrity of interactions does not need to be maintained and the biotinylated proteins can then be processed using strict lysis and washing steps followed by purification using streptavidin. Streptavidin-purified proteins are subsequently identified and quantified by mass spectrometry. Two classes of enzymes have been developed for proximity labeling: biotin protein ligases such as BioID [112] and TurboID [113], and peroxidases such as APEX2 [114].

While biotin ligases are useful in their ease of use, the speed of labeling using APEX2 presents an advantage when investigating dynamic processes. For example, APEX2 fusion to G-protein coupled receptors allowed parallel time-resolved quantitative analysis of thousands of protein-protein integrations, revealing insights on proteins involved in activation and internalization of these receptors [115].

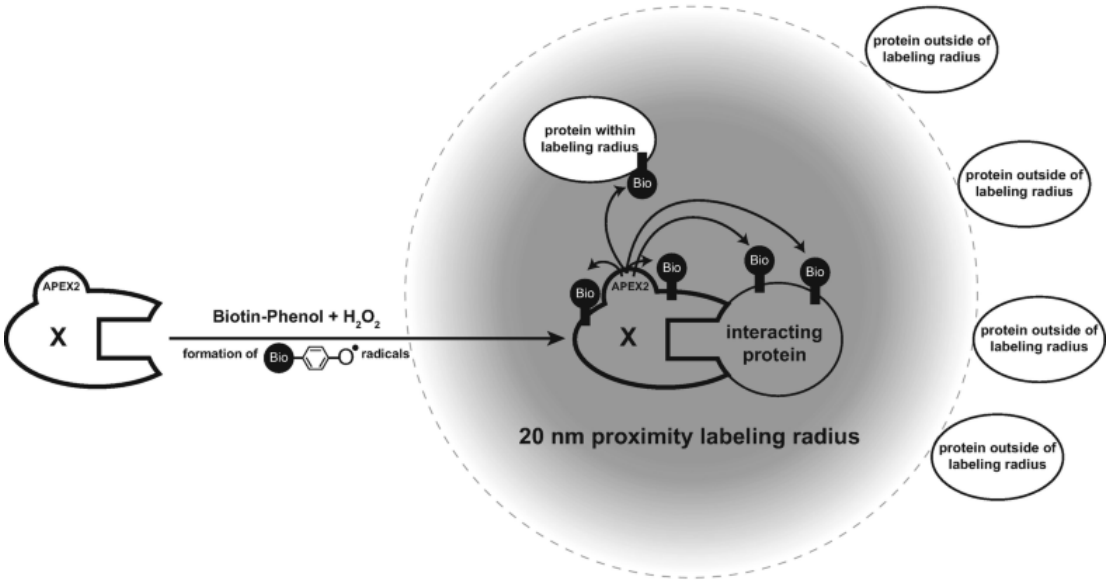

Figure 3. Illustration of peroxidase-catalyzed proximity labeling (APEX). A protein of interest (X) is expressed as a fusion protein with an engineered version of a plant ascorbate peroxidase (APEX2). In the presence of biotin-tyramide (biotin-phenol) and hydrogen peroxide (H_2O_2), free radicals of biotin-tyramide are formed. They react with surface-exposed tyrosine residues of interacting or neighboring proteins within the labeling radius and form covalent biotin adducts ("Bio," black). Labeling occurs within a radius of about 20 nm around the APEX2 module. Proteins outside of the labeling radius are not conjugated to biotin-tyramide. Adapted from [116].

Mass spectrometry can detect and quantify thousands of proteins from a sample of proteins and is a powerful tool when coupled with proximity labeling techniques. In particular, multiplexed proteomics using tandem mass tag (TMT) labeling allows robust analysis of several samples representing various conditions or replicates at the same time by tagging proteins from a sample with unique isobaric tags [117]. Some past proximity labeling studies have relied on label-free quantification, which is based on running multiple samples subsequently and usually

uses MS1 signal quantification [118, 119]. The requirement for multiple runs, therefore, can reduce throughput and introduce variation in results. TMT labeling on the other hand allows all tagged samples to be pooled and analyzed in a single mass spectrometry experiment so that relative abundances of thousands of proteins from up to 16 different samples are measured in a highly reproducible manner. Furthermore, quantification by SPS MS^3 rather than applying conventional tandem mass spectrometry (MS^2) has the advantage of reducing signal ratio distortion and improving the accuracy of peptide quantification [120]. To be sure, proximity proteomics coupled with TMT labeling and SPS MS^3 is an approach that is well-equipped to rigorously quantify changes in macromolecular complexes between multiple conditions.

Duchenne Muscular Dystrophy

Duchenne muscular dystrophy (DMD) is an X-linked recessive disorder caused by a loss-of-function mutation in the dystrophin gene [121]. Dystrophin is part of the large multimeric dystrophin-glycoprotein complex (DGC). The DGC is located in the sarcolemma and acts as a mechanical link between the actin cytoskeleton, the muscle membrane, and the extracellular matrix. Disruption of this complex leads to membrane fragility, making muscle cells susceptible to contraction-induced damage. As the disease progresses, regenerative processes are not able to compensate for the ongoing muscle damage, leading to progressive degeneration of myocytes and formation of fibrosis, resulting in muscle weakness [122]. DMD manifests as proximal weakness in the leg, shoulder, and pelvic girdle muscles and symptoms associated with cardiac defects can be masked by progressive muscle weakness and reduced physical activity. Cardiac involvement is evident after about 10 years of age and ubiquitous by 18 [123, 124]. Electrocardiographic abnormalities are first manifested, followed by progressive fibrosis

throughout the ventricular wall, a loss of contractility, and heart failure. With life expectancy estimated at about 25 years of age, the most common direct cause of death DMD is respiratory failure with the next leading cause of death being cardiac-related conditions such as heart failure brought on by dilated cardiomyopathy [125].

The *Dmd*^{mdx} mouse model, which has a total loss of functional dystrophin from the muscle tissue, has been used for decades for the majority of DMD research [126]. Ventricular cardiomyocytes isolated from *Dmd*^{mdx} mice exhibit a number of characteristics that reveal insights on the clinical phenotype of DMD patients. These include a fragile plasma membrane [127, 128], a disorganized microtubule cytoskeleton [129-131], impaired Ca^{2+} handling [132, 133], and a shift toward a more oxidative intracellular and mitochondrial redox state [134, 135]. The precise mechanisms leading to increased cell death and fibrosis are unclear, but augmented Ca^{2+} influx from membrane tears and stretch-activated channels are hypothesized to contribute to excessive mitochondrial Ca^{2+} uptake as well as increased Ca^{2+}-sensitive PKC phosphorylation of NAD(P)H oxidase [136, 137]. These events lead to abnormally high intracellular levels of reactive oxygen species and initiate necrotic and apoptotic processes that culminate in cell death and the development of cardiac fibrosis. Additionally, in *Dmd*^{mdx} mouse models it has been shown that loss of dystrophin leads to a decrease in Na^+ current, which is a known risk factor for arrhythmias and sudden cardiac death [102, 103]. It is currently unclear whether this disfunction is due to loss or redistribution of $Na_V1.5$ channels, or from changes in the $Na_V1.5$ macromolecular complex. Indeed, a combination of loss of Na^+ current and myocardial fibrosis may result in a markedly disturbed cardiac conduction and greatly increase the risk for potentially lethal arrhythmias in DMD patients.

Dissertation Outline

There are three primary components to my dissertation. My first aim is to determine whether PKA phosphorylation of $Ca_V1.2$ α_{1C} and β_2 subunits is required for β-adrenergic regulation of $Ca_V1.2$ in heart. Prior studies have indicated that conserved PKA phosphorylation sites on α_{1C} and several sites on β_2 are not necessary for regulation. This led to several hypotheses including that redundant regulation sites exist between subunits or that α_{1C} and β_2 subunits are not the functional phosphorylation target. To test this, we generated two doxycycline-inducible transgenic mice, one expressing α_{1C} with mutations at 35 intracellular predicted PKA phosphorylation sites and one expressing β_2 with mutations at 28 predicted PKA phosphorylation sites. We then cross these two mice to generate offspring that express both mutant subunits. We investigate the integrity of β-adrenergic regulation of $Ca_V1.2$ in all these models to provide the definitive answer about whether PKA phosphorylation of any α_{1C} or β_2 residues is necessary.

In my second aim, I focus on the effects of two auxiliary proteins—CaM and FGF13—on the function of $Na_V1.5$ expressed in cardiomyocytes. I hypothesized that, as in HEK cells, loss of CaM binding to voltage-gated Na^+ channels in cardiac cells will lead to increased $I_{Na,L}$. Transgenic mice were generated with inducible expression of IQ/AA $Na_V1.5$, a Na^+ channel harboring two mutated residues in the known CaM binding site. We found that IQ/AA did not increase Na^+ late current, indicating that endogenous protective mechanisms exist in cardiomyocytes that may be absent in HEK cells. Finally, we coexpressed the IQ/AA mutant $Na_V1.5$ with FGF13 in HEK cells to assess the ability of FGF13 to rescue the increased $I_{Na,L}$ phenotype.

My third aim is to identify alterations in the early stages of DMD, in which the absence of dystrophin predisposes affected individuals to arrhythmias and cardiac dysfunction. Here I posit that loss of dystrophin alters the macromolecular complexes of $Na_V1.5$ channels leading to changes in its electrophysiological properties. To provide a comprehensive understanding of the $Na_V1.5$ macromolecular complexes, we utilized the proximity labeling method by APEX2 to identify the interactome of $Na_V1.5$ in cardiomyocytes. We compared changes in the $Na_V1.5$ interactome to changes in the entire dystrophin-deficient *Dmd*^{mdx} myocyte proteome in control and young *Dmd*^{mdx} mice hearts, with the goal of precisely defining how DMD modifies the $Na_V1.5$ interactome to predispose to heart failure and arrhythmias. Finally, we leveraged the neighborhood-specificity of proteins at the lateral membrane, intercalated disk, and T-tubules to probe the effects of dystrophin-deficiency on $Na_V1.5$ localization.

Materials and Methods

Mouse Models

All transgenic mice were generated through the CUMC Shared Research Facilities Transgenic Mouse core. Plasmids used for pronuclear DNA microinjection were created in the laboratory. V5-TurboID-$Na_V1.5$ knock-in mice were generated by Cyagen. Both male and female mice were used in all experiments. The number of mice was always greater than three per genotype.

pWT α_{1C}, GFP–WT-β_{2B}, 35-α mutant, 28-β mutant, and 35-α X 28-β

Transgenic constructs were generated by fusing rabbit α_{1C} cDNA or human β_{2B} cDNA to the modified murine α-myosin heavy chain (α-MHC) tetracycline-inducible-promoter vector. A 3× Flag epitope was ligated in-frame to the N terminus of α_{1C}. The α_{1C} subunit was engineered to be dihydropyridine (DHP)-insensitive with the substitutions T1066Y and Q1070M [138, 139]. GFP was ligated to the N terminus of β_{2B}. In the background of the the pWT α_{1C} and GFP–WT-β_{2B}, the 35-α mutant and the 28-β mutant cDNA were generated by site-directed mutagenesis. We replaced 51 residues in rabbit α_{1C} with alanine at 35 potential phospho-regulatory domains in the 35-mutant α_{1C} construct, and replaced 37 residues with alanine at 28 putative phospho-regulatory domains of β_{2B}. We excluded those sites that were predicted to be extracellular or within the plasma membrane. Transgenic mice with non-targeted insertion of these tetracycline-regulated cDNAs were bred with α-MHC, doxycycline-regulated, codon-optimized reverse transcriptional transactivator (rtTA) mice (obtained via the Mutant Mouse Resource and Research Center) to generate double-transgenic mice.

pWT $Na_V1.5$, IQ/AA, F1759A, V5-APEX2-$Na_V1.5$, and V5-APEX2-$Na_V1.5$-Dmd^{mdx}

The pWT, IQ/AA, F1759A, and V5-APEX2-$Na_V1.5$ lines were generated by fusing human heart Na^+ channel α-subunit cDNA (hH1) to the modified murine α-MHC tetracycline-inducible-promoter vector. *SCN5A* was engineered to be either TTX sensitive by inserting a C374Y mutation or lidocaine-resistant by insertion a F1759A mutation. For IQ/AA mice, Ala/Ala was substituted at position IQ1908-1909. A 3× FLAG epitope was ligated in-frame to the N-terminus. The V5 epitope and APEX2 cDNA, created by gene synthesis, were conjugated to the N-terminus of human heart Na^+ channel α-subunit. These mice, in a B6CBA/F2 hybrid background, were bred with cardiac-specific rtTA mice in a FVB/N background, obtained via Mutant Mouse Resource & Research Center, to generate doxycycline-inducible transgenic mice. To create V5-APEX2-$Na_V1.5$-Dmd^{mdx} mice, the V5-APEX2-$Na_V1.5$ double transgenic mice were crossed with female Dmd^{mdx} mice (Jackson Laboratories, Stock 001801). Male mice were used in all V5-APEX2-$Na_V1.5$-Dmd^{mdx} experiments since dystrophin is X-linked.

V5-TurboID-$Na_V1.5$

The V5-TurboID-$Na_V1.5$ knock-in model was generated by Cyagen. The "Kozak-MG-HA tag-G-HA tag-G-HA tag-TurboID-V5 tag" (V5-TurboID) was created by gene synthesis and inserted upstream of the ATG start codon, which is in 2 of the Scn5a gene located on mouse chromosome 9. The targeting vector included homology arms generated by PCR using BAC clone RP23-386N9 or RP23-198L19 with V5-TruboID and a Neo cassette flanked by SDA (self-deletion anchor) sites. DTA was used for negative selection. The targeting construct was electroporated into ES cells. Positive clones were identified by PCR and confirmed by Southern

blotting. Five clones were injected in C57BL/6N blastocysts, and chimeras were crossed to C57BL/6 mice. Heterozygous mice were bred to produce homozygous offspring.

Biochemistry/Molecular Biology

Isolation of adult cardiac myocytes

Mice ventricular myocytes were isolated by enzymatic digestion using a Langendorff perfusion apparatus as described [140]. Cardiomyocytes were isolated from 8–12-week-old non-transgenic and transgenic mice. Only non-contracting rod-shaped cells with clear striations were used for electrophysiology studies.

Proximity labeling biotinylation

Isolated ventricular cardiomyocytes were incubated in labelling solution with 0.5 mM biotin-phenol (Iris-biotech) for 30 min. For some experiments, during the final 10 min of incubation, 1 μM isoproterenol (Sigma I5627) was added. To initiate labelling, H_2O_2 (Sigma H1009) was added to a final concentration of 1 mM for 1 min. Exactly 1 min after H_2O_2 treatment, the cells were washed three times with cold quenching solution containing 10 mM sodium ascorbate (VWR 95035-692), 5 mM Trolox (Sigma 238813) and 10 mM sodium azide (Sigma S2002). After cells were harvested by centrifugation, the quenching solution was aspirated, and the pellet was flash-frozen and stored at –80 °C until streptavidin pull-down. The cells were lysed with a hand-held tip homogenizer in a solution containing 50 mM Tris (tris(hydroxymethyl)aminomethane), 150 mM NaCl, 10 mM EGTA, 10 mM EDTA, 1% Triton X-100 (v/v), 0.1% SDS (w/v), 10 mM sodium ascorbate, 5 mM Trolox and 10 mM sodium azide, phosphatase inhibitors (Sigma 4906845001), protease inhibitors (Sigma 4693159001),

calpain inhibitor I (Sigma A6185) and calpain inhibitor II (Sigma A6060). Biotin labelling of the samples was confirmed after size fractionation of proteins on SDS–polyacrylamide gel electrophoresis (PAGE), transfer to nitrocellulose membranes, and probing with streptavidin-conjugated horseradish peroxidase (HRP) (Thermofisher, S911, lot number 1711896, 0.6 mg ml^{-1}). The response to isoproterenol was assessed by immunoblotting with an anti-phospho-Pln (Ser16/Thr17) antibody (Cell Signaling, number 8496, lot number 1; 1/1,000 dilution). Biotinylated proteins were bound to streptavidin magnetic beads (Thermo Fisher Scientific 88817), and the beads were washed three times with a solution containing 4 M urea, 0.5% SDS (w/v) and 100 mM sodium phosphate pH 8. Proteins were size-separated on SDS–PAGE, transferred to nitrocellulose membranes, and probed with anti-V5 antibody (Thermofisher, R960-25; 1/5,000 dilution), a custom-made anti-FGF13 antibody, and an anti-CaM antibody (Millipore Sigma, 05-173).

Immunoprecipitations

Cardiomyocytes were lysed with a hand-held tip homogenizer in a 1% (v/v) Triton X-100 buffer containing 50 mM Tris-HCl (pH 7.4) 150 mM NaCl, 10 mM EDTA, 10 mM EGTA and 0.01 mM calpain inhibitor I, 0.01 mM calpain inhibitor II, and complete protease inhibitors (1 per 7 ml, Roche). The lysates were incubated on ice for 30 min and centrifuged at 14,000 r.p.m at 4 °C for 10 min; supernatants were then collected. Anti-Flag antibody (Sigma, F7425, lot number 078M4886V) immunoprecipitations were performed overnight in a lysis buffer consisting of 50 mM Tris-HCl pH 7.4, 150 mM NaCl, 0.25%-1% Triton X-100 (v/v), 10 mM EDTA, 10 mM EGTA, 0.01 mM calpain inhibitor I, 0.01 mM calpain inhibitor II, and complete protease inhibitors (1 per 7 ml). Antibody–protein complexes were collected using protein-A-

conjugated agarose (Amersham) for 2 h, followed by three washes in lysis buffer. Proteins were size-separated by SDS, transferred to nitrocellulose membranes and probed with HRP-conjugated anti-Flag antibody (Sigma, A8592), a custom-made anti-β-antibody and HRP-conjugated secondary goat anti-rabbit antibody. Detection of luminescence was performed with a charge-coupled-device (CCD) camera (Carestream Imaging).

Immunofluorescence

Isolated cardiomyocytes from V5-APEX2-$Na_V1.5$ were first exposed to biotin-phenol and H_2O_2 as described above. After quenching, the cells were fixed for 15 min in 4% paraformaldehyde, washed with glycine/phosphate-buffered saline (PBS) twice, treated with 0.1% Triton X-100 (v/v) in PBS (PBST) for 5 min, and blocked with 3% bovine serum albumin (BSA; w/v) in PBS for 1 h. Indirect immunofluorescence was performed using 1/500 dilutions of anti-V5 antibody (Thermo Fisher, R960-25), 1/200 dilutions of Alexa594-labelled goat anti-mouse antibody (Thermo Fisher, A11032, lot 2069816) and 1/800 dilutions of streptavidin–Alexa Fluor 488 conjugate (Thermo Fisher, S32354, lot 1719656). Images were acquired using a confocal microscope.

Processing biotinylated proteins for mass spectromentry

Proteins were precipitated with trichloroacetic acid (TCA; MilliporeSigma, T9159) and then centrifuged at 21,130*g* at 4°C for 10 minutes. The pellet was washed with –20°C cold acetone (MilliporeSigma, 650501), vortexed, and centrifuged at 21,130*g* at 4°C for 10 minutes. Following centrifugation, acetone was aspirated and the pellet was acetone washed again 3 more times. After the last washing step, the pellet was resuspended in: 8M urea, 100 mM sodium

phosphate (pH 8), 100 mM NH_4HCO_3, and 1% SDS (w/v) and was rotated at room temperature until fully dissolved. Resuspended proteins were centrifuged at 21,130*g* at room temperature for 10 minutes, and the cleared supernatant was transferred to a new microcentrifuge tube. To reduce disulfides, 10 mM TCEP-HCl (Thermo Fisher Scientific, PG82089) in Milli-Q water titrated to pH 7.5 with NaOH was added. To alkylate free Cys, freshly prepared 400 mM iodoacetamide (Thermo Fisher Scientific, 90034) stock solution in 50 mM ammonium bicarbonate was added to the supernatant to a final concentration of 20 mM, immediately vortexed, and incubated in the dark for 25 minutes at room temperature. After alkylation, freshly prepared DTT (dithiothreitol) stock solution was added to 50 mM final concentration to quench alkylation. Water was added to each sample to reach a final concentration of 4 M urea and 0.5% (w/v) of SDS.

A 100 µl suspension equivalent per sample of streptavidin magnetic beads was washed twice with a solution containing 4 M urea, 0.5% SDS (w/v) and 100 mM sodium phosphate pH 8, and was added to each 1 mg of protein sample, diluting each sample with an equal amount of water to reach a final concentration of 2 M urea, 0.25% SDS (w/v), 50 mM sodium phosphate pH 8 during pull-down. The tubes were rotated overnight at 4 °C. Following streptavidin pull-down, the magnetic beads were washed three times with a solution containing 4 M urea, 0.5% SDS (w/v), 100 mM sodium phosphate pH 8, and three times with the same buffer without SDS. The beads were transferred to new tubes for the last wash step. Before final pulldown of the beads for mass-spectrometry analysis, streptavidin–HRP blotting was performed on 5% of the resuspended beads.

Quantitative real-time polymerase chain reaction (qRT-PCR)

PCR was performed using Applied Biosystems StepOne Plus PT-PCR system and inventoried following inventoried primers: human $Na_V1.5$ Hs00165693_m1; mouse $Na_V1.5$ Mm01342518_m1; mouse NaV1.6 Mm00488110_m1; mouse NaV1.8 Mm00501467_m1; mouse GAPDH Mm99999915_g1. PCR was performed, in triplicate, for 40 cycles with automated detection of crossing threshold.

Tandem Mass Tag Labeling and Mass Spectrometry Analysis

On-bead digestion and TMT labelling

On-bead digestion, TMT labeling, and mass spectrometry analysis were performed by Drs. Marian Kalocsay, Robyn Eisert, and Gary Bradshaw. Liquid reagents used were of high-performance liquid chromatography (HPLC) quality grade. Washed beads were resuspended in 50 µl of 200 mM 3-[4-(2-hydroxyethyl)-piperazin-1-yl]propane-1-sulfonic acid (EPPS) buffer pH 8.5, 2% acetonitrile (v/v) with 1 µl of LysC stock solution (2 mg ml^{-1}, Wako), vortexed briefly and incubated at 37 °C for 3 h. Then, 50 µl of trypsin stock (Promega V5111) diluted 1/100 (v/v) in 200 mM EPPS pH 8.5 was added. After mixing, digests were incubated at 37 °C overnight and beads were magnetically removed. Peptides were directly labelled after digest. For this, acetonitrile was added to a concentration of 30% (v/v) and peptides were labelled with TMT 10-plex or 11-plex reagents (Thermo Fisher Scientific 90406 and A34807) for 1 h. Reactions were quenched with hydroxylamine at a final concentration of 0.3% (v/v) for 15 min, and 1% of labelled peptides were analysed for efficiency of label incorporation and relative ratios by mass spectrometry. After quenching, peptide solutions were acidified with formic acid, trifluoroacetic acid (TFA) was added to a concentration of 0.1%, and peptides were desalted and fractionated by

high pH reversed phase chromatography (Thermo Fisher Scientific 84868). After loading of labelled peptides onto preconditioned columns and a single wash with water, excess unincorporated TMT label was removed by washing reversed phase columns once with 0.1% trimethylamine (TEA) buffer containing 5% acetonitrile. Samples were fractionated under alkaline conditions into 12 fractions with increasing concentrations of acetonitrile: 10%, 12.5%, 15%, 17.5%, 20%, 25%, 30%, 35%, 40%, 50%, 65% and 80%. Fractions 1 and 7, 2 and 8, 3 and 9, 4 and 10, 5 and 11, and 6 and 12 were pooled to obtain 6 final pooled fractions for subsequent analysis. Pooled fractions were dried to completion and further purified and desalted by acidic C_{18} solid phase extraction (StageTip). Labelled peptides were finally resuspended in 1% formic acid (v/v) and 3% acetonitrile (v/v).

Mass spectrometry analysis

Data collection followed a MultiNotch MS^3 TMT method using an Orbitrap Lumos mass spectrometer coupled to a Proxeon EASY-nLC 1200 liquid chromatography system (both Thermo Fisher Scientific). The capillary column used was packed with C_{18} resin (length 35 cm, inner diameter 75 μm, matrix 2.6 μm Accucore (Thermo Fisher Scientific)). Peptides of each fraction were separated for 4 h over acidic acetonitrile gradients by liquid chromatography before mass-spectrometry analysis. The scan sequence started with an MS^1 scan (Orbitrap analysis; resolution 120,000; mass range 400−1,400 Th). MS^2 analysis followed collision-induced dissociation (CID; CID energy = 35) with a maximum ion-injection time of 150–300 ms and an isolation window of 0.4 *m*/*z*. In order to obtain quantitative information, we fragmented MS^3 precursors by high-energy collision-induced dissociation (HCD) and analysed the fragments in the Orbitrap at a resolution of 50,000 at 200 Th.

Peptides were searched with a SEQUEST (v.28, rev. 12)-based software against a size-sorted forward and reverse database of the *Mus musculus* proteome (Uniprot 07/2014) with added common contaminant proteins. For this, spectra were first converted to mzXML. Searches were performed using a mass tolerance of 20 p.p.m. for precursors and a fragment-ion tolerance of 0.9 Da. For the searches, a maximum of two missed cleavages per peptide was allowed. We searched dynamically for oxidized methionine residues (+15.9949 Da) and, where indicated, for phospho-modification of serine, threonine and tyrosine residues (+79.9663 Da). We applied a target decoy database strategy and set a false discovery rate (FDR) of 1% for peptide–spectrum matches following filtering by linear discriminant analysis (LDA). The FDR for final collapsed proteins was 1%. We calibrated MS^1 data post-search and performed searches again. We used a modified version of the Ascore algorithm to quantify the confidence assignment of phosphorylation sites. Phosphorylation localized to particular residues required Ascore values of more than 13 ($P \leq 0.05$) for confident localization. Quantitative information on peptides was derived from MS^3 scans. Quant tables were generated requiring an MS^2 isolation specificity of more than 70% for each peptide and a sum of TMT signal-to-noise (s/n) ratios of more than 200 over all channels for any given peptide; the tables were exported to Excel and processed further therein. Details of the TMT intensity quantification method and further search parameters were described previously. Proteomics raw data and search results were deposited in the PRIDE archive and can be accessed under ProteomeXchange accession nunbers PXD014499, PXD014500 and PXD014501.

The relative summed TMT s/n ratios for proteins between two experimental conditions (referred to as ‘enriched’) were calculated from the sum of TMT s/n ratios for all peptides

quantified of a given protein. For enrichment of Gene Ontology (GO) terms, the BINGO package in Cytoscape was used. Scaled quantification data were subjected to two-way clustering (JMP software package) and changes in enrichment were analysed using Graphpad Prism 8 (Graphpad Software). Statistical significance was determined by multiple *t*-tests without correction for multiple comparisons and $\alpha = 0.05$.

Cellular Electrophysiology

Whole Cell Patch Clamp

Patch clamp experiments were performed by Dr. Alexander Katchman, Dr. Sergey Zakharov, and Daniel Roybal. Experiments were performed at room temperature. Membrane currents from non-contracting rod-shaped cells with clear striations were measured by the whole-cell patch-clamp method using a MultiClamp 700B amplifier or Axopath200B amplifier and pCLAMP 10.7 software. The pipette resistance was 1-3 MΩ for Ca^{2+} recordings and 0.4-1.0 MΩ for Na^{+} recordings. Capacitance transients and series resistance were compensated. Voltage was corrected for liquid junction potential (-10 mV) during analysis. Leak currents were subtracted by a P/4 protocol. The parameters of voltage-dependent activation were obtained using a modified Boltzmann distribution: $I(V) = G_{max} \times (V - E_{rev})/[1 + \exp(V - V_{50})/V_c)]$, where I(V) is the peak current, Gmax is the maximal conductance, E_{rev} is the reversal potential, V_{50} is the midpoint, and V_c is the slope factor.

For studies of Ca^{2+} recordings from pWT α_{1C}, 35-α mutant, 28-β mutant, and 35-α X 28-β cardiomyocytes, the pipette solution contained 40 mM CsCl, 80 mM cesium gluconate, 10 mM 1,2-bis(o-aminophenoxy)ethane-N,N,N′, N′-tetraacetic acid (BAPTA), 1 mM MgCl2, 4 mM Mg-

ATP, 2 mM $CaCl_2$ and 10 mM 4-(2-hydroxyethyl)-1-piperazineethanesulfonic acid (HEPES), adjusted to pH 7.2 with CsOH. After the isolated cardiomyocytes were dialyzed and adequately buffered with 10 mM BAPTA in the internal solution, cells were superfused with 140 mM tetraethylammonium chloride (TEA-Cl), 1.8 mM CaCl2, 1 mM MgCl2, 10 mM glucose and 10 mM HEPES, adjusted to pH 7.4 with CsOH. To measure peak currents, we held the cell membrane potential at −50 mV and stepped it to +0 mV for 350 ms every 10 s. To evaluate the current–voltage (I–V) relationship in cardiomyocytes, we repeated the same protocol with steps between −40 mV and +60 mV in 10-mV increments. Nisoldipine (Santa Cruz) was stored protected from light at −20 °C as 3 mM stock in ethanol. The final dilution of nisoldipine to 300 nM was in the extracellular recording solution immediately before the experiment. Isoproterenol (Sigma I5627) and forskolin (Santa Cruz) were prepared daily and diluted in extracellular solution.

For studies of Ca^{2+} recordings from transfected 35-α mutant, 28-β mutant, and Rad in HEK293T cells, we implemented the perforated whole-cell patch-clamp technique in order to minimize current run-down and preserve the intracellular milieu. Amphotericin B (Sigma A9528) was initially dissolved in DMSO (20 mg ml^{-1}) and used in the pipette solution at a final concentration of 200 μg ml^{-1}. The tip of the pipette was filled with amphotericin-free solution containing 80 mM caesium gluconate, 40 mM CsCl, 10 mM HEPES, 10 mM BAPTA, 1 mM MgCl2 and 1 mM Mg-ATP, pH adjusted to 7.2 with CsOH. The pipette was backfilled with 125 mM CsCl, 10 mM HEPES, 4 mM CaCl2, 1 mM MgCl2 pH 7.2 and CsOH containing amphotericin at 200 μg ml^{-1}. The external solution contained 130 mM tetraethylammonium methanesulfonate, 10 mM HEPES, 1 mM MgCl2, 10 mM (with Rad expression) or 2 mM

(without Rad expression) BaCl2, 5 mM glucose. For experiments with HEK293T cells, in addition to step protocols, we used a ramp protocol with a 200-ms voltage ramp from −60 mV to +60 mV (0.6 V s^{-1}) applied every 10 s to monitor the I–V relationship. Cells were selected on the basis of co-transfection of a vector containing GFP in the absence of Rad, or of a vector containing GFP-conjugated Rad.

For studies of pWT $Na_V1.5$, IQ/AA, F1759A, and V5-APEX2-$Na_V1.5$, the pipette solution contained 3 mM NaCl, 20 mM CsCl, 115 mM CsF, 10 mM HEPES, and 10 mM BAPTA (pH 7.4) titrated with CsOH. For measurement of peak Na^+ current, the extracellular solution contained 3 mM NaCl, 142 mM TEA-Cl, 10 mM HEPES, 1 mM MgCl2, 0.25 mM CaCl2, and 5 mM glucose (pH 7.4) titrated with CsOH. Peak transient currents in the F1759A mice were measured with 5 mM Na^+ in both intracellular and extracellular solutions (need to change int or ext sol to 3 or 5). Peak transient currents were measured by stepping the voltage from a holding potential of –110 mV to –30 mV. Peak transient currents for steady state activation were determined by stepping the voltage from a holding potential of–110mV to +5 mV in increments of 5 mV. For V5-APEX2-$Na_V1.5$ cardiomyocytes, steady-state inactivation was measured by stepping from a holding potential of-120 mV in increment of 5 mV to voltages from -110 mV to +5 mV for 100 ms, following step to -40 mV for 30 ms. For late current analysis of pWT $Na_V1.5$, IQ/AA, and F1759A cardiomyocytes, the bath solution contained 100 mM NaCl, 45 mM TEA-Cl, 10 mM HEPES, 1 mM MgCl2, 0.25 mM CaCl2, and 5 mM glucose (pH 7.4) titrated with CsOH. To determine late current, the cell membrane potential was held at –110 mM and stepped to –30 mV for 190 ms in the absence and in the presence of TTX (40 μM; nontransgenic and F1759A mice) or ranolazine (50 μM; pWT $Na_V1.5$ and IQ/AA mice). The

mean value of the current during the last 10 ms of the 190-ms pulse was measured. The difference of these values was used as a measure of late Na^+ current and later normalized to cell capacitance. The mean value of the late current was also normalized to the peak Na^+ current for each cell. For the cardiomyocytes isolated from F1759A mice, the fraction of transgenic current was assessed by applying 3 mM lidocaine. For these cardiomyocytes, the fraction of transgenic current was assessed by applying 20 nM TTX, which inhibits all mutant channels (IC_{50} < 1 nM) but has no effect on endogenous, nontransgenic channels. The current-voltage relationship of transgenic Na^+ currents for the pWT and IQ/AA cardiomyocytes were quantified as the difference between no TTX and 20 nM TTX across a range of voltages, from a holding potential of –110 mV to 0 mV.

Multichannel analysis of late Na^+ current

Multichannel analysis was performed by Drs. Nourdine Chakouri and Manu Ben-Johny. Multichannel records were obtained in the on-cell configuration with either HEK293 cells or in cardiomyocytes. The pipette contained (in mM): 140 NaCl, 10 HEPES, and 0.5 $CaCl_2$ at 300 mOsm adjusted with tetraethylammonium methanesulfonate, and pH 7.4 adjusted with tetraethylammonium hydroxide. To zero membrane potential, the bath contained (in mM): 132 K^+-glutamate, 5 KCl, 5 NaCl, 3 MgCl, 2 EGTA, 10 glucose, and 20 HEPES at 300 mOsm adjusted with glucose, and pH 7.4 adjusted with NaOH. Data were acquired at room temperature using the integrating mode of an Axopatch 200A amplifier (Axon Instruments, Molecular Devices). Patch pipettes (3–10 MΩ) were pulled from ultra-thick–walled borosilicate glass (BF200-116-10; Sutter Instruments) using horizontal puller (P-97, Sutter Instruments), fire polished with a microforge (Narishige), and coated with Sylgard (Dow Corning). Elementary

currents were low-pass filtered at 2 kHz with a 4-pole Bessel filter and digitized at 200 kHz with an ITC-18 unit (Instrutech), controlled by custom MATLAB software (Mathworks). For each pulse, we obtained P/8 leak pulses. Following leak subtraction, the unitary current for each patch was estimated using an amplitude histogram. Each stochastic trace was subsequently idealized. The ensemble average from 50 to 100 stochastic traces was computed for each patch and normalized to the peak current. The average late current for each patch ($R_{persist}$) was computed as the average normalized P_O following 50 ms of depolarization.

Chapter 1: Investigation of the Requirement of PKA Phosphorylation of $Ca_V\alpha$ and $Ca_V\beta$ for β-Adrenergic Regulation of $Ca_V1.2$

1.1 Introduction

In the heart, Ca^{2+} influx through $Ca_V1.2$ is an essential signal that initiates excitation-contraction (E-C) coupling, regulates cardiac excitability, and shapes the ventricular action potential [141, 142]. Physiologic β-adrenergic activation of PKA during the sympathetic "fight or flight" response increases Ca^{2+} influx through $Ca_V1.2$ in cardiomyocytes, leading to increased cardiac contractility [15] Although PKA activation is established as a fundamental process in the initiation of increased E-C coupling, the functional target phosphorylation site(s) that lead to $Ca_V1.2$ activation are unknown. My aim is to definitively determine whether phosphorylation of the pore-forming α_{1C} subunit and the accessory β_2 subunit are essential for β-adrenergic regulation of Ca^{2+} influx in the heart.

The long-standing dogma is that $Ca_V\alpha$ or $Ca_V\beta$ subunits are the functional PKA phosphorylation targets, although the data have been contradictory and controversial. Early reports suggested that Ser1928 on α_{1C} is the sole regulatory site [143, 144]. Studies in heterologous expression systems showed that Ala substitution of Ser1928 prevented upregulation of $Ca_V1.2$ [145] but, when this concept was tested in ventricular myocytes, it was shown that adrenergic regulation of $Ca_V1.2$ was unperturbed [146, 147]. After phosphorylation of Ser1928 was shown to be non-essential for β-adrenergic regulation of $Ca_V1.2$ in cardiomyocytes, phosphorylation of Ser1700 and Thr1704 was proposed [148, 149]. By generating transgenic mice expressing α_{1C} subunits with Ala-substitutions of Ser1700 and Thr1704, our lab showed that phosphorylation of these sites is unnecessary for β-adrenergic upregulation of $Ca_V1.2$ as

transgenic Ca^{2+} channels were still regulated by β-adrenergic receptor agonist isoproterenol and adenylyl cyclase activator forskolin [150]. Confusion on the relevance of these sites persisted after Fu et al. generated knock-in mice expressing mutant Ser1700 and Thr1704 and demonstrated the requirement of these sites for $Ca_V1.2$ upregulation [151]. They based their conclusion upon an unconventional metric: the difference in absolute current amplitude rather than the fold-increase after isoproterenol, which is the standard analysis. Their metric is valid only if the density of Ca^{2+} channels at the surface was unchanged, yet $Ca_V1.2$ membrane expression and basal Ca^{2+} currents were substantially reduced. Poomvanicha et al. subsequently created S1700A/T1704A knock-in mice and concluded that isoproterenol stimulated Ca^{2+} current in the control and mutant S1700A/T1704A cardiomyocytes to the same extent [152]. Furthermore, Poomvanicha et al. recalculated the data from Fu et al. and showed that in both groups' knock-in mice, the β-adrenergic stimulation for wild-type and mutant channels were equivalent.

Further complicating the search is the prospect of the $Ca_V\beta$ subunit as the functional PKA phosphorylation target. β_2 is the predominant $Ca_V\beta$ in the heart [153, 154]. Phosphorylation sites on the β_2 subunit have been demonstrated *in vivo* and *in vitro* on Ser459, Ser478 and Ser479 [155-157]. Subsequently, phosphorylation of β_{2a} at these sites was shown to be unnecessary for $Ca_V1.2$ upregulation in the heart by Miriyala et al. through the generation of an adenovirus encoding a mutated β_{2a} in which the 3 confirmed PKA phosphorylation sites were substituted with Ala [158]. Additionally, this group investigated the relationship between basal $Ca_V1.2$ current and capacity for regulation to better define the functional reserve for PKA modulation. They described an inverse relationship between the degree of channel modulation and basal

current density in both guinea pig and rat cells. Overexpression of β_{2a}, which uniquely increases single channel open probability, increased basal current amplitude to a larger degree than cells overexpressing other β subunits and exhibited the weakest β-adrenergic modulation. Later, Brandmayr et al. created a knock-in mouse expressing a β_2 subunit truncated prior to the putative phosphorylation sites [159]. These mice displayed normal PKA modulation of $Ca_V1.2$. Brandmayr et al. also recognized the possibility that PKA simultaneously phosphorylates sites at the $Ca_V\beta_2$ and the α_{1C} subunits, rationalizing that phosphorylation of each site could contribute a small amount to the overall regulation. To test this, they crossed the truncated β_2 mice with mice that expressed mutated α_{1C} at Ser1928. These mutations did not affect the β-adrenergic response of $Ca_V1.2$. Taken together, the prior studies demonstrated that the functional target of PKA in the $Ca_V1.2$ macromolecular complex was unknown.

1.2 Experimental Design and Approach

Full reconstitution of the β-adrenergic receptor signaling pathway in heterologous expression systems remains an unmet challenge that limits robust investigation [34]. Several controversies have arisen from attempts to reproduce reconstitution efforts, with no universally accepted results [160]. To study β-adrenergic regulation of $Ca_V1.2$ in native cardiomyocytes, a system is needed that allows the testing of multiple mutated sites and limits levels of mutant protein expression. Knock-in mice are considered the gold standard, but they are time-consuming and expensive to generate, and a phenotype of heart failure or death during perinatal period may preclude studies at later stages of development [151, 161]. Adenoviruses have been used to express $Ca_V1.2$ subunits in cardiomyocytes, but these cardiomyocytes need to be cultured for extended period, potentially inducing dedifferentiation. Additionally, the large size of the α_{1C}

insert is a limiting factor in the efficiency of knock-in and viral transduction methods. To circumvent previous problems that have limited progress in the field, our lab developed an approach of expressing doxycycline-inducible, tissue-specific rabbit α_{1C}. The rabbit isoform was chosen due to the previously observed enhancement of $Ca_V1.2$ in cardiomyocytes virally infected with rabbit α_{1C} [146]. Inducibility and tissue specificity were achieved by generating transgenic mice expressing the cDNA of rabbit α_{1C} ligated behind 7 tandem *tetO* sequences [162]. tetO-α_{1C} mice were crossed to transgenic mice expressing rtTA controlled by the cardiac-specific α-MHC promoter (Figure 1C). The bitransgenic tetracycline-regulated system enables acute expression of transgenic α_{1C} in the heart only when both transgenes and doxycycline are present. By acutely tuning transgene expression through feeding mice with doxycycline for 1-2 days, this approach limits overexpression of α_{1C} to preserve hormonal regulation of $Ca_V1.2$ and limit chronic effects secondary to altered expression [163].

Using this newly developed approach, our lab generated transgenic mice with inducible cardiomyocyte-specific expression of an N-terminal 3xFLAG-epitope–tagged DHP-resistant rabbit α_{1C} designated pseudo-wild-type ("pWT"). DHP-resistance was used to distinguish transgenic from endogenous Ca^{2+} channels. A concentration of 300 nM nisoldipine blocked >98% of heterologously expressed WT $Ca_V1.2$ current in tsA-201 cells, but only blocked 34.6% of DHP-insensitive α_{1C} [150]. In cardiomyocytes isolated from nontransgenic mice, 300 nM nisoldipine inhibited about 92.4% of peak $Ca_V1.2$ current. In the pWT background, our lab previously created transgenic mice ("22-mutant") expressing $Ca_V1.2$ with Ala substitutions of all conserved, previously not studied consensus PKA phosphorylation sites (17 mutations), and sites previously shown to be not required for β-adrenergic stimulation of $Ca_V1.2$ (rabbit Ser1517,

Ser1575, Ser1700, Thr1704, and Ser1928). Sites were only chosen if conserved in rabbit, rat, mouse, guinea pig, or human isoforms of $Ca_V1.2$ α_{1C}. In the cardiomyocytes isolated from 22-mutant transgenic mice, isoproterenol increased nisoldipine-resistant peak to a near-identical fold-change as the isoproterenol-induced augmentation of nisoldipine-resistant current in pWT cardiomyocytes [164].

Additionally, we reasoned that the functional PKA phosphorylation site exists on the CaVβ subunit. Our lab recently published results showing that the AID motif on α_{1C} is required for the high-affinity interaction between α_{1C} and β subunits [165]. We showed that when the AID motif is mutated, the β-less $Ca_V\alpha$ subunits were completely refractory to PKA activation, suggesting that $Ca_V\beta$ or an associated protein is the functional PKA phosphorylation target. It was previously demonstrated that C-terminal PKA phosphorylation sites were unnecessary for β-adrenergic regulation of $Ca_V1.2$ [159]. To test predicted phosphorylation sites that are upstream of the C-terminus, our lab identified and mutated to alanine 18 conserved Ser and Thr residues within 28 PKA-consensus phosphorylation sites before the C-terminal region previously deleted of human β_{2B} ("18-mutant"). Because there is no method to pharmacologically isolate $Ca_V1.2$ channels bound to transgenic β_2, we relied on overexpression of transgenic β_2 to outcompete endogenous CaVβ subunits [166]. GFP-tagged WT or 18-mutant β_{2B} mice were generated and isoproterenol increased peak $Ca_V1.2$ current to equal levels in non-transgenic, GFP-WT, and 18-mutant β2-expressing cells, indicating that direct PKA phosphorylation of sites upstream of the C-terminus on β2 might not be necessary for β-adrenergic regulation [165].

Although the 22-mutant α_{1C} cardiomyocytes exhibited unperturbed adrenergic regulation of $Ca_V1.2$, it remains possible that the functional PKA phosphorylation site is not conserved amongst species. Phenotypic differences in eukaryotic species —even those that are closely related—are observed in responses to adrenergic stimulation [167]. This can perhaps be explained by variation in phosphorylation sites, as gain or loss of phosphorylation sites is hypothesized to play a greater role in contributing to phenotypic differences among species than the gain or loss of protein kinases [168]. A recent example demonstrated that while parathyroid hormone-induced PKA phosphorylation of rabbit TRPV5 enhances channel activity, it did not stimulate human TRPV5 activity [169]. By mutating all conserved and non-conserved PKA phosphorylation sites between the 5 species mentioned above, we can test the following hypotheses that might explain why a consensus phosphorylation site hasn't been identified: (i) that the phosphorylation of any one of several $Ca_V\alpha$, $Ca_V\beta$, or both $Ca_V\alpha$ and $Ca_V\beta$ residues can induce the adrenergic stimulation of $Ca_V1.2$ current (redundancy), (ii) that each phosphorylated residue contributes a small fraction of the total effect, and/or (iii) that the critical PKA phosphorylation sites are not on $Ca_V\alpha$ or $Ca_V\beta$.

1.3 Results

To test the hypotheses outlined above, we started by replaced with Ala all consensus intracellular PKA phosphorylation sites in $Ca_V1.2$ α_{1C} that are conserved in the rabbit, human, guinea pig, mouse, and rat. The optimal PKA phosphorylation motif is a tetrapeptide with Arg at the second and third positions (termed -2 and -3) before the phosphorylated Ser or Thr and a large hydrophobic residue immediately thereafter (R-R-X-S/T-Φ) [170, 171]. The requirement for a positive charge is highest for residues at -2 and -3, but can be found for residues as far as

position −6 in PKA target sites [172]. The positions between -4 and -1 have a strong preference for Arg and, to a lesser extent, for His or Lys [171, 173]. We identified all potential intracellular PKA phosphorylation sites in rabbit α_{1C} using both manual sequence analysis and several web-based PKA phosphorylation prediction tools, including prediction of protein kinase A phosphorylation sites using the simplified kinase binding model (pKaPS) [174], Disorder-Enhanced Phosphorylation Sites Predictor (DISPHOS) [175], GPS [176], NetPhos [177], and Scansite [178]. For identified sites, we also mutated additional Ser and Thr within several amino acid residues C-terminal to the Arg or Lys to ensure that we fully tested each phosphoregulatory site (Figure 1A).

Our first goal was to determine whether elimination of conserved and non-conserved PKA phosphorylation sites in α_{1C} prevented $Ca_V1.2$'s responsiveness to β-adrenergic modulation in cardiomyocytes. Based on the list of potential PKA phosphorylation sites, we generated transgenic mice with inducible cardiomyocyte-specific expression of an N-terminal 3× FLAG-epitope–tagged DHP-resistant α_{1C} with Ala substitutions of all predicted Ser or Thr conserved and non-conserved between 5 species, including residues on the 22-mutant construct previously shown to be not required for β-adrenergic stimulation of $Ca_V1.2$ (Figure 1B). We mutated all 51 serine and threonine residues within the 35 intracellular PKA consensus phosphorylation sites of rabbit α_{1C} to alanine ("35-mutant"). Several predicted PKA phosphorylation sites in the transmembrane and extracellular regions were not mutated, as these are unlikely to have access to intracellular PKA. Additionally, two predicted sites that were very close to a transmembrane region (Ser607 and Ser680/683) were mutated in isolation and, when expressed heterologously, inhibited $Ca_V1.2$ basal function (data not shown). These sites were left out of the final 35-mutant.

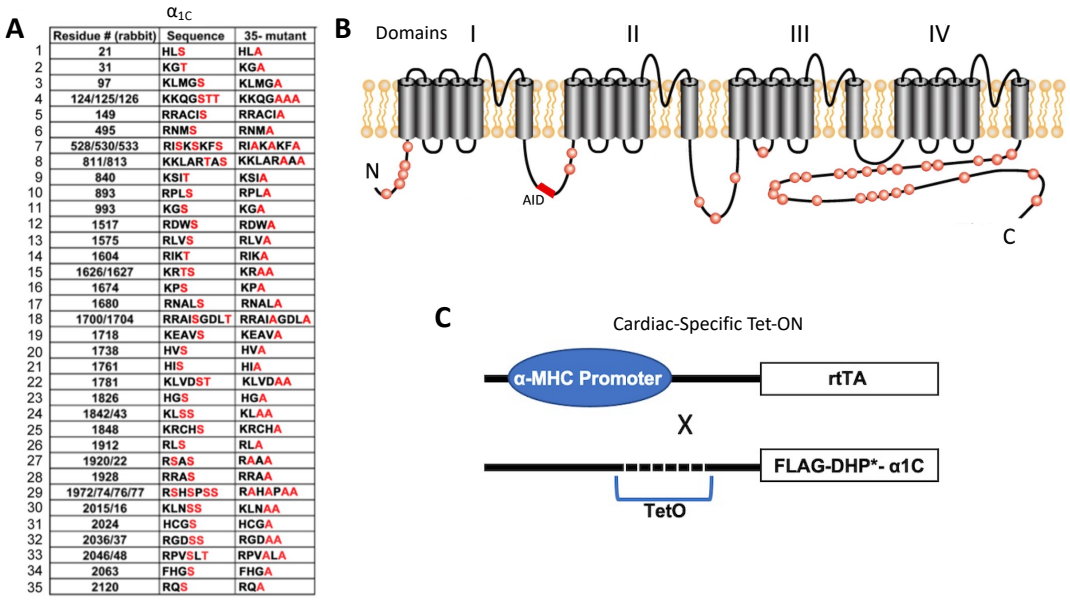

Figure 1. Cardiac-specific, DHP-resistant 35-mutant α_{1C}. (**A**) Left column, the 35 putative PKA phosphorylation sites in rabbit α_{1C}. Center, the 51 residues in red are either predicted phosphorylation sites or within the immediate region of the predicted phosphorylation sites. Right, all 51 residues were replaced with alanine in 35-mutant α_{1C} transgenic mice. (**B**) Diagram showing rabbit cardiac α_{1C}. Red dots indicate putative sites of phosphorylation by PKA. (**C**) Diagram showing the binary transgene system that permits robust expression of Flag-tagged DHP-resistant (DHP*) α_{1C} only in the presence of both rtTA and doxycycline (Tet-ON). The top diagram shows expression of the rtTA driven by the cardiac-specific α-myosin heavy chain (α-MHC) promoter. The lower diagram shows cDNA for Flag–DHP*–α_{1C} ligated behind seven tandem tetO sequences, which impart tetracycline regulation. Figures adapted from [179].

Previously generated pWT α_{1C} transgenic mice were compared to 35-mutant mice [150]. In pWT and 35-mutant cells, the transgenic and endogenous $Ca_V1.2$ currents are distinguishable by application of nisoldipine, a Ca^{2+}-channel DHP antagonist [150]. Nisoldipine (300 nM) inhibited about 70% of peak current in cardiomyocytes isolated from doxycycline-fed pWT α_{1C} transgenic mice and about 73% of peak current in doxycycline-fed 35-mutant α_{1C} transgenic mice (Figure 2A). This indicates that approximately 30% and 28% of the peak current in the cardiomyocytes isolated from pWT α_{1C} and 35-mutant doxycycline-treated transgenic mice, respectively, was insensitive to nisoldipine. In the cardiomyocytes isolated from pWT α_{1C} transgenic mice, isoproterenol increased the nisoldipine-insensitive peak current by a mean of

1.89 ± 0.08-fold (Figure 2B). In the cardiomyocytes isolated from the 35-mutant, isoproterenol and forskolin increased nisoldipine-resistant peak $Ca_V1.2$ current by a mean of 1.74 ± 0.08-fold, which is not significantly different from the isoproterenol-induced augmentation of nisoldipine-resistant current in pWT α_{1C} transgenic cardiomyocytes (Figure 2B). A hyperpolarizing shift in the V_{50} of activation from both transgenic mutants was observed, characteristic of β-adrenergic regulation of $Ca_V1.2$ (Figure 5C). These results indicate that phosphorylation of α_{1C} alone is not required for β-adrenergic regulation of $Ca_V1.2$.

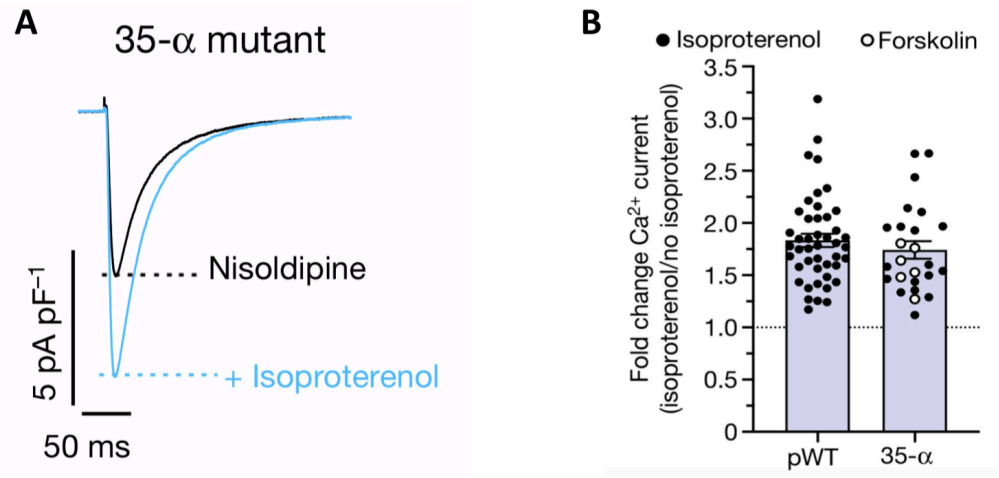

Figure 2. 35-mutant α_{1C} responds to adrenergic regulation. (**A**) Exemplar whole-cell Cav1.2 currents of 35-mutant α_{1C} cardiomyocytes (from transgenic mice) in nisoldipine before (black trace) and after (blue trace) treatment with isoproterenol. Representative of 25 experiments; pA pf^{-1}, picoamperes per picofarad. (**B**) Fold change in peak DHP-resistant Ca^{2+} current at 0 mV caused by isoproterenol or forskolin. Data are mean ± s.e.m.; P = 0.39 by unpaired two-tailed t-test; n = 45 cardiomyocytes from 5 mice (isoproterenol); n = 25 cardiomyocytes from 5 mice (forskolin). Figure adapted from [179].

The functional PKA phosphorylation site might also be on the $Ca_V\beta$ subunit. Although previous data have demonstrated that, separately, the N-terminal and the C-terminal putative PKA phosphorylation sites are not required for β-adrenergic regulation of $Ca_V1.2$ [159, 165], it remains possible that a redundancy exists such that a combination of sites on the N- and C-terminus confer channel regulation. In the same vein as the 35-mutant α_{1C}, we mutated to alanine

all 37 serine and threonine residues within 28 predicted PKA-consensus phosphorylation sites of human β_{2B} ("28-mutant") (Figure 3, A and B). We generated transgenic mice with inducible cardiomyocyte-specific expression of either GFP-tagged WT or 28-mutant β_{2B} subunits (Figure 3C).

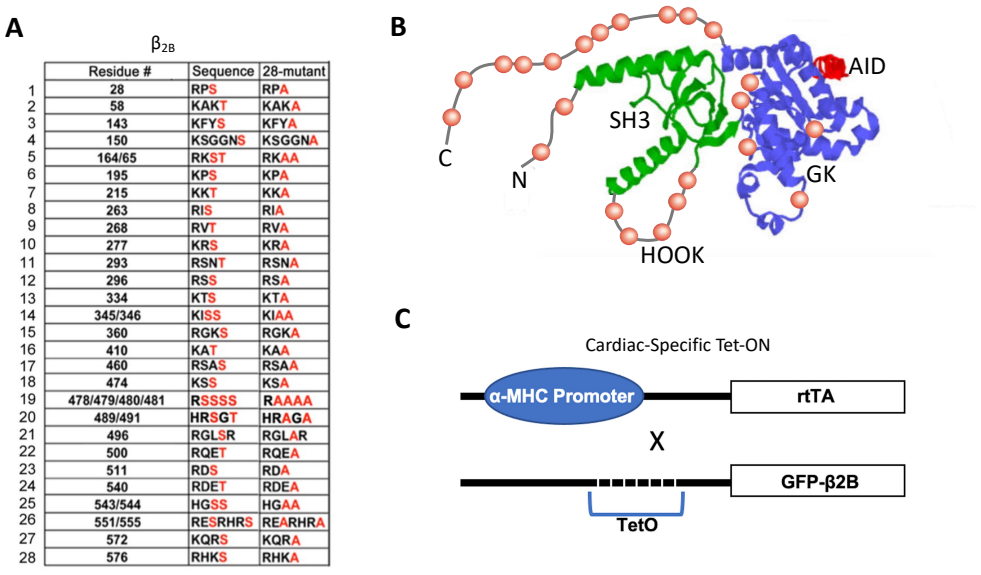

	Residue #	Sequence	28-mutant
1	28	RPS	RPA
2	58	KAKT	KAKA
3	143	KFYS	KFYA
4	150	KSGGNS	KSGGNA
5	164/65	RKST	RKAA
6	195	KPS	KPA
7	215	KKT	KKA
8	263	RIS	RIA
9	268	RVT	RVA
10	277	KRS	KRA
11	293	RSNT	RSNA
12	296	RSS	RSA
13	334	KTS	KTA
14	345/346	KISS	KIAA
15	360	RGKS	RGKA
16	410	KAT	KAA
17	460	RSAS	RSAA
18	474	KSS	KSA
19	478/479/480/481	RSSSS	RAAAA
20	489/491	HRSGT	HRAGA
21	496	RGLSR	RGLAR
22	500	RQET	RQEA
23	511	RDS	RDA
24	540	RDET	RDEA
25	543/544	HGSS	HGAA
26	551/555	RESRHRS	REARHRA
27	572	KQRS	KQRA
28	576	RHKS	RHKA

Figure 3. Cardiac-specific, 28-mutant β_{2B}. (**A**) Left, the 28 putative PKA phosphorylation sites in the N-terminal (NT), Hook, GK and C-terminal (CT) domains of β_{2B}. Centre, the 37 residues in red are either predicted phosphorylation sites or within the immediate vicinity of predicted phosphorylation sites, and were mutated to alanine in the 28-mutant GFP-tagged β_{2B} transgenic mice (right). (**B**) Diagram showing rabbit cardiac α_{1C} (ribbon diagram adapted from [180]). Red dots indicate putative sites of phosphorylation by PKA. GK, guanylate kinase domain; SH3, Src homology 3 domain; AID, alpha interaction domain; HOOK region. (**C**) Diagram showing the binary transgene system that permits robust expression of GFP-tagged β_{2B} only in the presence of both rtTA and doxycycline (Tet-ON). Format as in Figure 1C. Figures adapted from [179].

The GFP-WT and 28-mutant β_{2B} transgenic mice were fed doxycycline for up to 1 week, thus ensuring high levels of expression of the GFP-tagged β_2 subunits (Figure 4A). Cardiomyocytes expressing green fluorescent protein (GFP)-tagged WT β_{2B} displayed an isoproterenol and forskolin-induced stimulation of $Ca_V1.2$ current amplitude by 1.48 ± 0.05-fold. In the cardiomyocytes isolated from the 28-mutant, isoproterenol and forskolin increased peak $Ca_V1.2$ current by a mean of 1.60 ± 0.07-fold, which is not significantly different from the

isoproterenol-induced augmentation of current in GFP-WT β_{2B} transgenic cardiomyocytes (Figure 4, B and C). Interestingly, both of these fold-change values are lower than those observed in wild-type and even 35-mutant cardiomyocytes. It is likely that overexpression of $Ca_V\beta$ increased the number of functional channels in the sarcolemma and decreased the magnitude of PKA regulation relative to wild-type cells as previously reported [153, 158]. A hyperpolarizing shift in the V_{50} of activation in both transgenic mutants was observed, similar to the isoproterenol-induced shift observed for wild-type mice, pWT α_{1C}, and the 35-mutant (Figure 5C).

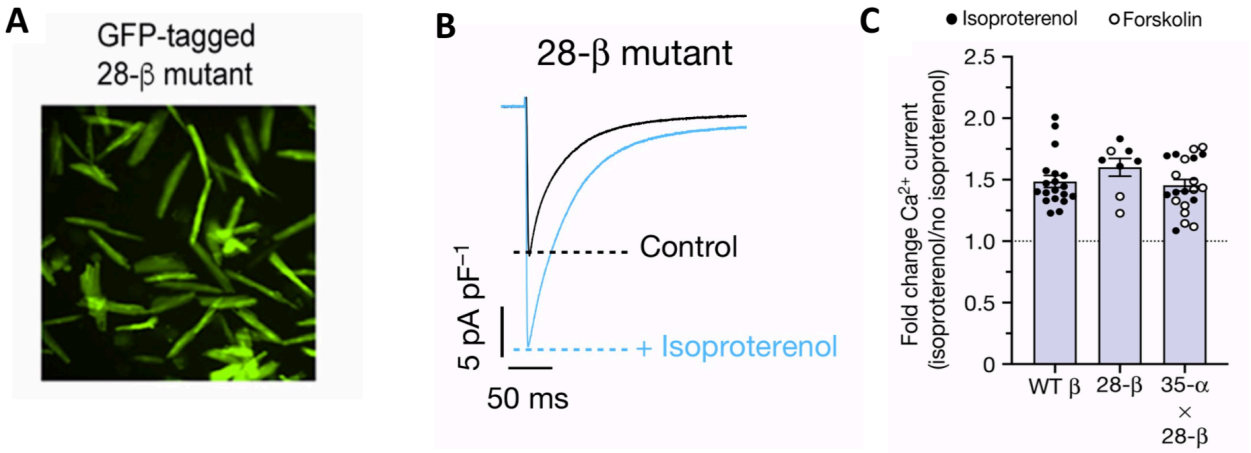

Figure 4. 28-mutant β_{2B} responds to adrenergic regulation. (**A**) Fluorescence imaging of isolated cardiomyocytes expressing the GFP-tagged 28-β mutant. Representative of images from more than five biologically independent mice. (**B**) Exemplar whole-cell $Ca_V1.2$ currents of cardiomyocytes from GFP-tagged 28-mutant β_{2B} transgenic mice in nisoldipine before (black trace) and after (blue trace) treatment with isoproterenol. (**C**) Fold change in peak Ca^{2+} current caused by isoproterenol or forskolin for cardiomyocytes isolated from transgenic mice expressing GFP-tagged wild-type (WT) β_{2B} subunit [165] and GFP-tagged 28-mutant β_{2B}, or both 35-mutant α1C and GFP-tagged 28-mutant β_{2B}. Data are mean ± s.e.m.; P = 0.27 by one way-ANOVA; n = 19, 8 and 21 cardiomyocytes from 4, 4 and 3 mice, from left to right. Figures adapted from [179].

The data thus far suggest that the functional PKA target for adrenergic regulation is likely not solely α_{1C} or solely on β_2, based on our observation that eliminating all conserved and non-conserved consensus PKA phosphorylation sites in α_{1C} and β_2 did not alter PKA-mediated upregulation of $Ca_V1.2$. This means that either there is redundancy between α_{1C} and β subunits,

such that PKA phosphorylation of either subunit is sufficient to mediate adrenergic regulation of Ca^{2+} channels in the heart, or that PKA phosphorylation of the core $Ca_V1.2$ subunits, α_{1C} and β, are not necessary for β-adrenergic regulation of the Ca^{2+} influx in the heart. To address this, we crossed 35-mutant α_{1C} with 28-mutant β_{2B} transgenic mice ("35α x 28β").

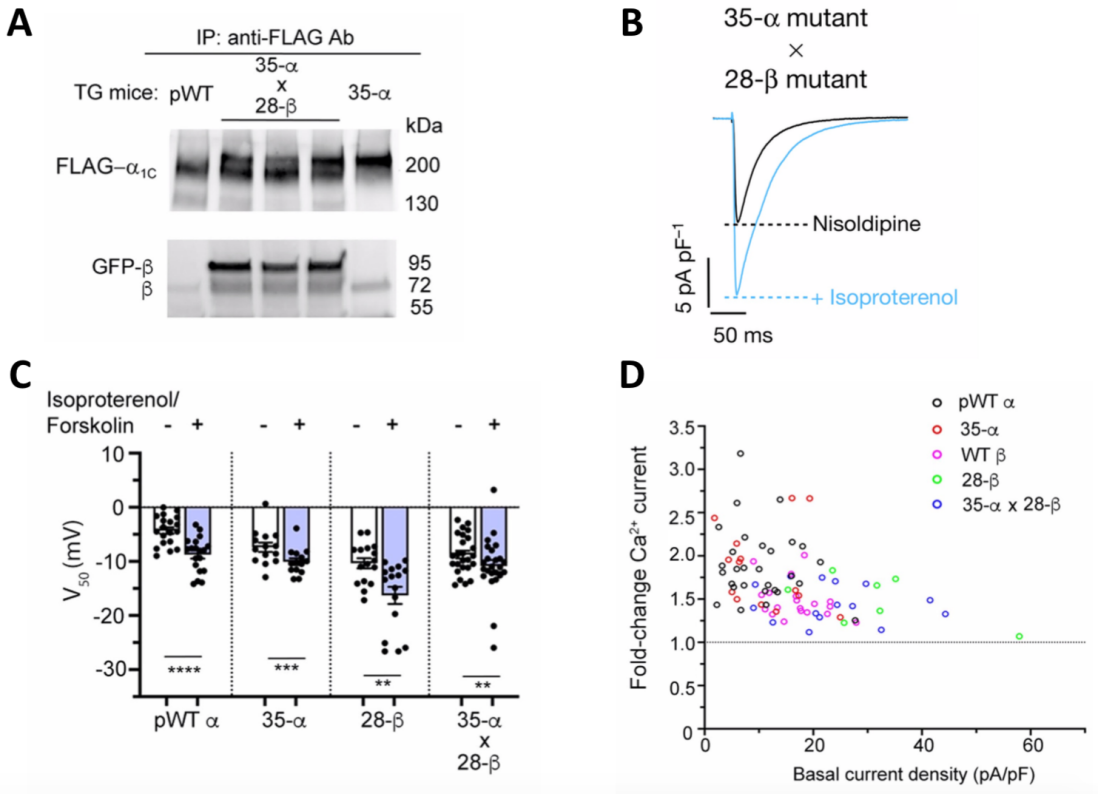

Figure 5. 35α x 28β exhibits unaltered adrenergic regulation. (**A**) Anti-Flag antibody (upper) and anti-β antibody (lower) immunoblots of anti-Flag antibody immunoprecipitations from cleared lysates of hearts from pWT, 35-α and three mice expressing 35-α × GFP-tagged-28-β. Representative images from two independent experiments. (**B**) Exemplar whole-cell $Ca_V1.2$ currents of cardiomyocytes from 35-mutant α_{1C} crossed with 28-mutant β_{2B} transgenic mice. (**C**) Combined bar and column scatter plot of Boltzmann function parameters, V50. Data are mean ± s.e.m. **P < 0.01; ***P < 0.001; ****P < 0.0001 by paired two-tailed t-test. pWT α, n = 19; 35-α mutant, n = 14; 28-β mutant, n = 16; 35-α mutant × 28-β mutant, n = 24. (**D**) Graph showing isoproterenol- and forskolin-induced increases in nisoldipine-resistant current, stratified by total basal current density before nisoldipine treatment. Figures adapted from [179].

Immunoprecipitation with anti-Flag antibody indicated that GFP-tagged 28-mutant β_{2B} subunits dominate in the 35-mutant α_{1C} complex (Figure 5A) in cardiomyocytes isolated from these mice. It has been previously demonstrated that acutely expressed exogenous β-subunits

out-compete β subunits present in channels preexisting in the plasma membrane in Xenopus oocytes [166]. 35α x 28β cardiomyocytes displayed an isoproterenol- and forskolin-induced increase in peak Ca^{2+} current by 1.45 ± 0.05-fold (Figure 4C and Figure 5B) and a hyperpolarizing shift in the V_{50} of activation (Figure 5C). As seen in pWT α_{1C}, 35-mutant α_{1C}, GFP-WT β, and 28-mutant β, the magnitude of the isoproterenol-induced increase in the nisoldipine-resistant Ca^{2+} current in cells from 35α x 28β mice was inversely correlated with the basal total $Ca_V1.2$ current (Figure 5D). These results indicate that β-adrenergic stimulation of $Ca_V1.2$ does not involve direct phosphorylation of α_{1C} or β2 subunits, providing the most definitive answer about whether PKA phosphorylation of any α_{1C} or β_2 residues is necessary.

Given the results above, our lab hypothesized that a $Ca_V1.2$ regulator in its macromolecular complex plays a role in PKA-mediated upregulation of channel function and may be the functional target of PKA phosphorylation. Work performed by other members of the Marx laboratory using proximity labeling and mass spectrometry observed the movement of Ca^{2+} channel inhibitor Rad away from $Ca_V1.2$ in cardiomyocytes after application of isoproterenol [179]. Heterologous expression of wild-type α_{1C}, β_{2B}, and Rad enabled reconstitution of forskolin-induced stimulation of $Ca_V1.2$ in HEK cells. As confirmation of my studies, we expressed in HEK293 cells 35-mutant α_{1C} and 28-mutant β_{2B} with and without Rad. Forskolin did not increase the maximal current density of $Ca_V1.2$ channels comprised of 35-mutant α_{1C} with 28-mutant β_{2B} (0.97 ± 0.04-fold change), but forskolin increased peak current density by 1.91 ± 0.12-fold when co-expressing 35-mutant α_{1C}, 28-mutant β_{2B}, and Rad (Figure 6, A and B). A forskolin-induced hyperpolarizing shift in the V_{50} of activation was observed for 35-mutant α_{1C}, 28-mutant β_{2B}, and Rad, but not in cells without Rad coexpression (Figure 6C). This implies

that similar to cardiomyocytes, phosphorylation of α_{1C} and β_{2B} subunits is not required for β-adrenergic upregulation of heterologously expressed $Ca_V1.2$ channels.

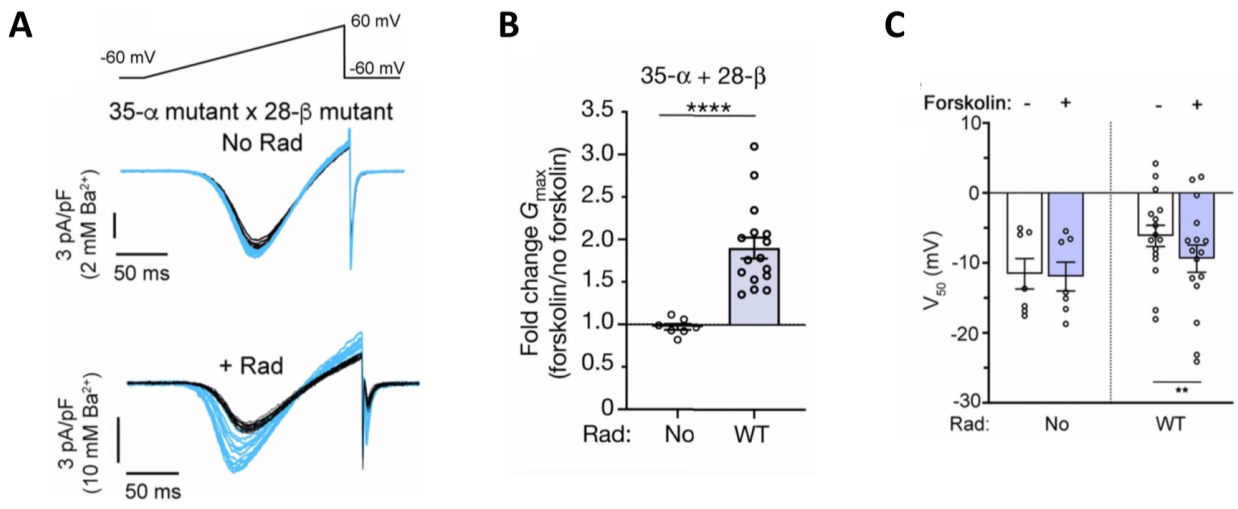

Figure 6. Rad is required for forskolin-induced activation of heterologously expressed $Ca_V1.2$ channels. (**A**) Upper, a 200-ms voltage ramp from −60 mV to +60 mV was applied every 10 s. Lower, Exemplar traces of Ba2+ currents in the absence and presence of Rad elicited by voltage ramp every 10 s. Black traces, before forskolin treatment; blue traces after treatment; no Rad, 7 cells; Rad, 16 cells. (**B**) Fold change in G_{max} induced by forskolin in the absence and presence of Rad. Data are mean ± s.e.m.; ****P < 0.0001 by unpaired two-tailed t-test. n = 7 and 16, from left to right. (**C**) Boltzmann function parameter V50. Data are mean ± s.e.m. **P < 0.01 by paired two-tailed t-test. n = 7 and 16, from left to right. Figures adapted from [179].

1.4 Discussion

Previously, our lab showed that in cardiomyocytes expressing α_{1C} with mutations at consensus PKA phosphorylation sites that are conserved between 5 species, β-adrenergic regulation of $Ca_V1.2$ was preserved [164]. Since our lab only investigated conserved residues, it could not be ruled out that predicted PKA phosphorylation sites that are not conserved amongst the 5 species contribute to adrenergic regulation of $Ca_V1.2$. Different eukaryotic species exhibit phenotypic differences in β-adrenergic regulation of the heart [181, 182], and variation of phosphorylation sites has been suggested as an explanation for these distinctions [168, 183]. Additionally, we previously showed that cardiomyocytes from transgenic mice expressing β_2

with mutated PKA sites upstream from the C-terminus did not show altered β-adrenergic regulation of $Ca_V1.2$ either [165]. These results foster several hypotheses. It was possible that redundancy existed between α_{1C} and β_2 so that phosphorylation of either subunit could cause in increase in Ca^{2+} current. If true, we would not observe alterations in regulation with coexpression of one a mutated subunit alongside endogenous expression of the other subunit. Expanding on this idea, redundancy might additionally exist between a conserved and non-conserved site the α_{1C} subunit, or between a C-terminal and N-terminal site the β_2 subunit. Finally, phosphorylation of several sites on α_{1C}, β_2, or both might each confer an incremental increase that amounts to the observed regulation. By mutating all conserved and non-conserved predicted PKA phosphorylation sites on both α_{1C} and β_2 and expressing the mutated subunits together, we were able to test these hypotheses. Adrenergic regulation was unperturbed in our experiments with these mutants in cardiomyocytes and in heterologous expression systems with Rad, providing the definitive answer that PKA phosphorylation of any α_{1C} and β_2 residues is not necessary for adrenergic stimulation of cardiac Ca^{2+} current.

Although heterologous expression of $Ca_V1.2$ channels has proven useful for investigating biophysical properties, it has not been as successful for exploring physiological modulation in a cardiomyocyte milieu. Our approach of expressing doxycycline-inducible, tissue-specific $Ca_V1.2$ subunits allowed us to study adrenergic regulation robustly in the native cardiomyocyte. There are drawbacks, however, to using our approach. Though acute, overexpression of α_{1C} or β_2 transgenes can reduce the hormonal regulation of the channel [158, 184]. Stratifying the magnitude of β-adrenergic-mediated upregulation of $Ca_V1.2$ current by total basal current density exemplifies this phenomenon (Figure 5D). Notably, GFP-WT β, 28-mutant β, and 35α x 28β all

had a relatively smaller fold-change after β-adrenergic stimulation compared to pWT α_{1C} and 35-mutant α_{1C}. This is likely due to an increased the number of functional channels in the sarcolemma as overexpression of the β_{2b} subunit in cardiomyocytes increases the maximum gating charge (Q_{max}; representing number of voltage-gated channels expressed in the membrane) and reduces response to β-adrenergic stimulation [153, 158]. This saturable modulation where an inverse hyperbolic relationship is observed between basal current and fold-change in current after β-adrenergic activation suggests a limiting resource for PKA modulation of $Ca_V1.2$. Recent results call Rad into question as the limiting factor in this process. If so, this would mean that as more channels are expressed, fewer are inhibited under basal conditions and capacity for upregulation is muted.

Another potential confounding variable in our results is the presence of non-transgenic current remaining after 300nM nisoldipine is applied to cardiomyocytes isolated from 35-mutant and 35α x 28β transgenic mice. The 35-mutant α_{1C} subunit was engineered to be relatively DHP-insensitive with the substitutions T1066Y and Q1070M [138, 139]. The IC_{50} for nisoldipine block of heterologously expressed WT α_{1C} was 12 nM, whereas the IC_{50} for pWT α_{1C} was 650 nM. A nisoldipine concentration of 300nM was the optimal concentration for inhibiting >98% of heterologously expressed WT α_{1C} and only 34.6% of heterologously expressed DHP-insensitive α_{1C}. In cardiomyocytes, 300nM nisoldipine blocked about 93% of current from non-transgenic mice, and about 70% of current from pWT α_{1C} mice. From these measurements, we can assume that about 7% of endogenous current is not blocked by nisoldipine and 65% of DHP-insensitive transgenic channels are not blocked by nisoldipine. Nisoldipine blocked about 73% of current in cardiomyocytes isolated from 35-mutant mice and about 58% of current in cardiomyocytes

isolated from 35α x 28β. The maximal contamination of nisoldipine-resistant currents by endogenous channels, determined by first calculating the fraction of endogenous current of total current, would be ~17% in 35-mutant cells and ~7% in the 35α x 28β cells [150]. These percentages are relatively small and would not materially impact our interpretations that the transgenic channels are regulated by adrenergic stimulation.

Previous results demonstrating phosphorylation of $Ca_V1.2$ at Ser1928, Ser1700, or other sites raises fundamental questions about the functional role of PKA phosphorylation of $Ca_V1.2$. $Ca_V1.2$ is the most abundant L-type Ca^{2+} channel isoform in the mammalian heart, brain, and vascular smooth muscle [185]. Its dysfunction leads to a range of disorders in these tissues, for example cardiac arrhythmias, autistic-like behavior, and developmental abnormalities in Timothy syndrome patients [22]. Due to this relative ubiquity, it would make sense that tissue-specific nuances exist to precisely tune $Ca_V1.2$ function. In hippocampal neurons, the β_2-adrenergic receptor binds directly to the C-terminus of $Ca_V1.2$, resulting in in localized cAMP signaling [186, 187]. Phosphorylation of Ser1928 in hippocampal neurons displaces the β_2-adrenergic receptor from $Ca_V1.2$ [188]. Single-channel recordings with isoproterenol in the pipette showed an increase in NP_O but, when cells were preincubated with isoproterenol, upregulation of channel activity was not observed unless the washout was 10 minutes long, indicating that displacement of the β_2-adrenergic receptor is a negative feedback regulatory mechanism for limiting Ca^{2+} influx that is unseen in cardiomyocytes. Of note, Ca^{2+} channel activator BayK8644 was used in the patch pipette solution, and it remains to be shown if results are dependent on the presence of BayK8644. Also, unlike cardiomyocytes, β_1-adrenergic receptor stimulation does not cause increase $Ca_V1.2$ activity in neuronal cultures [189]. In

smooth muscle cells, stimulation of β-adrenergic receptors leads to membrane hyperpolarization, indicating that K^+ channels are activated [190, 191]. Seemingly paradoxical results have shown that PKA-dependent phosphorylation of Ser1928 enhances vascular $Ca_V1.2$ activity, although this regulation is most apparent in conditions of high blood glucose [192]. AKAP50 is required for this regulation, leading to the hypothesis that compartmentalization of a subpopulation of $Ca_V1.2$ channels are responsible for activating K^+ channels. Supporting this, previous reports have demonstrated the association of Ca^{2+} channels and Ca^{2+}-activated BK channels in complex [193, 194].

1.5 Conclusion

PKA-mediated adrenergic regulation of $Ca_V1.2$ channels in the heart is key to normal cardiac physiology [30]. Using mutagenesis to eliminate all potential PKA phosphorylation targets on α_{1C} and β_2, we show that phosphorylation of these $Ca_V1.2$ subunits is not required for β-adrenergic upregulation of the channel in cardiomyocytes. Additionally, we reconstituted β-adrenergic regulation of $Ca_V1.2$ in heterologous expression systems using the cDNA of mutated α_{1C} and β_2 plus Rad. The identification of this mechanism could offer opportunities to develop specific modulators of the sympathetic nervous system modulation of Ca^{2+} currents for patients with heart failure for instance. Future projects will also explore the role of Rad phosphorylation using phospho-mutant knock-in mice, and how the neighborhood of the Ca^{2+} channels changes in disease states.

Chapter 2: Fibroblast Growth Factor Homologous Factors Tune Arrhythmogenic Late $Na_V1.5$ Current in Calmodulin Binding–Deficient Channels

2.1 Introduction

Incomplete inactivation of $Na_V1.5$ leads to persistent inward late Na^+ influx ($I_{Na,L}$). Even though $I_{Na,L}$ is diminutive compared with the peak Na^+ current, increased $I_{Na,L}$ counteracts repolarization and is sufficient to trigger LQT3 and cause structural and electrical remodeling in the atria of mice [195, 196]. Interaction of the $Na_V1.5$ III-IV linker and the C-terminus stabilizes fast inactivation and disruption of this interaction was found to increases $I_{Na,L}$, indicating a role for the C-terminus in modulating $I_{Na,L}$ [53]. The C-terminus of $Na_V1.5$ consists of several protein interaction domains and is a hotspot for mutations linked to LQT3, suggesting that these domains may be required for tuning physiologic $I_{Na,L}$ [197].

Calmodulin (CaM) is a Ca^{2+} sensing protein that interacts with the "IQ" domain within the C-terminus of $Na_V1.5$ via its C-lobe [198]. The IQ domain of nearly all Na_V channels binds to both Ca^{2+}-free CaM (apoCaM) and Ca^{2+}/CaM [199, 200]. Considerable efforts have been devoted to identifying the Ca^{2+} dependent effect on $Na_V1.5$ gating. Although some studies have shown that Ca^{2+} elevation elicits a depolarizing shift in channel steady-state inactivation, recent studies using rapid Ca^{2+} delivery techniques have suggested otherwise [54, 71]. Besides the Ca^{2+}-dependent effects, the loss of apoCaM binding to the $Na_V1.5$ by mutations of the IQ domain has been shown to increase $I_{Na,L}$ in heterologous expression systems [73], suggesting an impact of apoCaM in stabilizing the interaction between III-IV linker and the C-terminus [75]. Additionally, human mutations within the IQ motif or in close vicinity within the CaM binding pocket — including Q1909R, E1901Q, and R1913H — are associated with LQT3 and cause increased late Na^+ current when expressed

in heterologous cells [72]. Although these results are highly indicate loss of apoCaM increases $I_{Na,L}$, this has not been tested in native cardiomyocytes. $Na_V1.5$ function is exquisitely tuned by a rich repertoire of modulatory proteins that may be present in cardiomyocytes but not in heterologous expression systems, including fibroblast homologous growth factor (FHF) FGF13.

2.2 Experimental Design and Approach

Many of the prior studies on CaM and FGF13 regulation of $I_{Na,L}$ have been carried out in heterologous expression systems that might not properly represent the proteomic profile of cardiomyocytes. To study the effects of CaM binding in cardiomyocytes, we created transgenic mice with tetO–3XFLAG epitope–tagged, TTX-sensitive (C374Y) $Na_V1.5$ channels (designated pseudo-WT, pWT). The channel was engineered to be TTX sensitive with the substitution of C374Y [201], as $Na_V1.5$ channels are relatively resistant to TTX compared with neuronal and skeletal muscle isoforms. In the pWT background, we created additional transgenic mice expressing Ala substitutions for IQ motif (IQ/AA), which prevents CaM binding to the C-terminus of $Na_V1.5$. TTX-sensitivity was used to distinguish transgenic from endogenous Na^+ channels rather than lidocaine resistance (F1759A) as it had previously shown that this mutation results in significantly increased $I_{Na,L}$ [196]. Instead, we used a previously-made tetO-F1759A mutant mouse as a positive control for increased $I_{Na,L}$ relative to the pWT mouse. The tetO-$Na_V1.5$ mice were crossed to transgenic mice expressing rtTA controlled by the cardiac-specific α-MHC promoter (Figure 1A). The bitransgenic tetracycline-regulated system enables robust expression of the FLAG-tagged transgenic $Na_V1.5$ channels only when both transgenes and doxycycline were present. Since the expression of these channels is inducible and cardiac specific, there is a low likelihood of developmental or other compensatory mechanisms affecting

the phenotype. We use both whole-cell and cell-attached approaches in isolated cardiomyocytes from pWT and IQ/AA mice to explore of the effect of $Na_V1.5$ regulatory proteins on $I_{Na,L}$.

2.3 Results

The sum of the endogenous Na^+ currents and the transgenic $Na_V1.5$ current make up the total peak Na^+ current in the transgenic cardiomyocytes. Application of 20 nM TTX had no effect on peak endogenous Na^+ currents in cardiomyocytes isolated from nontransgenic animals due to the relative resistance of endogenous cardiac $Na_V1.5$ to TTX (Figure 1, B and E). In cardiomyocytes isolated from pWT or IQ/AA transgenic mice, in contrast, 20 nM TTX reduced the peak Na^+ current, implying that the transgenic channels were expressed, inserted in the membrane, and were functional (Figure 1, C-E). The difference between the total current and the remaining current after TTX infusion represents the current carried by the transgenic pWT or IQ/AA channels. The mean fraction of TTX-sensitive current, which can be attributed to the transgenic Na^+ channels, was 69% and 71% for pWT and IQ/AA, respectively (Figure 1, F).

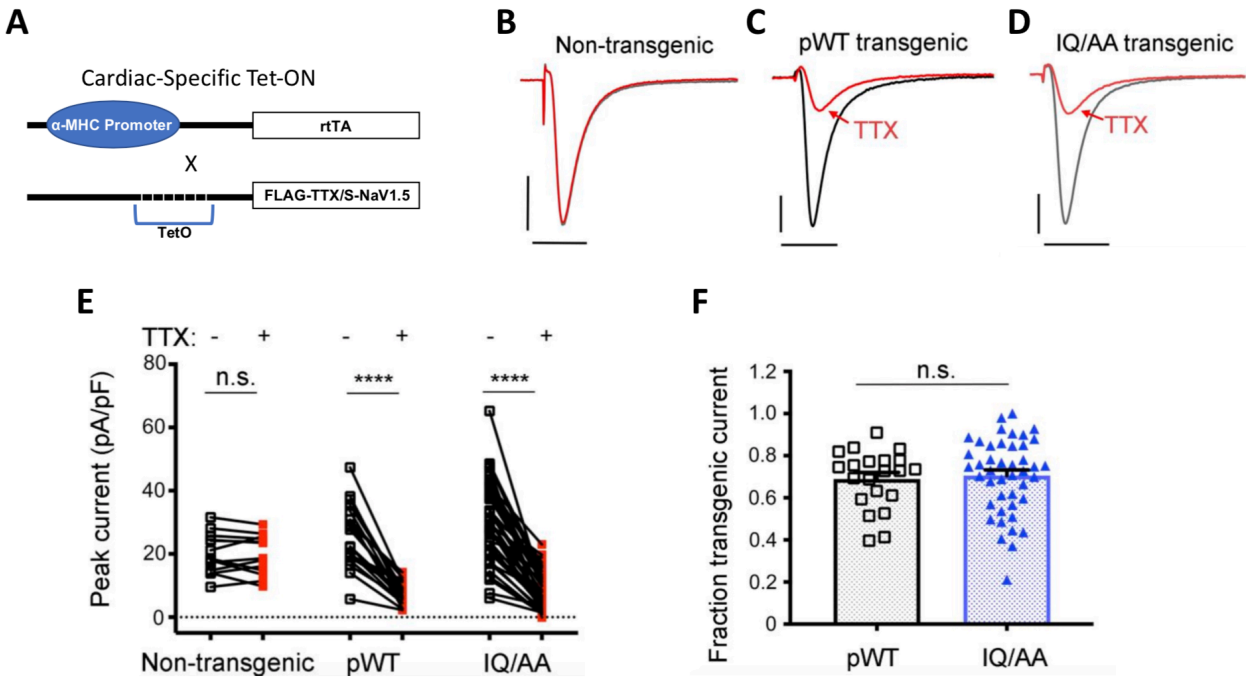

Figure 1. Cardiac-specific, FLAG-tagged TTX-sensitive Nav1.5-expressing transgenic mice. (**A**) Schematic of binary transgene system. The expression of reverse tetracycline-controlled transactivator (rtTA) is driven by the cardiac-specific α-myosin heavy chain promoter. The cDNAs for FLAG-F1759A-Nav1.5 or FLAG-tagged TTX-sensitive Nav1.5 were ligated behind 7 tandem *tetO* sequences. (**B–D**) Exemplar whole cell Na^+ current trace of ventricular cardiomyocyte from nontransgenic, pWT, and IQ/AA transgenic mice in the absence (black) and presence (red) of 20 nM TTX. Representative of $n = 13$, 21, and 44 cells, from left to right. Vertical scale bars: 10 pA/pF; horizontal scale bars: 5 ms. (**E**) Graph showing effect of 20 nM TTX on peak Na^+ current. ****$P < 0.0001$ by paired *t* test. For nontransgenic, $P = 0.61$. $n = 13$, 21, and 44 cells from left to right. (**F**) Graph of fraction transgenic Na^+ current for pWT and IQ/AA. Mean ± SEM. $n = 21$ and 44 cells from left to right. $P = 0.73$ by *t* test.

For whole-cell analysis, we normalized $I_{Na,L}$ to the peak Na^+ current in order to account for changes in peak Na^+ current that may occur due to variability in channel expression in a transgenic model [196]. To proceed this way, determination of extracellular Na^+ concentration when taking measurements of peak Na^+ current and $I_{Na,L}$ must be carefully considered due to the low magnitude of $I_{Na,L}$ in relation to the peak (<1%). Nonselective membrane leak or digitization artifacts could corrupt accurate resolution of small-amplitude $I_{Na,L}$ if the driving force is too small. On the other hand, when $I_{Na,L}$ is amplified by large ionic gradients, the amplitude of the peak I_{Na} becomes large and vulnerable to voltage-clamp artifacts. To overcome these limitations,

we devised a protocol whereby the $I_{Na,L}$ is measured using 100 mM Na^+ and the peak Na^+ current is measured using 3 mM or 5 mM Na^+ in the extracellular solution. $I_{Na,L}$ was quantified as the difference in currents during the final 10 ms of a 190-ms depolarization with 100 mM Na^+ in the extracellular solution, before and after application of either TTX or ranolazine, a selective blocker of $I_{Na,L}$ (Figure 2, A-D). After wash-out of ranolazine or TTX, peak current was measured with 3 mM Na^+ in the extracellular solution in the absence and presence of 20 nM TTX for pWT or IQ/AA transgenic mice or 3 mM lidocaine for F1759A transgenic mice. Normalization of $I_{Na,L}$ to the peak Na^+ current yielded a late-current ratio enabling comparison between transgenic models. All recordings were performed with BAPTA in the patch pipette to chelate intracellular Ca^{2+}, thus querying the role of apoCaM.

The late-current ratio was not different between nontransgenic and pWT cardiomyocytes, implying that overexpression of TTX-sensitive pWT in these cells does not increase $I_{Na,L}$ relative to nontransgenic cells (Figure 2E). Similarly, the late-current ratio was not increased in the IQ/AA mice compared with either the late-current ratio in nontransgenic or pWT mice (Figure 2E). This finding was different than previously reported results in a heterologous expression system showing disruption of CaM interaction causes increased $I_{Na,L}$ [72, 73]. Conversely, the late-current ratio from mutant F1759A cardiomyocytes was markedly increased compared with nontransgenic, pWT, and IQ/AA mice (Figure 2, D-E). This is consistent with previous reports of $I_{Na,L}$ investigations of the F1759A mutant in HEK cells [202].

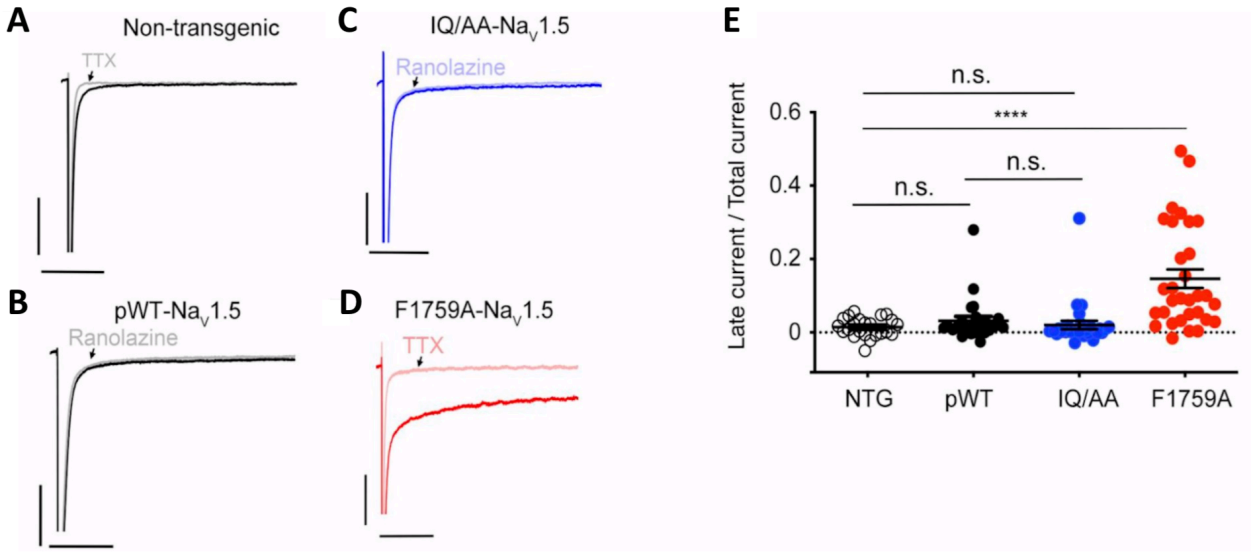

Figure 2. Whole-cell analysis demonstrated late Na^+ current is not increased in cardiomyocytes expressing IQ/AA Nav1.5. (**A–D**) Exemplar whole cell Na^+ current traces of ventricular cardiomyocytes isolated from nontransgenic, pWT, IQ/AA, and F1759A mice. Experiments designed to assess late Na^+ current using a 190 ms depolarization from a holding potential of –110 to –30 mV in the absence and presence of 500 μM ranolazine or 40 μM TTX; intracellular solution contained 5 mM Na^+ and extracellular solution contained 100 mM Na^+. Horizontal scale bars: 50 ms; vertical scale bars: 10 pA/pF. (**E**) Graph of fraction of late Na^+ current normalized to peak Na^+ current. Mean ± SEM, ****$P < 0.0001$ by Kruskal-Wallis test with Dunn's multiple comparison test. $n = 23$, 25, 29, and 31 cardiomyocytes from left to right.

To further dissect $I_{Na,L}$ in the pWT, IQ/AA, and F1759A transgenic models, we undertook cell-attached multichannel recordings to directly measure late-channel openings [67, 203]. A 300 ms depolarizing pulse from a holding potential of -120 to -30 elicits channel openings, as evident in a patch from pWT transgenic mice (Figure 3A). Rapid activation followed by inactivation of multiple channels within the patch result in stacked channel openings reflecting near-macroscopic peak current. Late openings can be observed following 50ms of depolarization and occur to the unitary current level, allowing the distinction from instrument noise and baseline level. For channels from pWT myocytes, we observed sparse late-channel openings, consistent with near-complete inactivation (Figure 3A, shaded area and inset). For each patch, we obtained 50–100 stochastic traces to compute an ensemble average current, which

is equal to the unitary current level (i) x the number of channels in the patch (N) x open probability (P_O). The ensemble average current was subsequently divided by the unitary current level (i) to obtain late NP_O. Peak NP_O is calculated from the ensemble average peak current. To assess late openings, we normalize late NP_O trace by peak NP_O to obtain a normalized time-dependent late P_O waveform for each patch (Figure 3B) and compute the mean value following 50 ms of depolarization (Figure 3G). Like pWT, multichannel recordings from IQ/AA transgenic cardiomyoyctes also showed minimal late-channel openings, as evident from exemplar trace (Figure 3C) and ensemble average (Figure 3D). By comparison, Na^+ channels from F1759A cardiomyocytes showed incomplete inactivation with frequent channel openings 50 ms following depolarization (Figure 3, E and F). The ratio of late-to-peak open probability was significantly increased for F1759A channels but not for IQ/AA channels compared with the control channels (Figure 3G).

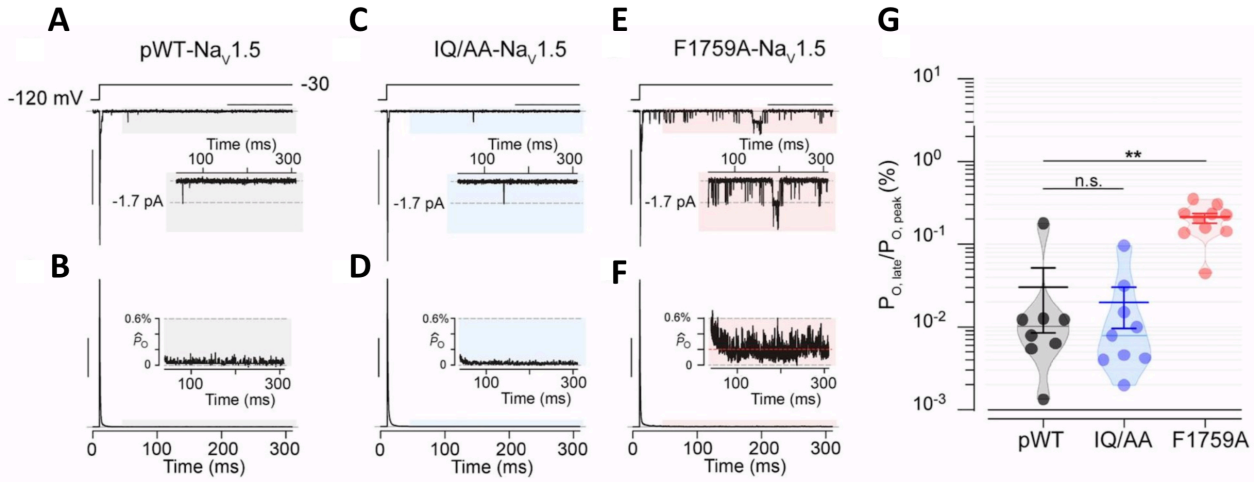

Figure 3. Multichannel macropatch analysis demonstrates late Na^+ current is not increased in cardiomyocytes expressing IQ/AA Na$_V$1.5. (**A**) Multichannel record from pseudo-WT myocyte shows rapid Na^+ channel activation and inactivation, followed by a rare opening in the late phase, following 50 ms of depolarization (gray shaded region). Inset shows lone Na$_V$1.5 opening to unitary current level (dashed line) in the late phase. Vertical scale bar: 10 pA; horizontal scale bar: 100 ms. (**B**) Normalized ensemble-average open probability relation computed from 50–80 stochastic records. Inset shows low levels of late P_O following 50 ms of depolarization. Vertical scale bar:

25% for normalized P_O ($P_O(t)/P_{O,peak}$). $P_O(t)$, time-dependent open probability; $P_{O,peak}$ denotes the peak open probability. (**C** and **D**) Multichannel recordings of Na^+ channels from IQ/AA mice show minimal late current similar to pWT myocytes. Format as in **A** and **B**. (**E** and **F**) Appreciable late Na^+–channel openings were detected for F1759A mutant. Format as in **A** and **B**. (**G**) Graph of P_O normalized to peak P_O. Mean ± SEM, $^{**}P < 0.001$ by Kruskal-Wallis test, $^{**}P < 0.01$ by Dunn's multiple comparison test. Multichannel macropatch analysis performed with the assistance of Nourdine Chakouri and Manu Ben-Johny.

In assessing possible mechanisms that might mask increased $I_{Na,L}$ in our transgenic models, we considered contributions of $I_{Na,L}$ from other Na^+ channel isoforms. $Na_V1.8$ (*Scn10a*) has been reported to play a role in promoting arrythmias, and immunohistochemistry methods have been used to show $Na_V1.6$ (*Scn8a*) expression in the heart [204, 205]. To test what Na^+ channel isoforms are present and are affected by transgene expression, we measured the transcript levels of endogenous mouse *Scn5*a, *Scn8a* and *Scn10a* and transgenic human *SCN5A* in mouse heart samples via rt-PCR. In pWT, IQ/AA, and F1759A mice, human *SCN5A* is substantially expressed (data not shown). *Scn8a* and *Scn10a*, on the other hand, did not reach the significant threshold value after 40 cycles in all mouse hearts, indicating negligible amount of expression.

Our results indicate the existence of $I_{Na,L}$ protective mechanisms present in the cardiomyocyte that are not in heterologous expression systems. We reasoned that a modulator uthat interacts with $Na_V1.5$ may play a protective role in prevention of increased $I_{Na,L}$. FHF proteins have been shown to modify multiple aspects of Na_V channel inactivation and $I_{Na,L}$ is increased in heterologously expressed $Na_V1.5$ channels with mutations at one of the hypothesized binding sites for FGF13 [74]. In heterologous expression systems, co-expression of FGF13 with $Na_V1.5$ reduced $I_{Na,L}$ compared to expression of $Na_V1.5$ alone [206]. We reasoned that FGF13 may be in part responsible for attenuating $I_{Na,L}$ of IQ/AA mutant *in vivo*.

We hypothesized that co-expression of FGF13 with mutant IQ/AA in HEK293 cells rescues the increased $I_{Na,L}$ phenotype previously observed in heterologous expression systems [72, 73]. As a control, we quantified late-channel openings from WT $Na_V1.5$ channels in the presence and absence of FGF13 using multichannel cell-attached recordings. At baseline, WT channels exhibited minimal late-channel openings (Figure 4, A and B), and FGF13 coexpression had no appreciable effect (Figure 4, C, D, I, and J). Per contra, expression of $Na_V1.5$ IQ/AA mutant alone revealed late-channel openings (Figure 4, E and F) with an 11-fold increase in $I_{Na,L}$ (Figure 4, I and J), consistent with previous studies. To mimic the colocalization of FHF with $Na_V1.5$ in cardiomyocytes, we coexpressed FGF13 with $Na_V1.5$ IQ/AA mutant. This maneuver resulted in a complete reversal of $I_{Na,L}$ to WT levels (Figure 4, G-J), suggesting that the addition of FGF13 eliminated $I_{Na,L}$ when the IQ motif was completely ablated and reminiscent of the absence of $I_{Na,L}$ in IQ/AA transgenic cardiomyocytes in which FGF13 is present. These findings suggest that endogenous FGF13 in cardiomyocytes may serve a protective function by preventing pathogenic late Na^+–channel openings.

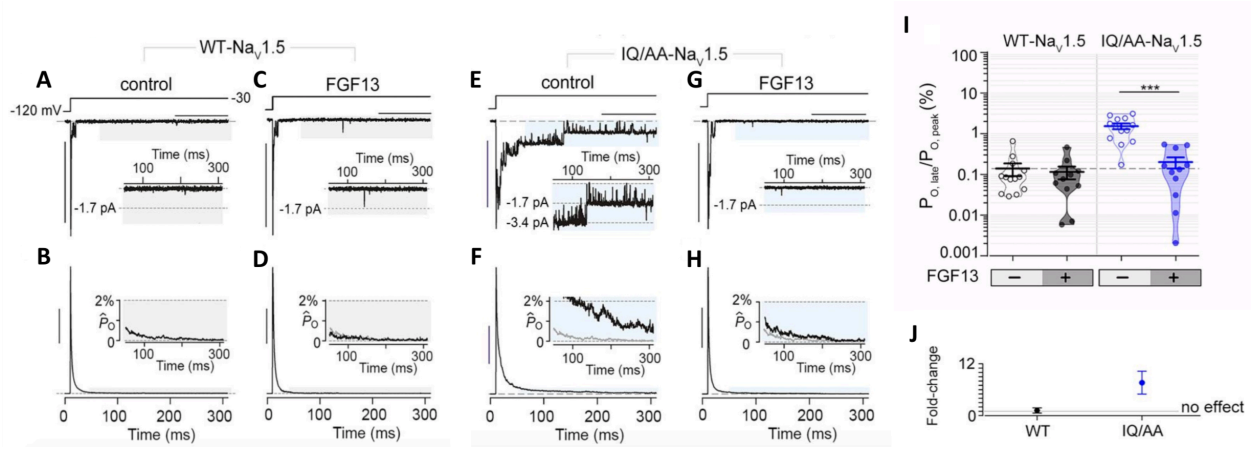

Figure 4. Expression of FGF13 reduces late Na+ current in IQ/AA NaV1.5. (**A** and **B**) Multichannel recordings show minimal late Na^+–channel openings for WT-$Na_V1.5$ expressed in HEK293 cells. Format as in Figure 2, F and G. Horizontal scale bar: 100 ms; vertical scale bar: 10 pA (**A**) and 25% for normalized P_O ($P_O(t)/P_{O,peak}$) (**B**). (**C** and **D**) Late current of WT-$Na_V1.5$ is unaffected by FGF13 overexpression. Same format as in **A** and **B**. (**E** and **F**) IQ/AA $Na_V1.5$ mutant channel showing enhanced late-channel openings compared with WT-$Na_V1.5$ in HEK293 cells. Same format as in **A** and **B**. (**G** and **H**) FGF13 coexpression with IQ/AA $Na_V1.5$ reverses the increase in late current to WT levels. Same format as in **A** and **B**. (**I**) Dot plot summary of $P_{O,late}$ for WT-$Na_V1.5$ and IQ/AA $Na_V1.5$ in the presence and absence of FGF13. Mean ± SEM, $***P < 0.0001$ by Kruskal-Wallis test with Dunn's multiple comparison test. (**J**) Graph shows fold-change in $P_{O,late}$ for WT-$Na_V1.5$ and IQ/AA $Na_V1.5$ by FGF13. Mean ± SEM, computed from aggregate data in **I**. Multichannel macropatch analysis performed with the assistance of Nourdine Chakouri and Manu Ben-Johny.

In cardiomyocytes, F1759A mutants exhibit a substantial $I_{Na,L}$ that causes cardiac arrhythmias in mice [196], raising the possibility that these channels are less sensitive to endogenous protective mechanisms. To test this possibility, we expressed the $Na_V1.5$ F1759A channels in HEK293 cells and undertook multichannel recordings. Similar to cardiomyocytes, recombinantly expressed F1759A mutant display markedly increased late openings (Figure 5, A and B), as previously reported [202]. Interestingly, the amount of $I_{Na,L}$ for F1759A is similar to the IQ/AA mutant in the absence of FHFs. In contrast to IQ/AA mutant, however, FGF13 overexpression exerted negligible effect on the $I_{Na,L}$ of F1759A mutation (Figure 5, C-F), thus confirming the reduced sensitivity of these channels for FGF13. In all, the differential modulation of IQ/AA versus F1759A mutant by FGF13 further elucidates role of FGF13 in tuning a pathogenic $I_{Na,L}$ of cardiac Na_V channels.

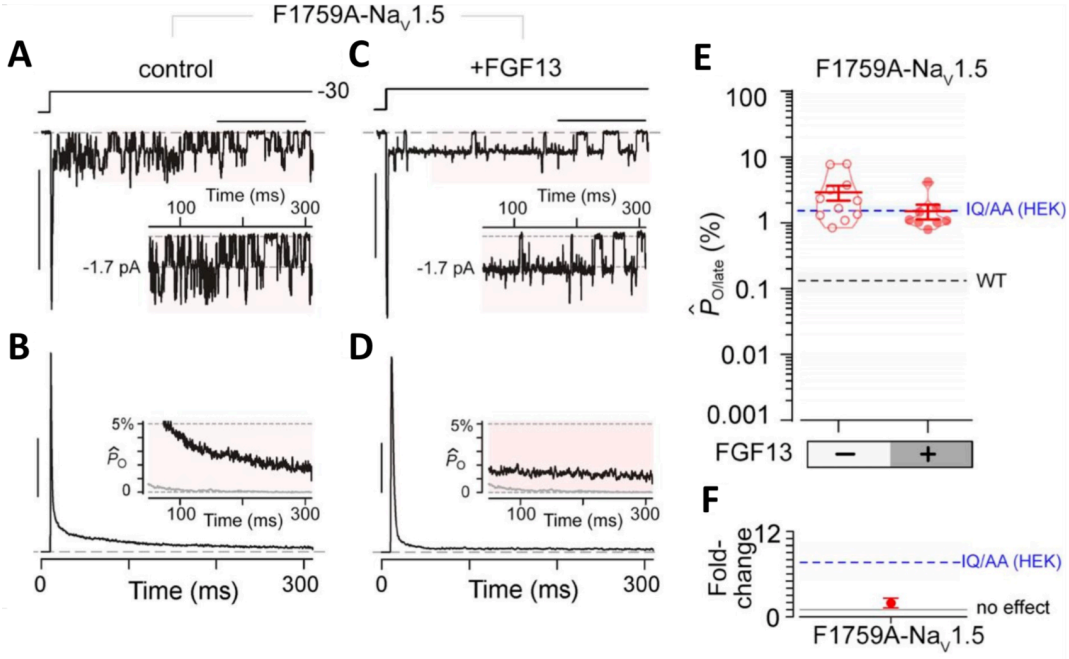

Figure 5. Late Na^+ current for F1759A-Na$_V$1.5 is minimally perturbed by FGF13. (**A** and **B**) Multichannel recordings show high late Na^+ current for F1759A-Na$_V$1.5 mutant when expressed in HEK293 cells. Format as in Figure 3, A and B. Horizontal scale bar: 100 ms; vertical scale bar: 10 pA (**A**) and 25% for normalized P_O ($P_O(t)/P_{O,peak}$) (**B**). (**C** and **D**) FGF13 coexpression with F1759A-Na$_V$1.5 mutant. Horizontal scale bar: 100 ms; vertical scale bar:10 pA (**C**) and 25% for normalized P_O ($P_O(t)/P_{O,peak}$) (**D**). (**E** and **F**) Population data confirm minimal change in late P_O for F1759A-Na$_V$1.5 with FGF13. Format as in Figure 7 I and J. Open probability of late Na^+ current from heterologously expressed IQ/AA Na$_V$1.5 (without FHF13) is shown by the dashed blue line. Multichannel macropatch analysis performed with the assistance of Nourdine Chakouri and Manu Ben-Johny.

2.4 Discussion

Increased $I_{Na,L}$ originates from failure of Na$_V$1.5 inactivation or the slowing of inactivation. Although $I_{Na,L}$ amounts to as little as 1% of the INa peak magnitude, increased $I_{Na,L}$ has been demonstrated in several mutant channels that associate with LQT3 [207]. Aberrant $I_{Na,L}$ counteracts repolarization and results in heterogenous action potential prolongation that may trigger atrial or ventricular arrhythmias [196, 208]. Sustained Na^+ influx also causes structural abnormalities such as those linked to dilated cardiomyopathy [209]. In heterologous expression systems, CaM was shown to regulate of $I_{Na,L}$ after mutations on the IQ motif demonstrated altered inactivation properties [72, 73]. This finding and multiple subsequent studies of

recombinant channels in heterologous expression systems has led to the current dogma that CaM is a powerful regulator of cardiac channels. We sought to test this result in in the native cardiomyocytes. To do this, we utilized an inducible platform for acutely expressing mutant $Na_V1.5$, minimizing previously reported electrophysiological abnormalities to investigate the primary effects of altered CaM binding. To this point, acute overexpression of transgenes did not alter ventricular repolarization, assessed by both QT interval assessment and optical voltage mapping, in pwt or IQ/AA cardiomyocytes relative to non-transgenic cells (data not shown) [208]. Furthermore, Na^+ current conveyed by the transgenic channels was isolated by pharmacological approaches, allowing us to specifically distinguish functional alterations of mutant channels from endogenous wild-type channels in the same cells.

To our surprise, we found that IQ/AA mutant did not increase $I_{Na,L}$ in cardiomyocytes. Both whole-cell analysis of $I_{Na,L}$ normalized to peak Na^+ current and multichannel macropatch analysis of late P_O normalized to peak P_O showed that each of these ratios from measurements in IQ/AA cardiomyocytes were not significantly different than those in pWT cardiomyocytes. These findings suggest the existence of endogenous protective mechanisms that counteract the increase in $I_{Na,L}$ that occurs with loss of CaM binding. We reasoned that additional $Na_V1.5$ interactors present in cardiomyocytes but perhaps not in HEK cells might play a role in tuning $I_{Na,L}$. FGF13 has been previously implicated in the regulation of $I_{Na,L}$ [74, 75]. Upon further investigation, FGF13 overexpression in HEK293 cells fully reversed the $I_{Na,L}$ phenotype of IQ/AA but minimally perturbs F1759A mutant.

CaM regulation of Na^+ channels is complex, with differing effects dependent on the expression system used, the channel isoform, and the presence of Ca^{2+}. For $Na_V1.5$, mutations in the IQ region on the C-terminus has been shown to diminish CaM interaction with $Na_V1.5$ [210]. Although the IQ domain of $Na_V1.5$ binds to both Ca^{2+}-free CaM and Ca^{2+}/CaM, [199, 200], prior analysis of endogenous $Na_V1.5$ in guinea pig ventricular myocytes revealed no Ca^{2+}-dependent effects [71]. $Na_V1.4$, by comparison, exhibits a reduction in peak current after transient elevation of intracellular Ca^{2+} concentration. We performed whole-cell experiments with BAPTA in the pipette solution, thus querying the role of apoCaM binding to $Na_V1.5$. Although BAPTA was not used in our multichannel recordings, we demonstrated the same findings of minimally perturbed $I_{Na,L}$ in IQ/AA cardiomyocytes. Our results demonstrate the differences in channel regulation between $Na_V1.5$ channels expressed in heterologous expression systems and cardiomyocytes. While loss of apoCaM preassociation to the $Na_V1.5$ IQ motif results in a marked elevation of $I_{Na,L}$ in heterologous systems, this effect is not observed in native cardiomyocytes.

The absence of an altered phenotype in cardiomyocytes and the rescue of the relatively increased $I_{Na,L}$ in HEK cells by FGF13 suggest that FGF13 plays a protective, and perhaps redundant, role in cardiomyocytes. FGF13 knockdown in mice leads to reduced Na^+ current density and decreased channel availability with a left shift in channel steady state inactivation [211]. Not unlike regulation of $Na_V1.5$ by CaM, inconsistent reports of $I_{Na,L}$ modulation by FGF13 have also been reported. Yang et al. showed that FGF13 had no effect on $I_{Na,L}$ in tsA201 cells and regulated steady state properties in an isoform-specific manner [212]. Only a year later did Burel et al. show that FGF13 decreased $I_{Na,L}$ in HEK293 cells, consistent with our

multichannel macropatch results in the same cell line [206]. Furthermore, these results were abrogated with $Na_V1.5$ mutants mimicking CAMKII phosphorylation, indicating that FGF13 interaction with the C-terminal tail is influenced by post-transitional modification. These results exemplify the variability in results from different cell types, even among heterologous expression systems. Consistent with the effect observed in HEK cells, conditional knockout of FGF13 in mouse hearts led to a prolonged action potential duration [213]. Future studies that knock out FGF13 in the IQ/AA transgenic model will help ascertain the precise contribution of FGF13 in attenuating the $I_{Na,L}$ in the setting of reduced CaM binding.

Based upon our results, we conclude that CaM and FGF play a redundant role in the heart to prevent arrhythmogenic increases in $I_{Na,L}$. This fails to explain, though, why human mutations in the IQ region such as Q1909R lead to LQT3 and arrhythmias [214]. One explanation is that FGF12, the predominant isoform in the human heart, does not prevent the increase in $I_{Na,L}$ in humans as FGF13 does in mice. FGF13 binds to the C-terminus of murine $Na_V1.5$ with an isothermal calorimetry–determined (ITC-determined) affinity of 16.6 nM, which is approximately 10-fold higher than the affinity of FGF12B which is the FHF isoform expressed in human cardiomyocytes [199]. Studies of inducible pluripotent stem cell–derived differentiated cardiomyocytes may further delineate the role of FGF12 in tuning CaM-deficient $Na_V1.5$ channels in humans. It also remains possible that post-translational modifications such as those described by Burel et al. reduce the interaction of FGF12 and $Na_V1.5$, unveiling the requirement for $I_{Na,L}$ tuning by CaM. Several cellular conditions have been shown to upregulate $I_{Na,L}$ including heart failure [215] and hypoxia [216], corroborating possibility that the phenotype of Q1909R manifests in specific circumstances. Finally, altered C-terminal interaction with other

protein regulators have been shown to influence $I_{Na,L}$ [76-78]. Future studies conducted in cardiomyocytes will delineate the involvement of endogenous factors.

2.5 Conclusion

The effect of IQ/AA mutation to increase $I_{Na,L}$ in heterologous expression systems has been established in the field for over 15 years. This finding and multiple subsequent studies of recombinant channels in cell lines has led to the dogma that CaM is a powerful regulator of cardiac channels. Here we have explored the effects of disrupting CaM binding to $Na_V1.5$ in cardiomyocytes. Our finding that IQ/AA mutant showed no apparent change in $I_{Na,L}$ in cardiac myocytes exemplifies the importance of performing experiments in native cells. Finally, we found that FGF13 diminished $I_{Na,L}$ of the IQ/AA, suggesting that endogenous FHFs may serve to prevent $I_{Na,L}$ in mouse cardiomyocytes.

Chapter 3: Dystrophin Deficiency-Induced Changes in Cardiac $Na_V1.5$ Macromolecular Complex Identified Using Proximity Proteomics

3.1 Background

SCN5A-encoded $Na_V1.5$ channels drive the rapid inward depolarizing current that initiates the cardiac action potential, thereby affecting proper cardiac impulse propagation and conduction through the myocardium [217]. Abnormalities in Na^+ channel function cause a broad spectrum of cardiac arrhythmias, such as LQT3, Brugada syndrome, atrial fibrillation, and heart failure [196, 209]. Some of these $Na_V1.5$-related clinical phenotypes are not solely accounted for by mutations in $Na_V1.5$. Normal physiologic function of $Na_V1.5$ has been shown to depend on the interaction of the channel with several proteins [84] and mutations in the genes that code for these regulating proteins have pathological consequences [218, 219]. These regulators exert an effect on $Na_V1.5$ in different ways, with some acting as adaptor proteins to traffic and anchor $Na_V1.5$ to the sarcolemma, some playing an enzymatic role in post-translationally modifying the channel, and some directly binding to and modulating the biophysical properties of $Na_V1.5$. Although several studies have provided details on the regulation of $Na_V1.5$ by other proteins, insights into how $Na_V1.5$ function is altered in disease through access to modulators of the $Na_V1.5$ macromolecular complex remain incomplete.

In this chapter, we apply proximity labeling and multiplexed quantitative proteomics approaches to define the $Na_V1.5$ macromolecular complex in healthy murine hearts and identify alterations in the early stages of Duchenne muscular dystrophy (DMD), in which the absence of dystrophin predisposes affected individuals to arrhythmias and cardiac dysfunction [121]. Although DMD is characterized by a relentless decline in skeletal muscle function, the major causes of death for individuals affected by DMD are arrhythmias and cardiac failure [220].

Dystrophin serves both as a protein cytolinker within the sarcolemma membrane dystrophin glycoprotein complex (DGC), which mediates mechanoprotective crosstalk between the cardiomyocyte cytoskeleton and the extracellular matrix [221]. The absence of dystrophin results in the dispersion of the DGC protein complex [222], altered ion channel function [223-225], a disorganized microtubule cytoskeleton [129, 130], and increased oxidative stress [126, 134], which in the DMD heart can initiate congestive heart failure and arrhythmias.

$Na_V1.5$ expression in the cardiomyocytes is hypothesized to segregate into different subcellular "pools" where they interact with location-specific proteins. Two pools have been described: one at the intercalated disc and one at the lateral membrane and t-tubules [106]. At the intercalated disc, $Na_V1.5$ interacts with connexin-43 [226], plakophilin-2 [96], and ankyrin-G [96] among other proteins, whereas $Na_V1.5$ at the lateral membrane associates with the DGC [85]. Interaction of the $Na_V1.5$ C-terminal PDZ domain-binding motif (SIV motif) with DGC members syntrophin and dystrophin (via syntrophin) was established by Gavillet et al [103]. They showed that, in the dystrophin-deficient *Dmd*^{mdx} mouse model, there was a significant ~50% reduction in $Na_V1.5$ expression and a corresponding ~30% decrease in whole-cell Na^+ current density. The conclusion was made that expression and function of $Na_V1.5$ at the lateral membrane is dependent upon its association with dystrophin and syntrophin. When expressed in HEK293 cells, mutations in α-syntrophin, however, caused ~1.5-fold increase in peak Na^+ current and ~2.5-fold increase in persistent Na^+ current [76], findings that are inconsistent with studies in cardiomyocytes and suggest cell type-specific regulatory mechanisms. Since the DGC complex is absent from the intercalated disc [227, 228], investigations of proteins that bound to the SIV motif at the this region revealed the interaction between $Na_V1.5$ and SAP97 [229, 230]. Knock-down of SAP97 in cultured

rat atrial myocytes via shRNA reduced sodium current density by 66%, and reduced $Na_V1.5$ immunostaining in ventricular rat heart tissue [229]. Dependence of $Na_V1.5$ expression on SAP97 was later challenged in reports of unaffected $Na_V1.5$ current and localization at the intercalated disc in SAP97 knockdown mice [231]. Again, differences in experimental models likely explain the discrepancy in results.

Cell-attached macropatch recordings have offered further insights on the macromolecular interactions and compartment-specific functions of $Na_V1.5$ at the lateral membrane and the intercalated disc. By placing electrodes and recording current from $Na_V1.5$ channels specifically at the lateral membrane and intercalated disc, Lin et al showed that at the intercalated disc, $Na_V1.5$ peak current was significantly larger, steady-state inactivation was more depolarized, and recovery from inactivation was faster, indicating that action potential upstroke results mostly from $Na_V1.5$ at the intercalated disc rather than those at the lateral membrane [108]. Macropatch analysis of hearts of knock-in mutant mice that lacked the SIV domain (ΔSIV) showed about a ~62% reduction of peak current at the lateral membrane, while peak current was unaffected at the intercalated disc [104]. A ~60% decrease in $Na_V1.5$ whole-cell current and reduction in channel immunostaining at the lateral membrane was also observed, indicating interaction of syntrophin with the SIV motif is required for partial expression of $Na_V1.5$ at the lateral membrane. It was proposed that the remaining current at the lateral membrane originates from $Na_V1.5$ channels at the T-tubules, although dystrophin and other DGC members are also expressed at the T-tubule [227, 232, 233]. Other explanations are that syntrophin is binding to the N-terminus in ΔSIV mice [234], or that a subset of $Na_V1.5$ channels at the lateral membrane are independent of the DGC. These hypotheses were subsequently tested with a syntrophin knockdown mouse, where

macropatch experiments demonstrated a ~24% decrease in lateral membrane $Na_V1.5$ current compared to control [105]. This decrease was not significantly different than macropatch currents at the lateral membrane in ΔSIV knock-in mice, suggesting the existence of $Na_V1.5$ channels at the lateral membrane that are independent of syntrophin and the SIV motif. $Na_V1.5$ expression was subsequently confirmed in the cardiomyocyte T-tubules by Vermij et al. using high-resolution single-molecule localization microscopy (SMLM). By quantifying colocalization of $Na_V1.5$ with T-tubule marker Bin-1, Vermij et al. showed that T-tubular $Na_V1.5$ expression is increased in cardiomyocytes from 16-week old *Dmd*^{mdx} mice, although the functional effect of this sub-compartment of $Na_V1.5$ remains in question as this group showed that whole-cell $Na_V1.5$ current was not different between control and detubulinated cells.

3.2 Experimental Design and Approach

Macromolecular complexes consisting of numerous proteins with specific roles are common and requisite functional units in cellular biology. Several techniques have been used in past studies to identify interactors and near-neighbors of $Na_V1.5$, but there are several limitations to the approaches used. The most frequently used approach to identify these interacting proteins has been based upon hypothesis-driven immunoprecipitation or immunohistochemistry, but these types of experiments inevitably result in a biased view of the numbers and types of interactions that may exist [235]. Even among those directly interacting proteins, many interactions may have dissociation constants >10-100 μM and fast off-rate constants such that after cell lysis with detergents, detection by immunoprecipitation methods is impossible [236]. To identify proteins within spatially resolved and potentially weakly interacting multicomponent complexes as they occur *in vivo*, we have adapted the APEX2 proximity labeling method [179, 237, 238]. After

application of biotin-phenol for 30 minutes, then H_2O_2 for 1 minute, APEX2 catalyzes the oxidation of phenol to create highly reactive phenoxyl radicals that are capable of covalently labeling exposed Tyr residues and, to a lesser extent, other electron-rich amino acids [238]. Biotinylated proteins are purified and quantified using tandem mass tag synchronous precursor selection triple-stage mass spectrometry (TMT SPS MS^3). The relative summed peptide TMT signal-to-noise ratio is used for relative protein quantification. We performed a two-tailed student's T-test without correction to determine statistical significance. This approach was previously used to show the biologically relevant change of Rad in proximity of $Ca_V1.2$ α_{1C} and β_2 subunits [179]. We generated transgenic mice with doxycycline-inducible, cardiomyocyte-specific expression of $Na_V1.5$ proteins with APEX2 and a V5 epitope conjugated to the N-terminus (V5-APEX2-$Na_V1.5$) [208], enabling live-cell biotin-labeling of proteins within ~20 nm of the $Na_V1.5$ subunit.

We show that cells isolated from V5-APEX2-$Na_V1.5$ are effective in labeling $Na_V1.5$-proximal proteins, including established $Na_V1.5$ modulators as well as proximal bystanders likely encountered during V5-APEX2-$Na_V1.5$ synthesis, maturation, and trafficking [208]. Although the comparison of samples labeled with the addition of H_2O_2 to no-label control samples without addition of H_2O_2 is useful for identifying proximal neighbors of $Na_V1.5$, this approach is limited in the ability to reveal useful quantitative information on protein dynamics. Hundreds of proteins that are in proximity of V5-APEX2-$Na_V1.5$ from genesis to degradation are labeled due to the complex molecular environment of the cell, making it difficult to distinguish bystanders from channel modulators. The true potential the APEX2 proximity labeling is revealed in comparisons where a perturbation is made, such as after application of a drug or the study of a disease state. In this way, proteins unrelated to the studied process are normalized, reducing the amount of

significantly changing proteins to those that are directly affected by the perturbation.

Here, we characterize of changes in the $Na_V1.5$ macromolecular complex that result from DMD. Dystrophin-deficiency has been shown to have a profound effect on $Na_V1.5$ function, but previous studies have largely described changes in NaV1.5 localization and function, rather than changes in the $Na_V1.5$ macromolecular complex. Using native cardiomyocytes from *Dmd*^{mdx} mice $\leq$ 2 months of age, we describe the fundamental mechanisms that precede the exacerbated phenotype observed in aged *Dmd*^{mdx} mice and human DMD patients. Our results portray a comprehensive view of alterations at the $Na_V1.5$ interactome as well as global changes in protein expression, broadening our understanding of factors that affect $Na_V1.5$ function.

3.3 Results

We adapted for application to cardiomyocytes the APEX2 proximity labeling method [237, 239], an approach we recently used to obtain a comprehensive proteome of $Ca_V1.2$ in cardiomyocytes [179]. We generated transgenic mice with doxycycline-inducible, cardiomyocyte-specific expression of V5-APEX2-$Na_V1.5$. Fusing APEX2 to $Na_V1.5$ did not affect $Na_V1.5$ subcellular localization and function, as assessed by cellular electrophysiology and anti-V5 antibody immunofluorescence (Figure 1A). Incubating isolated ventricular cardiomyocytes from V5-APEX2-$Na_V1.5$ mice with a solution containing biotin-phenol for 30 minutes, then application of H_2O_2 for 1 minute induced robust biotinylation of proteins at the sarcolemma, at the intercalated disk, and in a striated z-disk pattern, coinciding with the pattern of transgenic $Na_V1.5$ expression (Figure 1B).

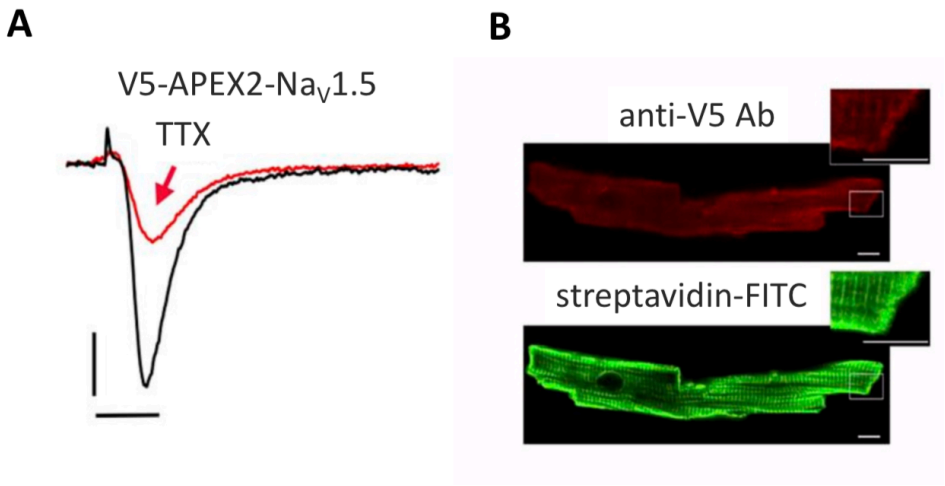

Figure 1. V5-APEX2-Na$_V$1.5 traffics to the cardiomyocyte membrane. (**A**) Exemplar whole cell Na^+ currents recorded from cardiomyocytes of TTX-sensitive Na$_V$1.5-V5-APEX2 transgenic mice, before (black trace) and after (red trace) 20 nM TTX. Representative of 3 similar recordings. Vertical scale bar: 5 pA/pF; horizontal scale bar: 5 ms. (**B**) Immunofluorescence of cardiomyocytes isolated from mice expressing Na$_V$1.5-V5-APEX2 exposed to biotin-phenol and H_2O_2. Staining is with anti-V5– and –Alexa 594–conjugated secondary antibodies (upper) and streptavidin-conjugated Alexa 488. Scale bar: 5 μm.

To probe for proteins that directly regulate Na$_V$1.5, we isolated cardiomyocytes from 4 V5-APEX2-Na$_V$1.5 mice. The cells from each mouse were exposed to biotin-phenol and then were split into 2 aliquots: one population to be labeled with the addition of H_2O_2 and the other without addition of H_2O_2 to be used as a no-label control. We quantified biotinylated proteins using TMT SPS MS^3. From the V5-APEX2-Na$_V$1.5 control mice we identified and quantified hundreds of biotinylated proteins, including proteins known to localize to the three main Na$_V$1.5 subcellular domains in cardiomyocytes: the intercalated disk, T-tubule and Z-disk, and lateral membrane (Figure 2A). Several known Na$_V$1.5 modulators were also identified. Many of the identified proteins are proximal bystanders rather than physically interacting with the channel, including the proteins of nearby organelles, such as subsarcolemmal mitochondria, which functionally couple with Na$_V$1.5 channels [240], or proteins encountered during Na$_V$1.5 synthesis, maturation, and trafficking. Non-significantly changing proteins were categorized as

endoplasmic reticulum membrane (GO:0005789), organelle inner membrane (GO:0019866), and mitochondrial inner membrane (GO:0005743) proteins, demonstrating the relative specificity of V5-APEX2-Nav1.5 in enriching Nav1.5 interactors and near-neighbors.

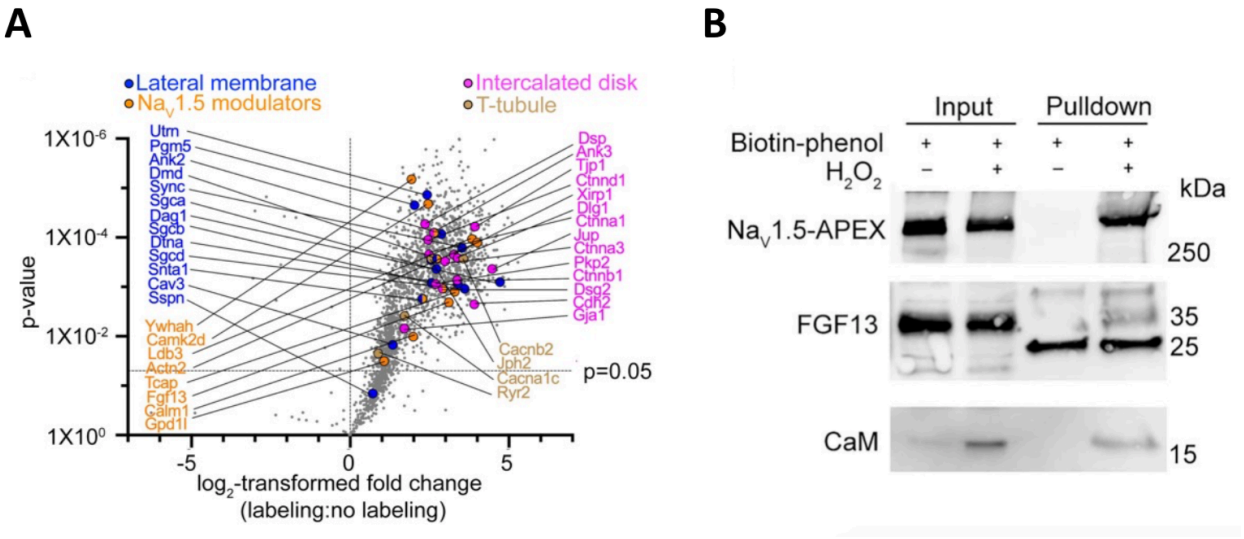

Figure 2. In situ biotin-labeling from V5-APEX2-Nav1.5 mice shows CaM and FGF13 in the Nav1.5 proteome. (**A**) Volcano plot showing differentially biotinylated proteins in V5-APEX2-Nav1.5 expressing cardiomyocytes compared to a no-labeling control. Data shown are means for four matching pairs of unlabeled and labeled sets of cardiomyocytes from four V5-APEX2 mice. Proteins of the lateral membrane (blue), intercalated disk (magenta), T-tubules (grey) and Nav1.5 modulators (orange) are highlighted. Non-adjusted unpaired two-tailed *t*-test. (**B**) Immunoblots of biotin-labeled proteins from cardiomyocytes of Nav1.5-APEX2 mice. NaV1.5, FGF13, and CaM are detected in streptavidin pull-down. Blots are representative of 2 independent experiments.

Both Nav1.5 interactors discussed in the last chapter, CaM and FGF13, were among the proteins enriched by APEX proximity labeling and identified by TMT SPS MS^3. As confirmation, we ran a western blot to show the biotinylation and streptavidin purification of both CaM and FGF13 (Figure 2B), confirming prior studies showing CaM and FGF13 interact with Nav1.5 [73, 198, 206, 241] and consistent with our results showing that CaM and FGF13 modulate Nav1.5 function.

After establishing the utility of V5-APEX2-Nav1.5 in identifying and quantifying proteins

in $Na_V1.5$ macromolecular complexes, our next goal was to apply this approach to define alterations in the $Na_V1.5$ interactome in the early stages of DMD. For all of our experiments, we limited our study to male mice ≤ 2 months of age to avoid macromolecular complex alterations secondary to the dystrophic heart failure phenotype that is characteristic of aged *Dmd*^{mdx} mice. Before performing proteomic analysis, we first applied whole-cell patch clamp analysis to understand the electrophysiologic phenotype of young *Dmd*^{mdx} mice. The peak Na^+ current in cardiomyocytes from *Dmd*^{mdx} mice is reduced compared to control mice (Figure 3A), as was previously reported in mice 10-14 weeks old [103]. Contrasting with previous reports, we found that the V_{50} for steady-state inactivation is shifted by +3.2 mV, indicating that $Na_V1.5$ availability is increased in young *Dmd*^{mdx} mice (Figure 3B).

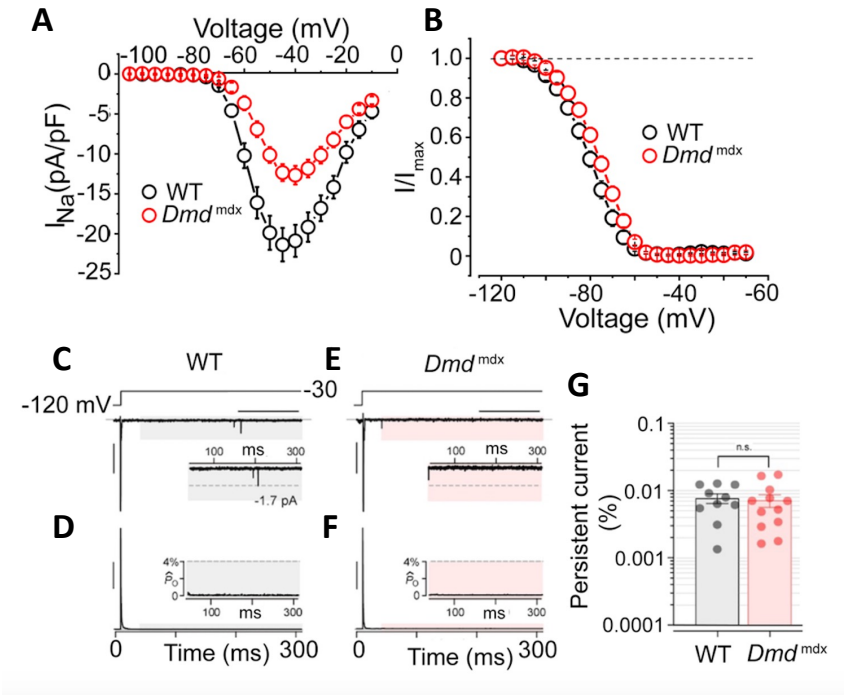

Figure 3. Dystrophin-deficiency causes changes in $Na_V1.5$ current in heart. (**A**) Sodium current-voltage relationship of 2-month-old WT and *Dmd*^{mdx} mice. n=22 for WT, 27 for *Dmd*^{mdx}. $P<0.0001$ at -40 mV by two-tailed *t*-test. The peak sodium current, determined by whole-cell patch clamp, in cardiomyocytes from *Dmd*^{mdx} mice is reduced compared to WT mice. (**B**) The V_{50} for steady-state inactivation is shifted by +3.2 mV. $P<0.05$ at V_{50} by two-tailed *t*-test. (**C, E**) Multi-channel record from WT and *Dmd*^{mdx} myocytes shows rapid sodium channel activation and inactivation followed by a rare opening in the late phase, following 50 ms of depolarization (gray and

pink shaded region for WT and *Dmd*^{mdx}, respectively). Inset shows lone $Na_V1.5$ opening to unitary current level (dashed line) in the late phase. Vertical scale bar = 10 pA, Horizontal scale bar = 100 ms. (**D, F**) Normalized ensemble-average open probability (P_o) relation computed from 50-80 stochastic records. Inset shows low levels of late P_o following 50 ms of depolarization. Vertical scale bar = 25% for normalized P_o. (**G**) Extent of late sodium current ($P_{o,\ late}$ normalized to peak P_o. Mean ± SEM, *P* =non-significant (n.s.) by *t*-test. Loss of dystrophin did not increase late sodium current implying that loss of dystrophin did not affect the inactivation of $Na_V1.5$ channels in cardiomyocytes. Multi-channel macropatch analysis performed with the assistance of Nourdine Chakouri and Manu Ben-Johny.

It was previously reported that mutations in α-syntrophin caused a ~2.5-fold increase in $I_{Na,L}$ in HEK293 cells [76]. To assess $I_{Na,L}$ in *Dmd*^{mdx} mice, we undertook cell-attached multichannel recordings to directly measure late channel openings [67, 203]. A 300 ms depolarizing pulse is used to elicit channel openings in cardiomyocytes from WT and *Dmd*^{mdx} mice (Figure 3, C and E). Rapid activation followed by inactivation of multiple channels within the patch resulted in stacked channel openings reflecting near-macroscopic peak current. For channels from WT and *Dmd*^{mdx} myocytes, we observed sparse late channel openings consistent with near-complete inactivation. For each patch we obtained 50-80 stochastic traces to compute an ensemble average current, which was subsequently divided by the unitary current level to obtain NP_o (channel number X open probability). To determine late current, we normalized NP_o trace by its peak value to obtain a normalized P_o waveform for each patch (Figure 3, D and F) and computed the mean value following 50 ms of depolarization. Loss of dystrophin did not increase late Na^+ current (Figure 3G) implying open-state inactivation of $Na_V1.5$ channels is not affected in early stages of DMD.

To elucidate the basis for the DMD-induced electrophysiological changes, we utilized previously-generated transgenic mice with doxycycline-inducible, cardiomyocyte-specific expression of V5-APEX2-$Na_V1.5$ [208]. These mice were crossed with female *Dmd*^{mdx} mice and,

because DMD is X-linked, we used only male mice for our studies. Isolated myocytes from 2-month-old V5-APEX2-Na$_V$1.5 control mice and V5-APEX2-Na$_V$1.5-*Dmd*^{mdx} mice were incubated with biotin-phenol before initiating labeling with H_2O_2. Western blots confirmed robust biotin-tyramide conjugation of cardiac proteins (Figure 4A). We used dual anti-V5 antibody/Alexa594 and streptavidin-Alexa488 fluorescence to detect localization of the transgenic Na$_V$1.5 channels and the biotin-labeled Na$_V$1.5 proteomic neighborhoods. V5 and streptavidin signals presented alike patterns in both control and *Dmd*^{mdx} cardiomyocytes (Figure 4B), suggesting that the absence of dystrophin causes minimal effects on Na$_V$1.5 subcellular localization.

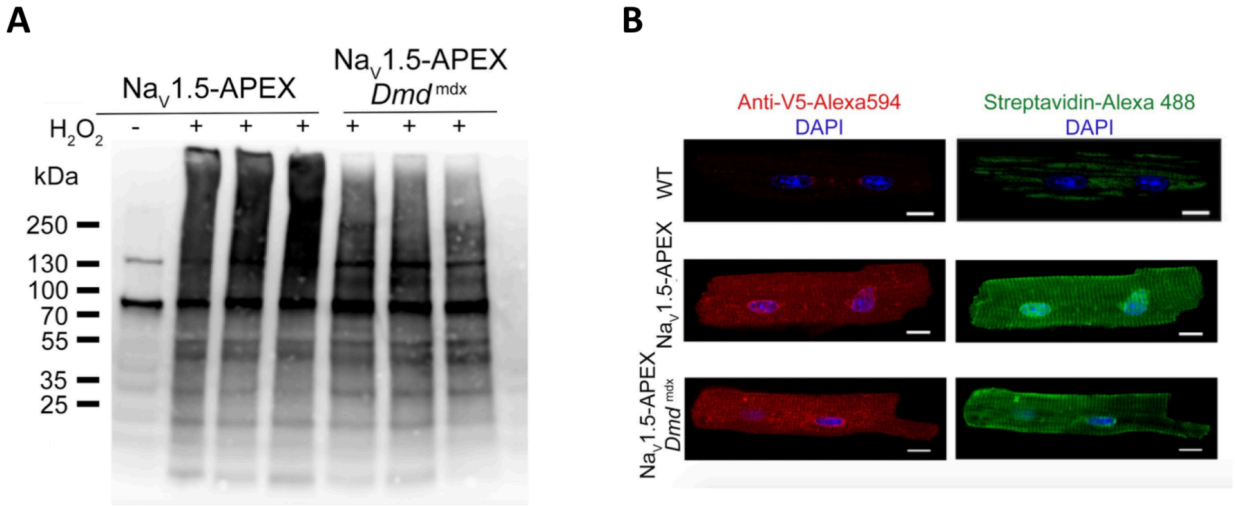

Figure 4. Biotin-labeling of cardiomyocyte proteins in Na$_V$1.5-APEX mice. (**A**) Streptavidin-HRP blot after biotin-labeling of proteins in isolated ventricular cardiomyocytes. Lysates from V5-APEX2-Na$_V$1.5 transgenic mice and V5-APEX2-Na$_V$1.5-*Dmd*^{mdx} were analyzed after proximity labeling (+H_2O_2) compared to no-labeling control (-H_2O_2). (**B**) Immuno-fluorescence of cardiomyocytes isolated from WT (upper), V5-APEX2-Na$_V$1.5 (middle) and V5-APEX2-Na$_V$1.5-*Dmd*^{mdx} (lower) mice exposed to biotin-phenol and H_2O_2. Staining is with anti-V5 and Alexa594-conjugated secondary antibodies (left), and streptavidin-conjugated Alexa488 (right). Nuclear labeling with DAPI stain. Scale bar = 5 μm.

We isolated and labeled cardiomyocytes from five V5-APEX2-Na$_V$1.5 mice and five V5-APEX2-Na$_V$1.5-*Dmd*^{mdx} mice. These samples were combined in a TMT multiplex for subsequent mass spec analysis (Figure 5A). We identified and quantified 3.2 thousand biotinylated proteins

between the two groups, including proteins known to localize to the three main $Na_V1.5$ subcellular domains in cardiomyocytes: the intercalated disc, T-tubule, and lateral membrane (Figure 5, B and C). Although there were several proteins that significantly changed in $Na_V1.5$ proximity between *Dmd*^{mdx} and non-diseased samples, it was unclear whether these alterations were due to recruitment or loss at the $Na_V1.5$ subdomain (from either relocation of $Na_V1.5$ or disease-responsive alterations) or if these alterations were reflective of the whole-cell changes in protein expression. To clarify this, we additionally quantified whole-cell protein lysates (not APEX2-biotinylated proteins) from V5-APEX2-$Na_V1.5$ mice and V5-APEX2-$Na_V1.5$-*Dmd*^{mdx} mice. We identified and quantified 4.9 thousand proteins between the two groups (Figure 5D).

As expected, a reduction in dystrophin by ~ 90% was observed in both the whole-cell and $Na_V1.5$ subdomain proteomes. The abundance of several other members of the DGC (e.g., dystrobrevin, α1-syntrophin and sarcospan) were also similarly reduced [222]. The DGC member utrophin, which increased in abundance both globally and within the $Na_V1.5$ neighborhood, was a notable exception (Figure 5, C and D) [102]. The compensatory increased expression of utrophin in *mdx* striated muscle is partially responsible for the reduced phenotype in murine vs. human DMD [242]. Our finding of increased utrophin within the $Na_V1.5$ neighborhood is also consistent with utrophin functionally compensating for the absence of dystrophin. Importantly, these local and global results are an independent validation of our proximity labeling approach.

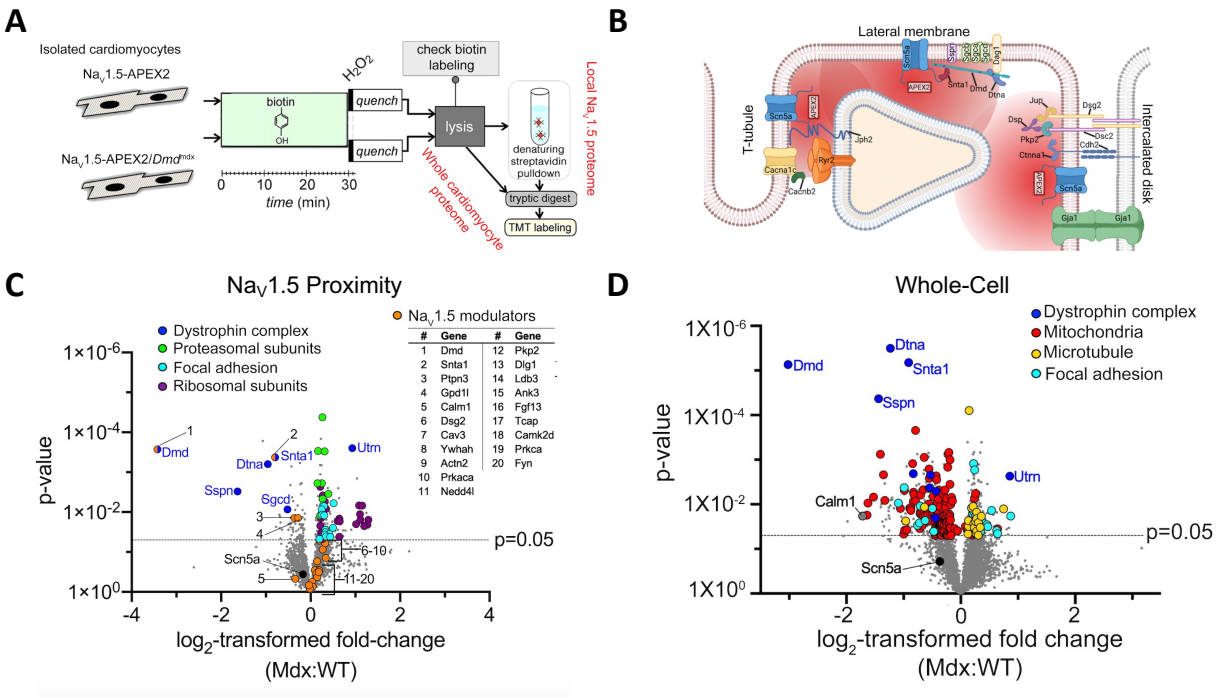

#	Gene	#	Gene
1	Dmd	12	Pkp2
2	Snta1	13	Dlg1
3	Ptpn3	14	Ldb3
4	Gpd1l	15	Ank3
5	Calm1	16	Fgf13
6	Dsg2	17	Tcap
7	Cav3	18	Camk2d
8	Ywhah	19	Prkca
9	Actn2	20	Fyn
10	Prkaca		
11	Nedd4l		

Figure 5. Changes in the cellular and Nav1.5 subdomain proteome induced by dystrophin deficiency. (**A**) Schematic of workflow for isolated cardiomyocytes from V5-APEX2-Nav1.5 and V5-APEX2-Nav1.5-*Dmd*^{mdx} mice. (**B**) Schematic depicting localization of V5-APEX2-Nav1.5 channels and regions of biotinylation at the intercalated disc, lateral membrane and T-tubules (created with Biorender.com). (**C**) Volcano plot of relative protein quantification of V5-APEX2-Nav1.5-*Dmd*^{mdx} and V5-APEX2-Nav1.5 proximal proteome. Data shown are means for five pairs of biologically independent samples. Numbers in plot refer to known Nav1.5 modulators in the inset chart. High-ranked gene ontology (GO) terms for significantly changed proteins in the Nav1.5 subdomain proteome are color-coded.(**D**) Volcano plot of relative protein quantification by TMT mass spectrometry of V5-APEX2-Nav1.5-*Dmd*^{mdx} and V5-APEX2-Nav1.5 whole-cell proteome. N= 3 V5-APEX2-Nav1.5-*Dmd*^{mdx} mice and 5 V5-APEX2-Nav1.5 mice samples. Non-adjusted unpaired two-tailed t-test. High-rank gene ontology (GO) terms for significantly changed proteins in the whole-cell proteome are color-coded.

In addition to the expected reduction in the DGC proteins within the Nav1.5 subdomain proteome of *Dmd*^{mdx} mice cardiomyocytes, gene ontology (GO) analysis demonstrated the enrichment of ribosomal proteins (GO:0022626), focal adhesion proteins (GO:0005925) and proteasomal proteins (GO:0010499) (Figure 5C). The relative abundance of a substantial number of Nav1.5 modulators was unchanged in the Nav1.5 subdomain proteome of *Dmd*^{mdx} cardiomyocytes compared to control cardiomyocytes, with some notable exceptions. We found a ~22% reduction in protein tyrosine phosphatase H1 (Ptpn3), a ~18% reduction of glycerol

phosphate dehydrogenase 1-like protein (Gdp1L), and a ~42% reduction of α1-syntrophin (Snta1). These significant values represent biologically relevant changes comparable to the ~30% decrease of Rad in proximity to $Ca_V\beta$ during β-adrenergic regulation of $Ca_V1.2$ [179]. Intriguingly, loss-of-enzymatic-function mutations in Gdp1L, observed in both Brugada syndrome and sudden infant death syndrome, lead to increased PKC-dependent phosphorylation of $Na_V1.5$ and reduced Na^+ current [243]. Furthermore, decreased Ptpn3 activity causes a shift in the $Na_V1.5$ availability towards depolarizing potentials [244]. Together these changes impact electrophysiology (decreased peak Na^+ current and a depolarizing shift in availability) in parallel to those in dystrophin-deficient cardiomyocytes, hinting that the changes in $Na_V1.5$ function in the *Dmd*^{mdx} mice may be multifactorial.

Our whole-cell dataset, obtained from young mice before the advent of heart failure, provide an informative contrast to a previous label-free mass spectrometric analysis of 20-month-old dystrophin-deficient mice that found changes in the proteome indicative of impaired mitochondrial metabolism, altered Ca^{2+}-handling, deficiencies in the basement membrane, fibrosis-related up-regulation of the extracellular matrix, and a heightened cellular stress response [245]. Some of these changes may have reflected secondary, end-stage processes that are characteristic of heart failure rather than dystrophin-deficiency-induced primary processes. Indeed, gene ontology (GO) analysis of the cardiomyocyte proteome of 2-month-old *Dmd*^{mdx} mice showed limited evidence for deficiencies in the basement membrane, fibrosis-related up-regulation of the extracellular matrix, or a heightened cellular stress response. Rather, the proteome of the 2-month-old *Dmd*^{mdx} mice was marked by an enrichment of focal adhesion proteins (GO:0005925) and microtubule cytoskeleton proteins (GO:0015630), and depletion of mitochondrial and

metabolic proteins (GO:0005739) (Figure 5D). These changes in the cardiomyocyte proteome of 2-month-old mice indicate that substantial alterations in metabolism presage the development of heart failure in older *Dmd*^{mdx} mice [246]. Notable significant whole-cell changes include CaM (Calm1), which was significantly reduced by ~70% globally but non-significantly reduced locally, and N-cadherin (Cdh2), which was significantly reduced by ~41% globally, but unchanged locally in the *Dmd*^{mdx} mice compared to control mice (Figure 5, C and D). These examples highlight the importance of parallel acquisition of whole-cell and local proteomic datasets and suggest a recruitment to the $Na_V1.5$ subdomain of CaM, thereby attenuating late current [72] as we observed in our *Dmd*^{mdx} macropatch experiments, and N-cadherin, which is proposed to enhance adhesion/excitability nodes at intercalated disks [247].

We then queried whether changes in the $Na_V1.5$ interactome within *Dmd*^{mdx} mice cardiomyocytes reflected overall changes in the cardiomyocyte proteome or indicated specific changes to the $Na_V1.5$ interactome. In general, for the proteins showing a significant change in abundance within the $Na_V1.5$ domain proteome, *Dmd*^{mdx}-induced changes in local $Na_V1.5$ neighborhood and the whole-cell proteome were highly correlated and the relationship was well-fit (slope = 1.05) using linear regression, nearly overlapping with the line of identity (Figure 6A). Thus, changes to the $Na_V1.5$ interactome, including focal adhesion and proteasomal proteins, generally reflect overall cellular changes due to loss of dystrophin. A notable exception, however, was that several large and small ribosomal subunit proteins were substantially enriched in the $Na_V1.5$ proteome, but not in the whole-cell proteome, of *Dmd*^{mdx} mice cardiomyocytes.

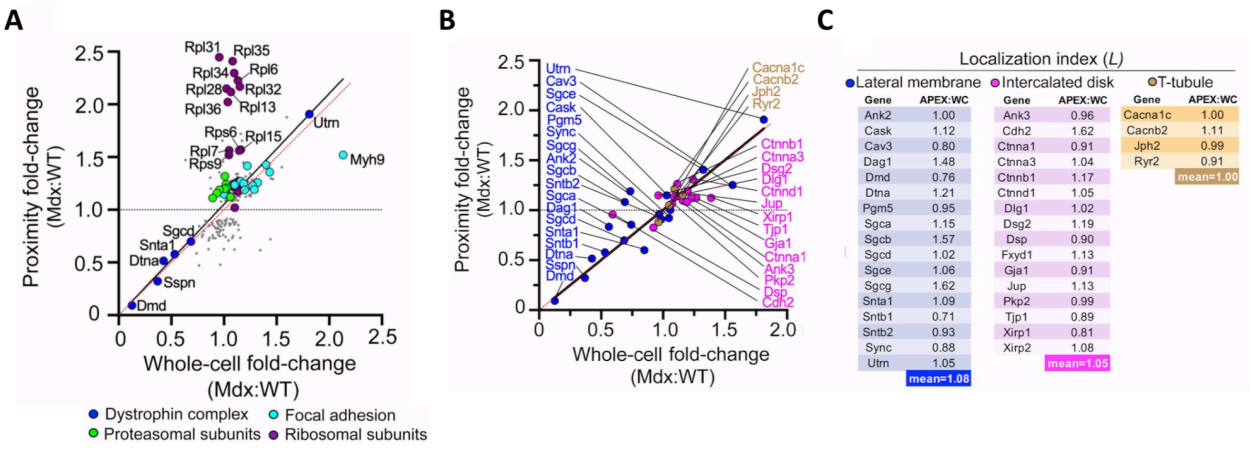

Figure 6. Comparison of *Dmd*^{mdx} proximity and whole-cell changes. (**A**) Graph showing relationship of dystrophin-deficiency induced changes in whole-cell proteome vs. changes within the Na$_V$1.5 subdomain for significantly changed proteins within the proximity of Na$_V$1.5. Linear regression fit (black line) and line of unity (red line) shown. Proteins above dashed line at Y=1 are significantly enriched in the *Dmd*^{mdx} Na$_V$1.5 complex. (**B**) Graph showing relationship of dystrophin-deficiency induced changes in whole-cell proteome vs. changes within the Na$_V$1.5 proximity for proteins principally localized to the lateral membrane, intercalated disk, and T-tubule. Overlapping linear regression fit (black line) and line of unity (dashed red line) shown. (**C**) The localization index, L, was calculated as a ratio of dystrophin-induced changes in Na$_V$1.5 subdomain as measured by proximity proteomics ("APEX") and dystrophin-induced changes in whole cell proteome ("WC"). These ratios are not significantly different (P = 0.73, ANOVA), implying that at early stages, dystrophin-deficiency does not cause redistribution of Na$_V$1.5 channels in cardiomyocytes.

Previous studies suggested that loss of dystrophin in *Dmd*^{mdx} cardiomyocytes and the consequent reduction in syntrophin led to redistribution of Na$_V$1.5 away from the lateral membrane [229], although later studies have suggested the existance of Na$_V$1.5 channels at the lateral membrane with membrane expression independent of syntrophin interation [105, 106]. To further characterize the location of Na$_V$1.5 in 2 week-old *Dmd*^{mdx} mice, we leveraged the neighborhood-specificity of proteins at the lateral membrane, intercalated disk, and T-tubules of cardiomyocytes. We devised a DMD-induced "localization index", *L*, defined as the ratio of local-to-global abundance of a specific protein to triangulate the subcellular localization of Na$_V$1.5 in cardiomyocytes based upon the identified neighbors. For instance, if dystrophin-deficiency induced changes in the local environment of Na$_V$1.5 channels such that the channels were depleted

from the lateral membrane, as was previously reported for *Dmd*^{mdx} mice [104, 229], the macromolecular complexes of $Na_V1.5$ channels would be biased towards proteins specific to the intercalated disk and T-tubule and depleted of lateral membrane-specific proteins and *L* would be < 1 for lateral membrane proteins. We identified subsets of proteins within the $Na_V1.5$ interactome and enriched for the distinct $Na_V1.5$ subcellular locations, and then calculated *L* for each protein and an average *L* for the location-enriched subset (Figure 6, B and C). At the lateral membrane, dystrophin-deficiency-induced changes in both the global and local abundance of most proteins were, for the most part, congruent, reflected by mean *L* of 1.08 for 17 proteins known to principally localize to the lateral membrane of cardiomyocytes. Similarly, the mean *L* was 1.05 for 16 proteins known to localize principally to the intercalated disk, and 1.0 for proteins known to localize principally to T-tubules. Together, these data imply that the subcellular distribution of $Na_V1.5$ channels is not substantially changed in *Dmd*^{mdx} cardiomyocytes. Nevertheless, individual outliers suggest some subtle changes to the $Na_V1.5$ interactome in *Dmd*^{mdx} mice cardiomyocytes, perhaps reflecting the remodeled DGC. Within the lateral membrane neighborhood, *L* increased for β and γ-sarcoglycan, indicating that these proteins have greater accessibility to V5-APEX2-$Na_V1.5$, and perhaps are closer to $Na_V1.5$ channels in *Dmd*^{mdx} mice. Within the intercalated disc associated neighbors, N-cadherin (Cdh2) was also an exception (*L*=1.62), as explained above.

3.4 Discussion

Taken together, our findings reveal insights in $Na_V1.5$ macromolecular complex remodeling in a disease state. Our results comparing labeled V5-APEX2-$Na_V1.5$ samples to an unlabeled control revealed proteins that are localized to the three $Na_V1.5$ subcellular compartments at the lateral membrane, the intercalated disc, and the T-tubule. We also identified several known

$Na_V1.5$ interactors including CaM and FGF13. The main findings exhibited in this chapter focus on the proteomic alterations of $Na_V1.5$ in dystrophin-deficient *Dmd*^{mdx} cardiomyocytes, a cellular model for Duchenne muscular dystrophy. We identified novel and known effects of dystrophin-deficiency on protein dynamics in the $Na_V1.5$ macromolecular complex as well as at the whole-cell level. We additionally used proximity proteomics to conclude that at an early stage of muscular dystrophy in mice, before heart failure has developed, $Na_V1.5$ channels localize with interacting proteins at the lateral membrane, T-tubule, and intercalated disc compartments in cardiomyocytes. This is in agreement with the hypothesis that the expression of some $Na_V1.5$ channels at the lateral membrane are not dependent of an intact DGC [105, 106]. While our findings confirm prior reports demonstrating that the $Na_V1.5$ macromolecular complex is altered in *Dmd*^{mdx} mice, our data do not reveal a significant redistribution among the key $Na_V1.5$ neighborhoods. Our results are novel in the use of quantitative TMT for cardiac mdx proteomic analysis and the application of proximity proteomics in a disease state mouse model.

Proteins related to focal adhesion, ribosomes, and proteasomal degradation are enriched in the $Na_V1.5$ neighborhood in the V5-APEX2-$Na_V1.5$-*Dmd*^{mdx} mice. These results can be interpreted in several ways. In cardiomyocytes, costameres are Z-line-associated structures that transmit contractile forces generated within the cardiomyocyte directly to the surrounding ECM [248]. There are two major protein complexes have been described at the costamere: the DGC and the integrin–vinculin–talin complex (IVTC), both of which play mechanical stabilizing and signaling roles in mediating interactions between the cytoskeleton, membrane, and extracellular matrix [221, 249]. The IVTC is analogous to the focal adhesion complex present in in non-muscle cells and it has been shown that almost all the same proteins that comprise the IVTC eventually reassemble

within focal adhesions cultured cardiomyocytes [250, 251]. It is likely that the proteins that were categorized as focal adhesion in our gene ontology analysis (GO:0005925) are actually proteins of the IVTC. Interestingly, it's been demonstrated that focal adhesion proteins in skeletal muscle are upregulated in dystrophin-deficient mice and protect against sarcolemmal damage [252, 253]. Our observations indicate that proteins of the IVTC may be upregulated at the costamere to compensate for the disrupted DGC observed in *Dmd*^{mdx} mice. Furthermore, relocation of ribosomes to focal adhesion complexes is dependent on complex mechanical coupling to ECM, perhaps explaining the dual increase of focal adhesion and ribosomal proteins in the *Dmd*^{mdx} $Na_V1.5$ environment, although these prior observations were made in non-muscle cell types [254, 255]. At the intercalated disc of the cardiomyocyte, enrichment of transcripts and translational machinery has been shown to increase upon hypertrophic stimulation [256]. The specific function of many of the significant ribosomal proteins recovered in our results is not known, although Rps6 regulates pro-survival ribosomal signaling [257]. The increased abundance of proteasomal proteins along with the reduced $Na_V1.5$ current in *Dmd*^{mdx} mice cardiomyocytes is consistent with a previous report that proteasomal degradation reduces $Na_V1.5$ protein levels and Na^+ current in dystrophin-deficient cardiomyocytes [258]. Dual increases in ribosomal and proteasomal proteins could be reflective of increased rates of protein synthesis and degradation in *Dmd*^{mdx} mice [259]. Future work in determining the effect of increased proximity of ribosomal and proteasomal proteins on $Na_V1.5$ functions may lead to therapeutic insights.

Our whole-cell proteomic results show enrichment of microtubule cytoskeleton proteins and focal adhesion proteins, and reduction of mitochondrial and metabolic proteins in our model for the 2-month-old *Dmd*^{mdx} mice. Differential expression patterns of mitochondrial and metabolic

proteins were previously described in 20-month-old dystrophin-deficient mice, although it was unclear if this was causal or adaptive [220, 245]. By using mice ≤ 2 months of age and minimizing involvement of cell death, fibrosis, and heart failure, our results suggest that an altered mitochondrial redox state precedes these events in increasing intracellular ROS that is known to contribute to the development of DMD [126, 260, 261]. The whole-cell proteomic results additionally align with reports detailing a denser and disorganized microtubule cytoskeleton described in dystrophin-deficient muscle [129, 130]. Of note, $Na_V1.5$ traffics to the cell membrane via microtubules and preferentially localizes to the N-cadherin-rich area composita, a process that is dependent on connexin-microtubule interaction at the intercalated disc [91, 262]. Interestingly, movement of connexin-43 from the intercalated disc to the lateral membrane has been described in *Dmd*^{mdx} mice, likely resulting from a disorganized microtubule network [131, 263]. Our studies show no significant whole-cell alterations in expression nor changes in $Na_V1.5$ proximity of connexin-43, and our APEX2 assay is not suitable to assess connexin-43 lateralization. N-cadherin, though, is significantly decreased at the whole-cell level but proximity to $Na_V1.5$ is unchanged, perhaps reflecting the presence of compensatory mechanisms that crucially preserve $Na_V1.5$ expression at the intercalated disc in the setting of altered connexin-microtubule interaction.

We found that many proteins that have previously been shown to modulate $Na_V1.5$ do not significantly change in proximity to $Na_V1.5$ between control and *Dmd*^{mdx} samples, with the exception of dystrophin, syntrophin, Gpd1l, and Ptpn3. Dystrophin and syntrophin were expected to decrease at the global and proximal level and it was previously hypothesized that loss $Na_V1.5$ interaction with these proteins results in a decrease in lateral membrane expression and concurrent

decrease in Na^+ current [103]. Our results showing a proximal decrease in Gpd1l and Ptpn3, a decrease in $Na_V1.5$ peak current, and a significantly right-shifted steady-state inactivation indicate that $Na_V1.5$ disfunction in *Dmd*^{mdx} might be multifactorial. Loss-of-enzymatic mutations in Gpd1l attenuate peak Na^+ current in heterologous expression systems and neonatal mouse myocytes [264, 265], resulting from increased PKC phosphorylation of $Na_V1.5$ [243]. For future experiments, we plan on applying a PKC inhibitor to cardiomyocytes isolated from *Dmd*^{mdx} mice and measuring peak Na^+ current. It is also possible that other proteins that regulate $Na_V1.5$ might be phosphorylated by the GPd1l pathway. For Ptpn3, loss-of-enzymatic mutations were shown to shift the voltage dependence of $Na_V1.5$ steady-state inactivation in a depolarized direction [244]. Ptpn3 is hypothesized to counter Tyr phosphorylation of $Na_V1.5$ by Fyn kinase and is dependent on the C-terminal SIV motif on $Na_V1.5$. Similar to experiments on Gpd1l, we are planning on applying a Tyr phosphatase inhibitor to *Dmd*^{mdx} cardiomyocytes to determine if reversal of the shift in steady-state inactivation occurs. Mass spectrometry phosphoproteomic analysis will also be important for determining if $Na_V1.5$ is differentially phosphorylated in *Dmd*^{mdx} cardiomyocytes. Finally, interaction of least four proteins (syntrophin, SAP97, CASK, and Ptpn3) with $Na_V1.5$ is dependent or influenced by the SIV motif, and knock-in mice lacking the SIV domain (ΔSIV) showed reduced $Na_V1.5$ expression by ~25% and Na^+ current by ~37% [104]. Future studies using proximity proteomics can elucidate the mechanisms behind the ΔSIV phenotype, while also revealing information on site-specificity and macromolecular complex components of different $Na_V1.5$ pools.

Although our inducible APEX2 proximity labeling method is a powerful technique for identifying specially resolved transient interactions, there are limitations to our approach.

Doxycycline-inducible transgenic overexpression of $Na_V1.5$ might not represent endogenous placement of $Na_V1.5$ at different subcellular compartments in the cardiomyocyte. The use of H_2O_2 for labeling also raises concern about potential oxidative stress and perturbation of cellular processes, although it was recently shown that addition of H_2O_2 for 1 minute did not statistically change quantification of proteins or post-translational modifications in iPSC-neurons [266]. Finally, the presence of thousands of proteins recovered in our proteomic analysis hinders robust analysis of relevant alterations and underscores the necessity for orthogonal validation. In order to address these limitations, we have generated a knock-in V5-TurboID-$Na_V1.5$ mouse model. TurboID is a biotin ligase that only requires the addition of non-toxic exogenous biotin for proximal labeling [113]. In our knock-in mouse, V5-TurboID-$Na_V1.5$ is expressed under the control of the wildtype gene regulatory elements, leading to expression of the transcript at endogenous levels. The labeling radius of TurboID is more restrictive than that of APEX2 and will provide a specific validation approach for our V5-APEX2-$Na_V1.5$ results. Western blot analysis of cardiomyocytes isolated from homozygous knock-in mice treated with biotin shows robust expression of V5-TurboID-$Na_V1.5$ and biotin-labeling of proteins (Figure 7, A and B).

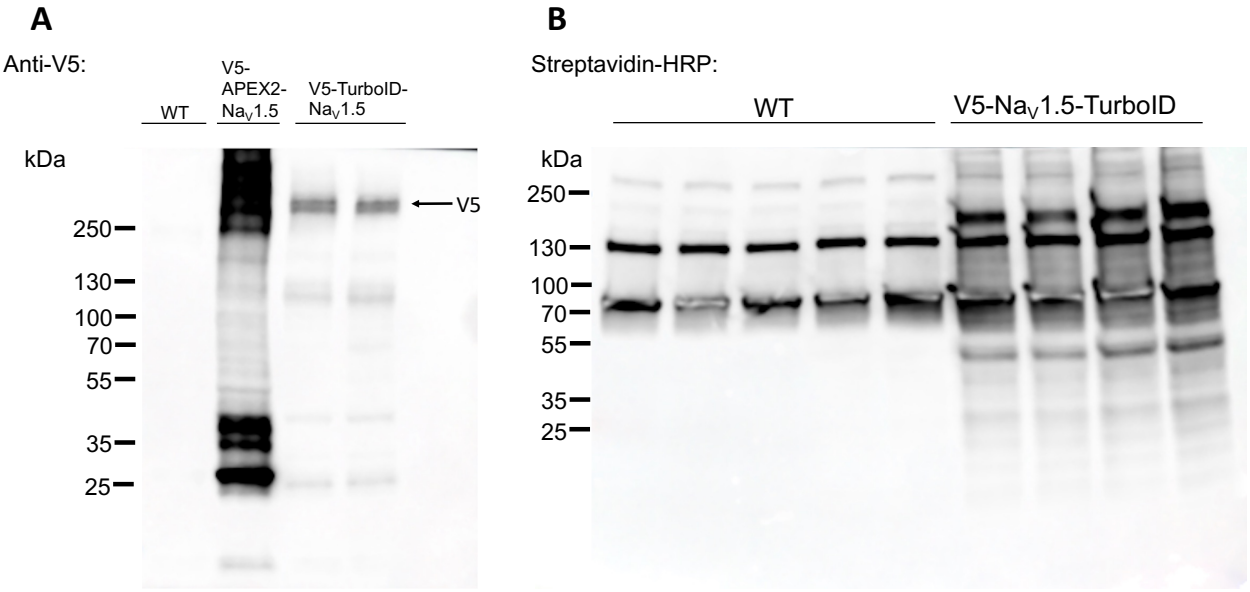

Figure 7. ***In situ*** **V5-TurboID-Na$_V$1.5 expresses and labels proteins.** (**A**) Anti-V5 western blot of lysates from V5-TurboID-Na$_V$1.5 and V5-APEX2-Na$_V$1.5 transgenic mice and wild-type (WT) control. (**B**) Streptavidin-HRP blot after biotin-labeling of proteins in isolated ventricular cardiomyocytes. Lysates from V5-TurboID-Na$_V$1.5 transgenic mice and WT control.

3.5 Conclusion

Evidence linking alterations of Na$_V$1.5 voltage-gated Na^+ channel function to arrhythmias or cardiomyopathy in the absence of Na$_V$1.5 mutations underscores the need to decode the protein components within Na$_V$1.5 macromolecular complexes. Prior studies offered only a superficial view of the Na$_V$1.5 interactome, thus limiting insights into disease-related Na$_V$1.5 dysfunction that is independent of mutations in Na$_V$1.5. Here, we apply proximity labeling and multiplexed quantitative proteomics approaches to define the Na$_V$1.5 macromolecular complex in the healthy murine heart. Additionally, we identified alterations in the early stages of DMD, in which the absence of dystrophin predisposes affected individuals to arrhythmias and cardiac dysfunction. Whole-cell protein expression fold-change results were used to reveal the altered global expression

profile and to place context behind $Na_V1.5$-proximal changes. Finally, we leveraged the neighborhood-specificity of proteins at the lateral membrane, intercalated disc, and T-tubules of cardiomyocytes to demonstrate that $Na_V1.5$ channels can traffic to all three membrane compartments even in the absence of dystrophin, contrary to previous reports. Thus, the approach of proximity labeling in cardiomyocytes from an animal model of human disease offers new insights into molecular mechanisms of $Na_V1.5$ dysfunction in DMD and provides a framework for similar investigations on other cardiac diseases.

Conclusion

Ionic currents were studied in fine detail by Alan Hodgekin and Andrew Huxely in 1952, and it was subsequently shown that these currents were mediated by selective ion channels. Since these discoveries, the critical role of ion channels for normal physiologic function has been extensively demonstrated. $Ca_V1.2$ and $Na_V1.5$ each contribute to the cardiac action potential, rapidly initiating the steep upstroke in phase 0 and balancing K^+ efflux to form the phase 2 plateau, respectively. Functional defects in these channels can occur at any level— from mutations in the genome to altered interactions with enzymes and proteins that modulate the biophysical activity of the channel. Perturbations in channel modulation have been shown to result in electrophysiological and structural disease of the heart. For this reason, understanding the mechanisms and effects of channel modulation is essential for therapy development.

In Chapter 1, we investigated whether the α_{1C} subunit and β_2 subunit of $Ca_V1.2$ are the functional PKA phosphorylation targets for β-adrenergic regulation of $Ca_V1.2$. Increased Ca^{2+} entry into the myocytes via $Ca_V1.2$, mediated by both β_1- and β_2-adrenergic receptors, substantially contributes to the positive inotropic effect of β-adrenergic activation. Dozens of past studies have supported and ruled out putative PKA phosphorylation sites on the α_{1C} and β_2 subunits, complicating the search and leading to no consensus answer. After mutating all putative and predicted PKA phosphorylation sites on the α_{1C} and β_2 subunits, then co-expressing the mutated subunits, we showed that β-adrenergic regulation of $Ca_V1.2$ was unaltered. This provided the definitive answer that neither subunit is the functional PKA phosphorylation site.

These results were the basis for later studies revealing that the Ca^{2+} channel inhibitor Rad is the functional PKA phosphorylation target, a finding that was supported by our demonstration of intact β-adrenergic regulation of $Ca_V1.2$ after heterologous coexpression of Rad with mutant $Ca_V1.2$ subunits.

In Chapter 2, we characterized the disruption of CaM binding to the IQ region on the $Na_V1.5$ C-terminus in cardiomyocytes. The C-terminus is a hotspot for mutations identified in patients with LQT3, which can be caused by an increase in $I_{Na,L}$. Coexpression of $Na_V1.5$ channels mutated at the IQ region (IQ/AA) with CaM in heterologous expression systems causes increased $I_{Na,L}$, leading to the hypothesis that mutations that abrogate the CaM-$Na_V1.5$ interaction in cardiomyocytes also increase $I_{Na,L}$ and are the basis for the observed QT interval prolongation in LQT patients. Surprisingly, we found no differences in $I_{Na,L}$ between cardiomyocytes expressing wild-type $Na_V1.5$ and those expressing mutant IQ/AA $Na_V1.5$. Since prior studies have demonstrated that FGF13 modulates $I_{Na,L}$, we tested the ability of FGF13 to rescue the late current phenotype of IQ/AA channels in HEK293 cells. After confirming prior studies showing increased $I_{Na,L}$ in HEK293 cells expressing IQ/AA channels, we showed that additional coexpression of FGF13 significantly ablated $I_{Na,L}$. We conclude that FGF13 serves as an endogenous protective mechanism in cardiomyocytes that counteracts the increase in $I_{Na,L}$ after loss of CaM binding.

In Chapter 3, we applied proximity proteomics to describe changes in the $Na_V1.5$ macromolecular complex as they occur in living cardiomyocytes. Previous studies of $Na_V1.5$ in dystrophin-deficient *Dmd*^{mdx} cardiomyocytes showed a decrease in Na^+ current and a loss of Na^+

channels specifically from the lateral membrane of the cardiomyocyte, but failed to completely describe alterations of interactions between $Na_V1.5$ and modulating proteins. To do this, we expressed $Na_V1.5$ fused to APEX2 in *Dmd*^{mdx} mice and isolated cardiomyocytes when mice were $\leq$ 2 months of age in order to minimize the effects of dystrophic cardiomyopathy. We first showed that Na^+ current was decreased and voltage-dependence of steady-state inactivation was significantly depolarized in young *Dmd*^{mdx} mice compared to wild-type control mice. Our proteomic analysis revealed changes in the $Na_V1.5$ macromolecular complex that partially accounted for these changes, including a decrease in Ptpn3 and Gdp1l and an increase in proteasomal machinery. Finally, we quantified whole-cell proteomic changes and used these values to define a "localization index" that described the changes in the proximity of subcellular location-specific neighbors of $Na_V1.5$. Localization index values were used to show that $Na_V1.5$ traffics to the intercalated disk, T-tubules, and lateral membrane of the cardiomyocyte. Altogether, our results provide in-depth details on the regulation of Ca^{2+} and Na^+ channels of the heart by enzymes and direct modulators. These mechanistic insights represent a step toward the future development of therapies and our approaches provide a framework for further investigations.

References

1. Catterall, W.A., G. Wisedchaisri, and N. Zheng, *The chemical basis for electrical signaling.* Nat Chem Biol, 2017. **13**(5): p. 455-463.
2. Hille, B., *Ionic selectivity, saturation, and block in sodium channels. A four-barrier model.* J Gen Physiol, 1975. **66**(5): p. 535-60.
3. Nerbonne, J.M. and R.S. Kass, *Molecular physiology of cardiac repolarization.* Physiol Rev, 2005. **85**(4): p. 1205-53.
4. Catterall, W.A., *Voltage-gated sodium channels at 60: structure, function and pathophysiology.* J Physiol, 2012. **590**(11): p. 2577-89.
5. Catterall, W.A., *Voltage-gated calcium channels.* Cold Spring Harb Perspect Biol, 2011. **3**(8): p. a003947.
6. Singh, H.W.a.S., *Modeling of generation and propagation of cardiac action potential using fractional capacitance.* 2015.
7. Buraei, Z. and J. Yang, *The ss subunit of voltage-gated Ca2+ channels.* Physiol Rev, 2010. **90**(4): p. 1461-506.
8. Muller, C.S., et al., *Quantitative proteomics of the Cav2 channel nano-environments in the mammalian brain.* Proc Natl Acad Sci U S A, 2010. **107**(34): p. 14950-7.
9. Catterall, W.A., *Structure and regulation of voltage-gated Ca2+ channels.* Annu Rev Cell Dev Biol, 2000. **16**: p. 521-55.
10. Striessnig, J., *Pharmacology, structure and function of cardiac L-type Ca(2+) channels.* Cell Physiol Biochem, 1999. **9**(4-5): p. 242-69.
11. Link, S., et al., *Diversity and developmental expression of L-type calcium channel beta2 proteins and their influence on calcium current in murine heart.* J Biol Chem, 2009. **284**(44): p. 30129-37.
12. Opatowsky, Y., et al., *Structural analysis of the voltage-dependent calcium channel beta subunit functional core and its complex with the alpha 1 interaction domain.* Neuron, 2004. **42**(3): p. 387-99.
13. Van Petegem, F., et al., *Alanine-scanning mutagenesis defines a conserved energetic hotspot in the CaValpha1 AID-CaVbeta interaction site that is critical for channel modulation.* Structure, 2008. **16**(2): p. 280-94.
14. McDonald, T.F., et al., *Regulation and modulation of calcium channels in cardiac, skeletal, and smooth muscle cells.* Physiol Rev, 1994. **74**(2): p. 365-507.
15. Yue, D.T., S. Herzig, and E. Marban, *Beta-adrenergic stimulation of calcium channels occurs by potentiation of high-activity gating modes.* Proc Natl Acad Sci U S A, 1990. **87**(2): p. 753-7.
16. Hering, S., et al., *Molecular determinants of inactivation in voltage-gated Ca2+ channels.* J Physiol, 2000. **528 Pt 2**: p. 237-49.
17. Zuhlke, R.D., et al., *Calmodulin supports both inactivation and facilitation of L-type calcium channels.* Nature, 1999. **399**(6732): p. 159-62.

18. Morales, D., T. Hermosilla, and D. Varela, *Calcium-dependent inactivation controls cardiac L-type Ca(2+) currents under beta-adrenergic stimulation.* J Gen Physiol, 2019. **151**(6): p. 786-797.
19. Findlay, I., et al., *Physiological modulation of voltage-dependent inactivation in the cardiac muscle L-type calcium channel: a modelling study.* Prog Biophys Mol Biol, 2008. **96**(1-3): p. 482-98.
20. Marks, M.L., D.L. Trippel, and M.T. Keating, *Long QT syndrome associated with syndactyly identified in females.* Am J Cardiol, 1995. **76**(10): p. 744-5.
21. Reichenbach, H., E.M. Meister, and H. Theile, *[The heart-hand syndrome. A new variant of disorders of heart conduction and syndactylia including osseous changes in hands and feet].* Kinderarztl Prax, 1992. **60**(2): p. 54-6.
22. Splawski, I., et al., *Ca(V)1.2 calcium channel dysfunction causes a multisystem disorder including arrhythmia and autism.* Cell, 2004. **119**(1): p. 19-31.
23. Nielsen, M.W., et al., *The genetic component of Brugada syndrome.* Front Physiol, 2013. **4**: p. 179.
24. Sun, X.H., et al., *Molecular architecture of membranes involved in excitation-contraction coupling of cardiac muscle.* J Cell Biol, 1995. **129**(3): p. 659-71.
25. Fawcett, D.W. and N.S. McNutt, *The ultrastructure of the cat myocardium. I. Ventricular papillary muscle.* J Cell Biol, 1969. **42**(1): p. 1-45.
26. Louch, W.E., et al., *Reduced synchrony of Ca2+ release with loss of T-tubules-a comparison to Ca2+ release in human failing cardiomyocytes.* Cardiovasc Res, 2004. **62**(1): p. 63-73.
27. Bers, D.M., *Cardiac excitation-contraction coupling.* Nature, 2002. **415**(6868): p. 198-205.
28. Fabiato, A. and F. Fabiato, *Calcium release from the sarcoplasmic reticulum.* Circ Res, 1977. **40**(2): p. 119-29.
29. Gordon, A.M., E. Homsher, and M. Regnier, *Regulation of contraction in striated muscle.* Physiol Rev, 2000. **80**(2): p. 853-924.
30. Bers, D.M., *Calcium cycling and signaling in cardiac myocytes.* Annu Rev Physiol, 2008. **70**: p. 23-49.
31. Cannon, W.B., *Bodily changes in pain, hunger, fear, and rage; an account of recent researches into the function of emotional excitement*. 1915, New York, London,: D. Appleton and Company. xiii, 311 p.
32. Tsien, R.W., et al., *Mechanisms of calcium channel modulation by beta-adrenergic agents and dihydropyridine calcium agonists.* J Mol Cell Cardiol, 1986. **18**(7): p. 691-710.
33. Turnham, R.E. and J.D. Scott, *Protein kinase A catalytic subunit isoform PRKACA; History, function and physiology.* Gene, 2016. **577**(2): p. 101-8.
34. Roybal, D., J.A. Hennessey, and S.O. Marx, *The quest to identify the mechanism underlying adrenergic regulation of cardiac Ca(2+) channels.* Channels (Austin), 2020. **14**(1): p. 123-131.
35. Kirchberber, M.A., M. Tada, and A.M. Katz, *Phospholamban: a regulatory protein of the cardiac sarcoplasmic reticulum.* Recent Adv Stud Cardiac Struct Metab, 1975. **5**: p. 103-15.

36. Rao, V., et al., *PKA phosphorylation of cardiac troponin I modulates activation and relaxation kinetics of ventricular myofibrils.* Biophys J, 2014. **107**(5): p. 1196-1204.
37. Benkusky, N.A., et al., *Intact beta-adrenergic response and unmodified progression toward heart failure in mice with genetic ablation of a major protein kinase A phosphorylation site in the cardiac ryanodine receptor.* Circ Res, 2007. **101**(8): p. 819-29.
38. Houser, S.R., *Role of RyR2 phosphorylation in heart failure and arrhythmias: protein kinase A-mediated hyperphosphorylation of the ryanodine receptor at serine 2808 does not alter cardiac contractility or cause heart failure and arrhythmias.* Circ Res, 2014. **114**(8): p. 1320-7; discussion 1327.
39. Marx, S.O., et al., *PKA phosphorylation dissociates FKBP12.6 from the calcium release channel (ryanodine receptor): defective regulation in failing hearts.* Cell, 2000. **101**(4): p. 365-76.
40. Wang, Q., et al., *Genomic organization of the human SCN5A gene encoding the cardiac sodium channel.* Genomics, 1996. **34**(1): p. 9-16.
41. Catterall, W.A., *From ionic currents to molecular mechanisms: the structure and function of voltage-gated sodium channels.* Neuron, 2000. **26**(1): p. 13-25.
42. Jiang, D., et al., *Structure of the Cardiac Sodium Channel.* Cell, 2020. **180**(1): p. 122-134 e10.
43. Numa, S. and M. Noda, *Molecular structure of sodium channels.* Ann N Y Acad Sci, 1986. **479**: p. 338-55.
44. Catterall, W.A. and N. Zheng, *Deciphering voltage-gated Na(+) and Ca(2+) channels by studying prokaryotic ancestors.* Trends Biochem Sci, 2015. **40**(9): p. 526-34.
45. Yarov-Yarovoy, V., et al., *Structural basis for gating charge movement in the voltage sensor of a sodium channel.* Proc Natl Acad Sci U S A, 2012. **109**(2): p. E93-102.
46. Guy, H.R. and P. Seetharamulu, *Molecular model of the action potential sodium channel.* Proc Natl Acad Sci U S A, 1986. **83**(2): p. 508-12.
47. George, A.L., Jr., *Inherited disorders of voltage-gated sodium channels.* J Clin Invest, 2005. **115**(8): p. 1990-9.
48. Kellenberger, S., et al., *Molecular analysis of the putative inactivation particle in the inactivation gate of brain type IIA Na+ channels.* J Gen Physiol, 1997. **109**(5): p. 589-605.
49. West, J.W., et al., *A cluster of hydrophobic amino acid residues required for fast Na(+)-channel inactivation.* Proc Natl Acad Sci U S A, 1992. **89**(22): p. 10910-4.
50. Valenzuela, C. and P.B. Bennett, Jr., *Gating of cardiac Na+ channels in excised membrane patches after modification by alpha-chymotrypsin.* Biophys J, 1994. **67**(1): p. 161-71.
51. Wei, J., et al., *Congenital long-QT syndrome caused by a novel mutation in a conserved acidic domain of the cardiac Na+ channel.* Circulation, 1999. **99**(24): p. 3165-71.
52. Bankston, J.R., et al., *A novel LQT-3 mutation disrupts an inactivation gate complex with distinct rate-dependent phenotypic consequences.* Channels (Austin), 2007. **1**(4): p. 273-80.
53. Motoike, H.K., et al., *The Na+ channel inactivation gate is a molecular complex: a novel role of the COOH-terminal domain.* J Gen Physiol, 2004. **123**(2): p. 155-65.

54. Sarhan, M.F., et al., *Crystallographic basis for calcium regulation of sodium channels.* Proc Natl Acad Sci U S A, 2012. **109**(9): p. 3558-63.
55. Van Petegem, F., P.A. Lobo, and C.A. Ahern, *Seeing the forest through the trees: towards a unified view on physiological calcium regulation of voltage-gated sodium channels.* Biophys J, 2012. **103**(11): p. 2243-51.
56. Catterall, W.A., *Structure and function of voltage-gated sodium channels at atomic resolution.* Exp Physiol, 2014. **99**(1): p. 35-51.
57. Balser, J.R., et al., *External pore residue mediates slow inactivation in mu 1 rat skeletal muscle sodium channels.* J Physiol, 1996. **494 (Pt 2)**: p. 431-42.
58. Todt, H., et al., *Ultra-slow inactivation in mu1 Na+ channels is produced by a structural rearrangement of the outer vestibule.* Biophys J, 1999. **76**(3): p. 1335-45.
59. Zaza, A., L. Belardinelli, and J.C. Shryock, *Pathophysiology and pharmacology of the cardiac "late sodium current.".* Pharmacol Ther, 2008. **119**(3): p. 326-39.
60. Belardinelli, L., et al., *Cardiac late Na(+) current: proarrhythmic effects, roles in long QT syndromes, and pathological relationship to CaMKII and oxidative stress.* Heart Rhythm, 2015. **12**(2): p. 440-8.
61. Bennett, P.B., et al., *Molecular mechanism for an inherited cardiac arrhythmia.* Nature, 1995. **376**(6542): p. 683-5.
62. Nuyens, D., et al., *Abrupt rate accelerations or premature beats cause life-threatening arrhythmias in mice with long-QT3 syndrome.* Nat Med, 2001. **7**(9): p. 1021-7.
63. Clancy, C.E. and Y. Rudy, *Linking a genetic defect to its cellular phenotype in a cardiac arrhythmia.* Nature, 1999. **400**(6744): p. 566-9.
64. Heijman, J., et al., *Cellular and molecular electrophysiology of atrial fibrillation initiation, maintenance, and progression.* Circ Res, 2014. **114**(9): p. 1483-99.
65. Lemoine, M.D., et al., *Arrhythmogenic left atrial cellular electrophysiology in a murine genetic long QT syndrome model.* Cardiovasc Res, 2011. **92**(1): p. 67-74.
66. Lindegger, N., et al., *Diastolic transient inward current in long QT syndrome type 3 is caused by Ca2+ overload and inhibited by ranolazine.* J Mol Cell Cardiol, 2009. **47**(2): p. 326-34.
67. Maltsev, V.A. and A.I. Undrovinas, *A multi-modal composition of the late Na+ current in human ventricular cardiomyocytes.* Cardiovasc Res, 2006. **69**(1): p. 116-27.
68. Nagatomo, T., et al., *Rate-dependent QT shortening mechanism for the LQT3 deltaKPQ mutant.* Cardiovasc Res, 2002. **54**(3): p. 624-9.
69. Schwartz, P.J., et al., *Genotype-phenotype correlation in the long-QT syndrome: gene-specific triggers for life-threatening arrhythmias.* Circulation, 2001. **103**(1): p. 89-95.
70. Schwartz, P.J., et al., *Long QT syndrome patients with mutations of the SCN5A and HERG genes have differential responses to Na+ channel blockade and to increases in heart rate. Implications for gene-specific therapy.* Circulation, 1995. **92**(12): p. 3381-6.
71. Ben-Johny, M., et al., *Conservation of Ca2+/calmodulin regulation across Na and Ca2+ channels.* Cell, 2014. **157**(7): p. 1657-70.
72. Yan, H., et al., *Calmodulin limits pathogenic Na+ channel persistent current.* J Gen Physiol, 2017. **149**(2): p. 277-293.
73. Kim, J., et al., *Calmodulin mediates Ca2+ sensitivity of sodium channels.* J Biol Chem, 2004. **279**(43): p. 45004-12.

74. Musa, H., et al., *SCN5A variant that blocks fibroblast growth factor homologous factor regulation causes human arrhythmia.* Proc Natl Acad Sci U S A, 2015. **112**(40): p. 12528-33.
75. Gade, A.R., S.O. Marx, and G.S. Pitt, *An interaction between the III-IV linker and CTD in NaV1.5 confers regulation of inactivation by CaM and FHF.* J Gen Physiol, 2020. **152**(2).
76. Cheng, J., et al., *Alpha1-syntrophin mutations identified in sudden infant death syndrome cause an increase in late cardiac sodium current.* Circ Arrhythm Electrophysiol, 2009. **2**(6): p. 667-76.
77. Cronk, L.B., et al., *Novel mechanism for sudden infant death syndrome: persistent late sodium current secondary to mutations in caveolin-3.* Heart Rhythm, 2007. **4**(2): p. 161-6.
78. Vatta, M., et al., *Mutant caveolin-3 induces persistent late sodium current and is associated with long-QT syndrome.* Circulation, 2006. **114**(20): p. 2104-12.
79. Tateyama, M., et al., *Modulation of cardiac sodium channel gating by protein kinase A can be altered by disease-linked mutation.* J Biol Chem, 2003. **278**(47): p. 46718-26.
80. Echt, D.S., et al., *Mortality and morbidity in patients receiving encainide, flecainide, or placebo. The Cardiac Arrhythmia Suppression Trial.* N Engl J Med, 1991. **324**(12): p. 781-8.
81. Greene, H.L., et al., *The Cardiac Arrhythmia Suppression Trial: first CAST ... then CAST-II.* J Am Coll Cardiol, 1992. **19**(5): p. 894-8.
82. Moreno, J.D. and C.E. Clancy, *Pathophysiology of the cardiac late Na current and its potential as a drug target.* J Mol Cell Cardiol, 2012. **52**(3): p. 608-19.
83. Fredj, S., et al., *Molecular basis of ranolazine block of LQT-3 mutant sodium channels: evidence for site of action.* Br J Pharmacol, 2006. **148**(1): p. 16-24.
84. Abriel, H., *Cardiac sodium channel Na(v)1.5 and interacting proteins: Physiology and pathophysiology.* J Mol Cell Cardiol, 2010. **48**(1): p. 2-11.
85. Shy, D., L. Gillet, and H. Abriel, *Cardiac sodium channel NaV1.5 distribution in myocytes via interacting proteins: the multiple pool model.* Biochim Biophys Acta, 2013. **1833**(4): p. 886-94.
86. Delmar, M., *The intercalated disk as a single functional unit.* Heart Rhythm, 2004. **1**(1): p. 12-3.
87. Noorman, M., et al., *Cardiac cell-cell junctions in health and disease: Electrical versus mechanical coupling.* J Mol Cell Cardiol, 2009. **47**(1): p. 23-31.
88. Zong, L., et al., *Gap junction mediated miRNA intercellular transfer and gene regulation: A novel mechanism for intercellular genetic communication.* Sci Rep, 2016. **6**: p. 19884.
89. Dusek, R.L., L.M. Godsel, and K.J. Green, *Discriminating roles of desmosomal cadherins: beyond desmosomal adhesion.* J Dermatol Sci, 2007. **45**(1): p. 7-21.
90. Wang, Q., et al., *Xin proteins and intercalated disc maturation, signaling and diseases.* Front Biosci (Landmark Ed), 2012. **17**: p. 2566-93.
91. Agullo-Pascual, E., et al., *Super-resolution imaging reveals that loss of the C-terminus of connexin43 limits microtubule plus-end capture and NaV1.5 localization at the intercalated disc.* Cardiovasc Res, 2014. **104**(2): p. 371-81.

92. Geisler, S.B., et al., *Ordered assembly of the adhesive and electrochemical connections within newly formed intercalated disks in primary cultures of adult rat cardiomyocytes.* J Biomed Biotechnol, 2010. **2010**: p. 624719.
93. Oxford, E.M., et al., *Connexin43 remodeling caused by inhibition of plakophilin-2 expression in cardiac cells.* Circ Res, 2007. **101**(7): p. 703-11.
94. Yang, L., et al., *Loss of beta-adrenergic-stimulated phosphorylation of CaV1.2 channels on Ser1700 leads to heart failure.* Proc Natl Acad Sci U S A, 2016. **113**(49): p. E7976-E7985.
95. Lowe, J.S., et al., *Voltage-gated Nav channel targeting in the heart requires an ankyrin-G dependent cellular pathway.* J Cell Biol, 2008. **180**(1): p. 173-86.
96. Sato, P.Y., et al., *Loss of plakophilin-2 expression leads to decreased sodium current and slower conduction velocity in cultured cardiac myocytes.* Circ Res, 2009. **105**(6): p. 523-6.
97. Cerrone, M., et al., *Sodium current deficit and arrhythmogenesis in a murine model of plakophilin-2 haploinsufficiency.* Cardiovasc Res, 2012. **95**(4): p. 460-8.
98. Rizzo, S., et al., *Intercalated disc abnormalities, reduced Na(+) current density, and conduction slowing in desmoglein-2 mutant mice prior to cardiomyopathic changes.* Cardiovasc Res, 2012. **95**(4): p. 409-18.
99. Gomes, J., et al., *Electrophysiological abnormalities precede overt structural changes in arrhythmogenic right ventricular cardiomyopathy due to mutations in desmoplakin-A combined murine and human study.* Eur Heart J, 2012. **33**(15): p. 1942-53.
100. Jansen, J.A., et al., *Reduced heterogeneous expression of Cx43 results in decreased Nav1.5 expression and reduced sodium current that accounts for arrhythmia vulnerability in conditional Cx43 knockout mice.* Heart Rhythm, 2012. **9**(4): p. 600-7.
101. Agullo-Pascual, E., M. Cerrone, and M. Delmar, *Arrhythmogenic cardiomyopathy and Brugada syndrome: diseases of the connexome.* FEBS Lett, 2014. **588**(8): p. 1322-30.
102. Albesa, M., et al., *Regulation of the cardiac sodium channel Nav1.5 by utrophin in dystrophin-deficient mice.* Cardiovasc Res, 2011. **89**(2): p. 320-8.
103. Gavillet, B., et al., *Cardiac sodium channel Nav1.5 is regulated by a multiprotein complex composed of syntrophins and dystrophin.* Circ Res, 2006. **99**(4): p. 407-14.
104. Shy, D., et al., *PDZ domain-binding motif regulates cardiomyocyte compartment-specific NaV1.5 channel expression and function.* Circulation, 2014. **130**(2): p. 147-60.
105. Rougier, J.S., et al., *A Distinct Pool of Nav1.5 Channels at the Lateral Membrane of Murine Ventricular Cardiomyocytes.* Front Physiol, 2019. **10**: p. 834.
106. Vermij, S.H., et al., *Single-Molecule Localization of the Cardiac Voltage-Gated Sodium Channel Reveals Different Modes of Reorganization at Cardiomyocyte Membrane Domains.* Circ Arrhythm Electrophysiol, 2020. **13**(7): p. e008241.
107. Verkerk, A.O., et al., *Effects of heart failure on brain-type Na+ channels in rabbit ventricular myocytes.* Europace, 2007. **9**(8): p. 571-7.
108. Lin, X., et al., *Subcellular heterogeneity of sodium current properties in adult cardiac ventricular myocytes.* Heart Rhythm, 2011. **8**(12): p. 1923-30.
109. Mousson, F., et al., *Quantitative proteomics reveals regulation of dynamic components within TATA-binding protein (TBP) transcription complexes.* Mol Cell Proteomics, 2008. **7**(5): p. 845-52.

110. Iacobucci, I., et al., *From classical to new generation approaches: An excursus of -omics methods for investigation of protein-protein interaction networks.* J Proteomics, 2021. **230**: p. 103990.
111. Martell, J.D., et al., *Engineered ascorbate peroxidase as a genetically encoded reporter for electron microscopy.* Nat Biotechnol, 2012. **30**(11): p. 1143-8.
112. Roux, K.J., et al., *A promiscuous biotin ligase fusion protein identifies proximal and interacting proteins in mammalian cells.* J Cell Biol, 2012. **196**(6): p. 801-10.
113. Branon, T.C., et al., *Efficient proximity labeling in living cells and organisms with TurboID.* Nat Biotechnol, 2018. **36**(9): p. 880-887.
114. Lam, S.S., et al., *Directed evolution of APEX2 for electron microscopy and proximity labeling.* Nat Methods, 2015. **12**(1): p. 51-4.
115. Paek, J., et al., *Multidimensional Tracking of GPCR Signaling via Peroxidase-Catalyzed Proximity Labeling.* Cell, 2017. **169**(2): p. 338-349 e11.
116. Kalocsay, M., *APEX Peroxidase-Catalyzed Proximity Labeling and Multiplexed Quantitative Proteomics.* Methods Mol Biol, 2019. **2008**: p. 41-55.
117. Thompson, A., et al., *Tandem mass tags: a novel quantification strategy for comparative analysis of complex protein mixtures by MS/MS.* Anal Chem, 2003. **75**(8): p. 1895-904.
118. Lobingier, B.T., et al., *An Approach to Spatiotemporally Resolve Protein Interaction Networks in Living Cells.* Cell, 2017. **169**(2): p. 350-360 e12.
119. Vandemoortele, G., et al., *A Well-Controlled BioID Design for Endogenous Bait Proteins.* J Proteome Res, 2019. **18**(1): p. 95-106.
120. Ting, L., et al., *MS3 eliminates ratio distortion in isobaric multiplexed quantitative proteomics.* Nat Methods, 2011. **8**(11): p. 937-40.
121. Duan, D., et al., *Duchenne muscular dystrophy.* Nat Rev Dis Primers, 2021. **7**(1): p. 13.
122. Wallace, G.Q. and E.M. McNally, *Mechanisms of muscle degeneration, regeneration, and repair in the muscular dystrophies.* Annu Rev Physiol, 2009. **71**: p. 37-57.
123. Perloff, J.K., *Cardiac rhythm and conduction in Duchenne's muscular dystrophy: a prospective study of 20 patients.* J Am Coll Cardiol, 1984. **3**(5): p. 1263-8.
124. Nigro, G., et al., *The incidence and evolution of cardiomyopathy in Duchenne muscular dystrophy.* Int J Cardiol, 1990. **26**(3): p. 271-7.
125. Kieny, P., et al., *Evolution of life expectancy of patients with Duchenne muscular dystrophy at AFM Yolaine de Kepper centre between 1981 and 2011.* Ann Phys Rehabil Med, 2013. **56**(6): p. 443-54.
126. Yucel, N., et al., *Humanizing the mdx mouse model of DMD: the long and the short of it.* NPJ Regen Med, 2018. **3**: p. 4.
127. Yasuda, S., et al., *Dystrophic heart failure blocked by membrane sealant poloxamer.* Nature, 2005. **436**(7053): p. 1025-9.
128. Fanchaouy, M., et al., *Pathways of abnormal stress-induced Ca2+ influx into dystrophic mdx cardiomyocytes.* Cell Calcium, 2009. **46**(2): p. 114-21.
129. Khairallah, R.J., et al., *Microtubules underlie dysfunction in duchenne muscular dystrophy.* Sci Signal, 2012. **5**(236): p. ra56.
130. Prins, K.W., et al., *Dystrophin is a microtubule-associated protein.* J Cell Biol, 2009. **186**(3): p. 363-9.
131. Himelman, E., et al., *Prevention of connexin-43 remodeling protects against Duchenne muscular dystrophy cardiomyopathy.* J Clin Invest, 2020. **130**(4): p. 1713-1727.

132. Ullrich, N.D., et al., *Hypersensitivity of excitation-contraction coupling in dystrophic cardiomyocytes.* Am J Physiol Heart Circ Physiol, 2009. **297**(6): p. H1992-2003.
133. Williams, I.A. and D.G. Allen, *Intracellular calcium handling in ventricular myocytes from mdx mice.* Am J Physiol Heart Circ Physiol, 2007. **292**(2): p. H846-55.
134. Jung, C., et al., *Dystrophic cardiomyopathy: amplification of cellular damage by Ca2+ signalling and reactive oxygen species-generating pathways.* Cardiovasc Res, 2008. **77**(4): p. 766-73.
135. Williams, I.A. and D.G. Allen, *The role of reactive oxygen species in the hearts of dystrophin-deficient mdx mice.* Am J Physiol Heart Circ Physiol, 2007. **293**(3): p. H1969-77.
136. Robert, V., et al., *Alteration in calcium handling at the subcellular level in mdx myotubes.* J Biol Chem, 2001. **276**(7): p. 4647-51.
137. Jiang, F., Y. Zhang, and G.J. Dusting, *NADPH oxidase-mediated redox signaling: roles in cellular stress response, stress tolerance, and tissue repair.* Pharmacol Rev, 2011. **63**(1): p. 218-42.
138. Hockerman, G.H., et al., *Construction of a high-affinity receptor site for dihydropyridine agonists and antagonists by single amino acid substitutions in a non-L-type Ca2+ channel.* Proc Natl Acad Sci U S A, 1997. **94**(26): p. 14906-11.
139. He, M., et al., *Motif III S5 of L-type calcium channels is involved in the dihydropyridine binding site. A combined radioligand binding and electrophysiological study.* J Biol Chem, 1997. **272**(5): p. 2629-33.
140. O'Connell, T.D., M.C. Rodrigo, and P.C. Simpson, *Isolation and culture of adult mouse cardiac myocytes.* Methods Mol Biol, 2007. **357**: p. 271-96.
141. Fabiato, A. and F. Fabiato, *Calcium and cardiac excitation-contraction coupling.* Annu Rev Physiol, 1979. **41**: p. 473-84.
142. Beeler, G.W., Jr. and H. Reuter, *Membrane calcium current in ventricular myocardial fibres.* J Physiol, 1970. **207**(1): p. 191-209.
143. De Jongh, K.S., et al., *Specific phosphorylation of a site in the full-length form of the alpha 1 subunit of the cardiac L-type calcium channel by adenosine 3',5'-cyclic monophosphate-dependent protein kinase.* Biochemistry, 1996. **35**(32): p. 10392-402.
144. Mitterdorfer, J., et al., *Identification of PK-A phosphorylation sites in the carboxyl terminus of L-type calcium channel alpha 1 subunits.* Biochemistry, 1996. **35**(29): p. 9400-6.
145. Gao, T., et al., *cAMP-dependent regulation of cardiac L-type Ca2+ channels requires membrane targeting of PKA and phosphorylation of channel subunits.* Neuron, 1997. **19**(1): p. 185-96.
146. Ganesan, A.N., et al., *Beta-adrenergic stimulation of L-type Ca2+ channels in cardiac myocytes requires the distal carboxyl terminus of alpha1C but not serine 1928.* Circ Res, 2006. **98**(2): p. e11-8.
147. Lemke, T., et al., *Unchanged beta-adrenergic stimulation of cardiac L-type calcium channels in Ca v 1.2 phosphorylation site S1928A mutant mice.* J Biol Chem, 2008. **283**(50): p. 34738-44.
148. Fuller, M.D., et al., *Molecular mechanism of calcium channel regulation in the fight-or-flight response.* Sci Signal, 2010. **3**(141): p. ra70.

149. Emrick, M.A., et al., *Beta-adrenergic-regulated phosphorylation of the skeletal muscle Ca(V)1.1 channel in the fight-or-flight response.* Proc Natl Acad Sci U S A, 2010. **107**(43): p. 18712-7.
150. Yang, L., et al., *beta-adrenergic regulation of the L-type Ca2+ channel does not require phosphorylation of alpha1C Ser1700.* Circ Res, 2013. **113**(7): p. 871-80.
151. Fu, Y., et al., *Phosphorylation sites required for regulation of cardiac calcium channels in the fight-or-flight response.* Proc Natl Acad Sci U S A, 2013. **110**(48): p. 19621-6.
152. Poomvanicha, M., et al., *Beta-adrenergic regulation of the heart expressing the Ser1700A/Thr1704A mutated Cav1.2 channel.* J Mol Cell Cardiol, 2017. **111**: p. 10-16.
153. Colecraft, H.M., et al., *Novel functional properties of Ca(2+) channel beta subunits revealed by their expression in adult rat heart cells.* J Physiol, 2002. **541**(Pt 2): p. 435-52.
154. Hullin, R., et al., *Calcium channel beta subunit heterogeneity: functional expression of cloned cDNA from heart, aorta and brain.* EMBO J, 1992. **11**(3): p. 885-90.
155. Haase, H., et al., *In-vivo phosphorylation of the cardiac L-type calcium channel beta-subunit in response to catecholamines.* Mol Cell Biochem, 1996. **163-164**: p. 99-106.
156. Bunemann, M., et al., *Functional regulation of L-type calcium channels via protein kinase A-mediated phosphorylation of the beta(2) subunit.* J Biol Chem, 1999. **274**(48): p. 33851-4.
157. Gerhardstein, B.L., et al., *Identification of the sites phosphorylated by cyclic AMP-dependent protein kinase on the beta 2 subunit of L-type voltage-dependent calcium channels.* Biochemistry, 1999. **38**(32): p. 10361-70.
158. Miriyala, J., et al., *Role of CaVbeta subunits, and lack of functional reserve, in protein kinase A modulation of cardiac CaV1.2 channels.* Circ Res, 2008. **102**(7): p. e54-64.
159. Brandmayr, J., et al., *Deletion of the C-terminal phosphorylation sites in the cardiac beta-subunit does not affect the basic beta-adrenergic response of the heart and the Ca(v)1.2 channel.* J Biol Chem, 2012. **287**(27): p. 22584-92.
160. Weiss, S., et al., *Regulation of cardiac L-type Ca(2)(+) channel CaV1.2 via the beta-adrenergic-cAMP-protein kinase A pathway: old dogmas, advances, and new uncertainties.* Circ Res, 2013. **113**(5): p. 617-31.
161. Domes, K., et al., *Truncation of murine CaV1.2 at Asp-1904 results in heart failure after birth.* J Biol Chem, 2011. **286**(39): p. 33863-71.
162. Hambleton, M., et al., *Inducible and myocyte-specific inhibition of PKCalpha enhances cardiac contractility and protects against infarction-induced heart failure.* Am J Physiol Heart Circ Physiol, 2007. **293**(6): p. H3768-71.
163. Tang, M., et al., *Enhanced basal contractility but reduced excitation-contraction coupling efficiency and beta-adrenergic reserve of hearts with increased Cav1.2 activity.* Am J Physiol Heart Circ Physiol, 2010. **299**(2): p. H519-28.
164. Katchman, A., et al., *Proteolytic cleavage and PKA phosphorylation of alpha1C subunit are not required for adrenergic regulation of CaV1.2 in the heart.* Proc Natl Acad Sci U S A, 2017. **114**(34): p. 9194-9199.
165. Yang, L., et al., *Cardiac CaV1.2 channels require beta subunits for beta-adrenergic-mediated modulation but not trafficking.* J Clin Invest, 2019. **129**(2): p. 647-658.
166. Hidalgo, P., et al., *The alpha1-beta-subunit interaction that modulates calcium channel activity is reversible and requires a competent alpha-interaction domain.* J Biol Chem, 2006. **281**(34): p. 24104-10.

167. Xiao, R.P., et al., *Recent advances in cardiac beta(2)-adrenergic signal transduction.* Circ Res, 1999. **85**(11): p. 1092-100.
168. Trost, B., A. Kusalik, and S. Napper, *Computational Analysis of the Predicted Evolutionary Conservation of Human Phosphorylation Sites.* PLoS One, 2016. **11**(4): p. e0152809.
169. van Goor, M.K., et al., *Interspecies differences in PTH-mediated PKA phosphorylation of the epithelial calcium channel TRPV5.* Pflugers Arch, 2017. **469**(10): p. 1301-1311.
170. Bramson, H.N., E.T. Kaiser, and A.S. Mildvan, *Mechanistic studies of cAMP-dependent protein kinase action.* CRC Crit Rev Biochem, 1984. **15**(2): p. 93-124.
171. Moore, M.J., J.A. Adams, and S.S. Taylor, *Structural basis for peptide binding in protein kinase A. Role of glutamic acid 203 and tyrosine 204 in the peptide-positioning loop.* J Biol Chem, 2003. **278**(12): p. 10613-8.
172. Feramisco, J.R., D.B. Glass, and E.G. Krebs, *Optimal spatial requirements for the location of basic residues in peptide substrates for the cyclic AMP-dependent protein kinase.* J Biol Chem, 1980. **255**(9): p. 4240-5.
173. Kemp, B.E., et al., *Role of multiple basic residues in determining the substrate specificity of cyclic AMP-dependent protein kinase.* J Biol Chem, 1977. **252**(14): p. 4888-94.
174. Neuberger, G., G. Schneider, and F. Eisenhaber, *pkaPS: prediction of protein kinase A phosphorylation sites with the simplified kinase-substrate binding model.* Biol Direct, 2007. **2**: p. 1.
175. Iakoucheva, L.M., et al., *The importance of intrinsic disorder for protein phosphorylation.* Nucleic Acids Res, 2004. **32**(3): p. 1037-49.
176. Zhou, F.F., et al., *GPS: a novel group-based phosphorylation predicting and scoring method.* Biochem Biophys Res Commun, 2004. **325**(4): p. 1443-8.
177. Blom, N., S. Gammeltoft, and S. Brunak, *Sequence and structure-based prediction of eukaryotic protein phosphorylation sites.* J Mol Biol, 1999. **294**(5): p. 1351-62.
178. Obenauer, J.C., L.C. Cantley, and M.B. Yaffe, *Scansite 2.0: Proteome-wide prediction of cell signaling interactions using short sequence motifs.* Nucleic Acids Res, 2003. **31**(13): p. 3635-41.
179. Liu, G., et al., *Mechanism of adrenergic CaV1.2 stimulation revealed by proximity proteomics.* Nature, 2020. **577**(7792): p. 695-700.
180. Takahashi, S.X., et al., *A CaVbeta SH3/guanylate kinase domain interaction regulates multiple properties of voltage-gated Ca2+ channels.* J Gen Physiol, 2005. **126**(4): p. 365-77.
181. Kaumann, A.J., et al., *Beta 2-adrenoceptor activation by zinterol causes protein phosphorylation, contractile effects and relaxant effects through a cAMP pathway in human atrium.* Mol Cell Biochem, 1996. **163-164**: p. 113-23.
182. Lundby, A., et al., *In vivo phosphoproteomics analysis reveals the cardiac targets of beta-adrenergic receptor signaling.* Sci Signal, 2013. **6**(278): p. rs11.
183. Freschi, L., M. Osseni, and C.R. Landry, *Functional divergence and evolutionary turnover in mammalian phosphoproteomes.* PLoS Genet, 2014. **10**(1): p. e1004062.
184. Muth, J.N., et al., *Cardiac-specific overexpression of the alpha(1) subunit of the L-type voltage-dependent Ca(2+) channel in transgenic mice. Loss of isoproterenol-induced contraction.* J Biol Chem, 1999. **274**(31): p. 21503-6.

185. Dai, S., D.D. Hall, and J.W. Hell, *Supramolecular assemblies and localized regulation of voltage-gated ion channels.* Physiol Rev, 2009. **89**(2): p. 411-52.
186. Davare, M.A., et al., *A beta2 adrenergic receptor signaling complex assembled with the Ca2+ channel Cav1.2.* Science, 2001. **293**(5527): p. 98-101.
187. Joiner, M.L., et al., *Assembly of a beta2-adrenergic receptor--GluR1 signalling complex for localized cAMP signalling.* EMBO J, 2010. **29**(2): p. 482-95.
188. Patriarchi, T., et al., *Phosphorylation of Cav1.2 on S1928 uncouples the L-type Ca2+ channel from the beta2 adrenergic receptor.* EMBO J, 2016. **35**(12): p. 1330-45.
189. Qian, H., et al., *Phosphorylation of Ser1928 mediates the enhanced activity of the L-type Ca2+ channel Cav1.2 by the beta2-adrenergic receptor in neurons.* Sci Signal, 2017. **10**(463).
190. Prehn, J.L. and J.A. Bevan, *Facial vein of the rabbit. Intracellularly recorded hyperpolarization of smooth muscle cells induced by beta-adrenergic receptor stimulation.* Circ Res, 1983. **52**(4): p. 465-70.
191. Miyoshi, H. and Y. Nakaya, *Activation of ATP-sensitive K+ channels by cyclic AMP-dependent protein kinase in cultured smooth muscle cells of porcine coronary artery.* Biochem Biophys Res Commun, 1993. **193**(1): p. 240-7.
192. Nystoriak, M.A., et al., *Ser1928 phosphorylation by PKA stimulates the L-type Ca2+ channel CaV1.2 and vasoconstriction during acute hyperglycemia and diabetes.* Sci Signal, 2017. **10**(463).
193. Liu, G., et al., *Assembly of a Ca2+-dependent BK channel signaling complex by binding to beta2 adrenergic receptor.* EMBO J, 2004. **23**(11): p. 2196-205.
194. Berkefeld, H., et al., *BKCa-Cav channel complexes mediate rapid and localized Ca2+-activated K+ signaling.* Science, 2006. **314**(5799): p. 615-20.
195. Wang, Q., et al., *SCN5A mutations associated with an inherited cardiac arrhythmia, long QT syndrome.* Cell, 1995. **80**(5): p. 805-11.
196. Wan, E., et al., *Aberrant sodium influx causes cardiomyopathy and atrial fibrillation in mice.* J Clin Invest, 2016. **126**(1): p. 112-22.
197. Kass, R.S., *Sodium channel inactivation in heart: a novel role of the carboxy-terminal domain.* J Cardiovasc Electrophysiol, 2006. **17 Suppl 1**: p. S21-S25.
198. Tan, H.L., et al., *A calcium sensor in the sodium channel modulates cardiac excitability.* Nature, 2002. **415**(6870): p. 442-7.
199. Wang, C., et al., *Crystal structure of the ternary complex of a NaV C-terminal domain, a fibroblast growth factor homologous factor, and calmodulin.* Structure, 2012. **20**(7): p. 1167-76.
200. Yoder, J.B., et al., *Ca(2+)-dependent regulation of sodium channels NaV1.4 and NaV1.5 is controlled by the post-IQ motif.* Nat Commun, 2019. **10**(1): p. 1514.
201. Satin, J., et al., *A mutant of TTX-resistant cardiac sodium channels with TTX-sensitive properties.* Science, 1992. **256**(5060): p. 1202-5.
202. Carboni, M., et al., *Slow sodium channel inactivation and use-dependent block modulated by the same domain IV S6 residue.* J Membr Biol, 2005. **207**(2): p. 107-17.
203. Kiyosue, T. and M. Arita, *Late sodium current and its contribution to action potential configuration in guinea pig ventricular myocytes.* Circ Res, 1989. **64**(2): p. 389-97.
204. Bengel, P., et al., *Contribution of the neuronal sodium channel NaV1.8 to sodium- and calcium-dependent cellular proarrhythmia.* J Mol Cell Cardiol, 2020. **144**: p. 35-46.

205. Kaufmann, S.G., et al., *Distribution and function of sodium channel subtypes in human atrial myocardium.* J Mol Cell Cardiol, 2013. **61**: p. 133-141.
206. Burel, S., et al., *C-terminal phosphorylation of NaV1.5 impairs FGF13-dependent regulation of channel inactivation.* J Biol Chem, 2017. **292**(42): p. 17431-17448.
207. Liu, H., et al., *Mutations in cardiac sodium channels: clinical implications.* Am J Pharmacogenomics, 2003. **3**(3): p. 173-9.
208. Abrams, J., et al., *Fibroblast growth factor homologous factors tune arrhythmogenic late NaV1.5 current in calmodulin binding-deficient channels.* JCI Insight, 2020. **5**(19).
209. Wilde, A.A.M. and A.S. Amin, *Clinical Spectrum of SCN5A Mutations: Long QT Syndrome, Brugada Syndrome, and Cardiomyopathy.* JACC Clin Electrophysiol, 2018. **4**(5): p. 569-579.
210. Deschenes, I., et al., *Isoform-specific modulation of voltage-gated Na(+) channels by calmodulin.* Circ Res, 2002. **90**(4): p. E49-57.
211. Hennessey, J.A., et al., *FGF12 is a candidate Brugada syndrome locus.* Heart Rhythm, 2013. **10**(12): p. 1886-94.
212. Yang, J., et al., *FGF13 modulates the gating properties of the cardiac sodium channel Nav1.5 in an isoform-specific manner.* Channels (Austin), 2016. **10**(5): p. 410-420.
213. Wang, X., et al., *Conditional knockout of Fgf13 in murine hearts increases arrhythmia susceptibility and reveals novel ion channel modulatory roles.* J Mol Cell Cardiol, 2017. **104**: p. 63-74.
214. Kapplinger, J.D., et al., *Enhanced Classification of Brugada Syndrome-Associated and Long-QT Syndrome-Associated Genetic Variants in the SCN5A-Encoded Na(v)1.5 Cardiac Sodium Channel.* Circ Cardiovasc Genet, 2015. **8**(4): p. 582-95.
215. Maltsev, V.A. and A. Undrovinas, *Late sodium current in failing heart: friend or foe?* Prog Biophys Mol Biol, 2008. **96**(1-3): p. 421-51.
216. Plant, L.D., et al., *Hypoxia Produces Pro-arrhythmic Late Sodium Current in Cardiac Myocytes by SUMOylation of NaV1.5 Channels.* Cell Rep, 2020. **30**(7): p. 2225-2236 e4.
217. Abriel, H., *Roles and regulation of the cardiac sodium channel Na v 1.5: recent insights from experimental studies.* Cardiovasc Res, 2007. **76**(3): p. 381-9.
218. Cerrone, M. and S.G. Priori, *Genetics of sudden death: focus on inherited channelopathies.* Eur Heart J, 2011. **32**(17): p. 2109-18.
219. Mizusawa, Y. and A.A. Wilde, *Brugada syndrome.* Circ Arrhythm Electrophysiol, 2012. **5**(3): p. 606-16.
220. Shirokova, N. and E. Niggli, *Cardiac phenotype of Duchenne Muscular Dystrophy: insights from cellular studies.* J Mol Cell Cardiol, 2013. **58**: p. 217-24.
221. Gao, Q.Q. and E.M. McNally, *The Dystrophin Complex: Structure, Function, and Implications for Therapy.* Compr Physiol, 2015. **5**(3): p. 1223-39.
222. Ohlendieck, K. and K.P. Campbell, *Dystrophin-associated proteins are greatly reduced in skeletal muscle from mdx mice.* J Cell Biol, 1991. **115**(6): p. 1685-94.
223. Koenig, X., J. Ebner, and K. Hilber, *Voltage-Dependent Sarcolemmal Ion Channel Abnormalities in the Dystrophin-Deficient Heart.* Int J Mol Sci, 2018. **19**(11).
224. Sadeghi, A., A.D. Doyle, and B.D. Johnson, *Regulation of the cardiac L-type Ca2+ channel by the actin-binding proteins alpha-actinin and dystrophin.* Am J Physiol Cell Physiol, 2002. **282**(6): p. C1502-11.

225. Rubi, L., et al., *Decreased inward rectifier potassium current IK1 in dystrophin-deficient ventricular cardiomyocytes.* Channels (Austin), 2017. **11**(2): p. 101-108.
226. Rhett, J.M., et al., *Cx43 associates with Na(v)1.5 in the cardiomyocyte perinexus.* J Membr Biol, 2012. **245**(7): p. 411-22.
227. Kaprielian, R.R., et al., *Distinct patterns of dystrophin organization in myocyte sarcolemma and transverse tubules of normal and diseased human myocardium.* Circulation, 2000. **101**(22): p. 2586-94.
228. Stevenson, S.A., et al., *High-resolution en-face visualization of the cardiomyocyte plasma membrane reveals distinctive distributions of spectrin and dystrophin.* Eur J Cell Biol, 2005. **84**(12): p. 961-71.
229. Petitprez, S., et al., *SAP97 and dystrophin macromolecular complexes determine two pools of cardiac sodium channels Nav1.5 in cardiomyocytes.* Circ Res, 2011. **108**(3): p. 294-304.
230. Milstein, M.L., et al., *Dynamic reciprocity of sodium and potassium channel expression in a macromolecular complex controls cardiac excitability and arrhythmia.* Proc Natl Acad Sci U S A, 2012. **109**(31): p. E2134-43.
231. Gillet, L., et al., *Cardiac-specific ablation of synapse-associated protein SAP97 in mice decreases potassium currents but not sodium current.* Heart Rhythm, 2015. **12**(1): p. 181-92.
232. Klietsch, R., et al., *Dystrophin-glycoprotein complex and laminin colocalize to the sarcolemma and transverse tubules of cardiac muscle.* Circ Res, 1993. **72**(2): p. 349-60.
233. Peri, V., et al., *Dystrophin predominantly localizes to the transverse tubule/Z-line regions of single ventricular myocytes and exhibits distinct associations with the membrane.* Mol Cell Biochem, 1994. **130**(1): p. 57-65.
234. Matamoros, M., et al., *Nav1.5 N-terminal domain binding to alpha1-syntrophin increases membrane density of human Kir2.1, Kir2.2 and Nav1.5 channels.* Cardiovasc Res, 2016. **110**(2): p. 279-90.
235. Dolphin, A.C., *Age of quantitative proteomics hits voltage-gated calcium channels.* Proc Natl Acad Sci U S A, 2010. **107**(34): p. 14941-2.
236. Rees, J.S., et al., *Protein Neighbors and Proximity Proteomics.* Mol Cell Proteomics, 2015. **14**(11): p. 2848-56.
237. Hung, V., et al., *Proteomic mapping of the human mitochondrial intermembrane space in live cells via ratiometric APEX tagging.* Mol Cell, 2014. **55**(2): p. 332-41.
238. Hung, V., et al., *Spatially resolved proteomic mapping in living cells with the engineered peroxidase APEX2.* Nat Protoc, 2016. **11**(3): p. 456-75.
239. Rhee, H.W., et al., *Proteomic mapping of mitochondria in living cells via spatially restricted enzymatic tagging.* Science, 2013. **339**(6125): p. 1328-1331.
240. Perez-Hernandez, M., et al., *Structural and Functional Characterization of a Nav1.5-Mitochondrial Couplon.* Circ Res, 2021. **128**(3): p. 419-432.
241. Wang, C., et al., *Fibroblast growth factor homologous factor 13 regulates Na+ channels and conduction velocity in murine hearts.* Circ Res, 2011. **109**(7): p. 775-82.
242. Tinsley, J., et al., *Expression of full-length utrophin prevents muscular dystrophy in mdx mice.* Nat Med, 1998. **4**(12): p. 1441-4.

243. Valdivia, C.R., et al., *GPD1L links redox state to cardiac excitability by PKC-dependent phosphorylation of the sodium channel SCN5A.* Am J Physiol Heart Circ Physiol, 2009. **297**(4): p. H1446-52.
244. Jespersen, T., et al., *Cardiac sodium channel Na(v)1.5 interacts with and is regulated by the protein tyrosine phosphatase PTPH1.* Biochem Biophys Res Commun, 2006. **348**(4): p. 1455-62.
245. Murphy, S., et al., *Proteomic analysis of dystrophin deficiency and associated changes in the aged mdx-4cv heart model of dystrophinopathy-related cardiomyopathy.* J Proteomics, 2016. **145**: p. 24-36.
246. Lopaschuk, G.D., et al., *Cardiac Energy Metabolism in Heart Failure.* Circ Res, 2021. **128**(10): p. 1487-1513.
247. Leo-Macias, A., et al., *Nanoscale visualization of functional adhesion/excitability nodes at the intercalated disc.* Nat Commun, 2016. **7**: p. 10342.
248. Sit, B., D. Gutmann, and T. Iskratsch, *Costameres, dense plaques and podosomes: the cell matrix adhesions in cardiovascular mechanosensing.* J Muscle Res Cell Motil, 2019. **40**(2): p. 197-209.
249. Peter, A.K., et al., *The costamere bridges sarcomeres to the sarcolemma in striated muscle.* Prog Pediatr Cardiol, 2011. **31**(2): p. 83-88.
250. Decker, M.L., et al., *Morphological analysis of contracting and quiescent adult rabbit cardiac myocytes in long-term culture.* Anat Rec, 1990. **227**(3): p. 285-99.
251. Samarel, A.M., *Costameres, focal adhesions, and cardiomyocyte mechanotransduction.* Am J Physiol Heart Circ Physiol, 2005. **289**(6): p. H2291-301.
252. Liu, J., et al., *beta1D chain increases alpha7beta1 integrin and laminin and protects against sarcolemmal damage in mdx mice.* Hum Mol Genet, 2012. **21**(7): p. 1592-603.
253. Sen, S., et al., *Upregulation of paxillin and focal adhesion signaling follows Dystroglycan Complex deletions and promotes a hypertensive state of differentiation.* Eur J Cell Biol, 2011. **90**(2-3): p. 249-60.
254. Chicurel, M.E., et al., *Integrin binding and mechanical tension induce movement of mRNA and ribosomes to focal adhesions.* Nature, 1998. **392**(6677): p. 730-3.
255. Willett, M., et al., *Localization of ribosomes and translation initiation factors to talin/beta3-integrin-enriched adhesion complexes in spreading and migrating mammalian cells.* Biol Cell, 2010. **102**(5): p. 265-76.
256. Scarborough, E.A., et al., *Microtubules orchestrate local translation to enable cardiac growth.* Nat Commun, 2021. **12**(1): p. 1547.
257. Yano, T., et al., *Pivotal role of mTORC2 and involvement of ribosomal protein S6 in cardioprotective signaling.* Circ Res, 2014. **114**(8): p. 1268-80.
258. Rougier, J.S., B. Gavillet, and H. Abriel, *Proteasome inhibitor (MG132) rescues Nav1.5 protein content and the cardiac sodium current in dystrophin-deficient mdx (5cv) mice.* Front Physiol, 2013. **4**: p. 51.
259. MacLennan, P.A. and R.H. Edwards, *Protein turnover is elevated in muscle of mdx mice in vivo.* Biochem J, 1990. **268**(3): p. 795-7.
260. Erickson, J.R., et al., *CaMKII in the cardiovascular system: sensing redox states.* Physiol Rev, 2011. **91**(3): p. 889-915.
261. Gervasio, O.L., et al., *TRPC1 binds to caveolin-3 and is regulated by Src kinase - role in Duchenne muscular dystrophy.* J Cell Sci, 2008. **121**(Pt 13): p. 2246-55.

262. Casini, S., et al., *Tubulin polymerization modifies cardiac sodium channel expression and gating.* Cardiovasc Res, 2010. **85**(4): p. 691-700.
263. Chkourko, H.S., et al., *Remodeling of mechanical junctions and of microtubule-associated proteins accompany cardiac connexin43 lateralization.* Heart Rhythm, 2012. **9**(7): p. 1133-1140 e6.
264. Van Norstrand, D.W., et al., *Molecular and functional characterization of novel glycerol-3-phosphate dehydrogenase 1 like gene (GPD1-L) mutations in sudden infant death syndrome.* Circulation, 2007. **116**(20): p. 2253-9.
265. London, B., et al., *Mutation in glycerol-3-phosphate dehydrogenase 1 like gene (GPD1-L) decreases cardiac Na+ current and causes inherited arrhythmias.* Circulation, 2007. **116**(20): p. 2260-8.
266. Frankenfield, A.M., et al., *Development and Comparative Evaluation of Endolysosomal Proximity Labeling-Based Proteomic Methods in Human iPSC-Derived Neurons.* Anal Chem, 2020. **92**(23): p. 15437-15444.